POLITECNICO DI MILANO

Scuola di Ingegneria Civile, Ambientale e Territoriale

Corso di Laurea Magistrale in Ingegneria Civile

GEOTECHNICAL MODELLING OF CPR GROUTING

Relatore: Prof. Giancarlo GIODA

Tesi di Laurea di:

Alessandro Cirone

Matr. 801689

Anno Accademico 2015-2016

Acknowledgments

This Thesis has been written thanks to the cooperation between the partner universities Politecnico di Milano and Pontifícia Universidade Católica do Rio de Janeiro under the Double Degree Programme.

First of all I wish to express my thanks to my supervisor at PUC Rio Prof. Euripides Vargas for his advice and guidance. I am also indebted to Prof.ra Raquel Velloso for her stimulation and encouragement during the discussions that we had in different phases of the research. I would thank also my supervisor at Polimi Prof. Giancarlo Gioda for having placed his trust in me.

I would also to thank all the employees of the Engegraut Company for their kindly help.

Last, but by no means least, I would like to thank my parents for their continuous encouragement and my beloved Rose, who has always been able to bring me peace and serenity during the challenges of my research.

Contents

List of Figures

List of Tables

List of symbols

a, a_0	radius of the cavity, initial radius of the cavity
a_c	column replacement factor
a_1, a_2, a_3	coefficients
A	area
A_c	area of the column
A_s	area of the soil surrounding the column
b	outer radius of spherical thick walled shell
c	cohesion
c_v	coefficient of consolidation
C_c	compression index
C_s	swelling index
d_e	equivalent diameter of PVD unit cell
d_n	nozzle diameter
d_s	diameter of smear zone
d_w	equivalent diameter of drain
D	equivalent diameter of CPR Grouting unit cell
e	void ratio
E	elastic modulus
E_{oed}	oedometric modulus
F	resistance factor for PVD
G	shear modulus
H_d	length of drainage path
k	hydraulic conductivity
k_v, k_h	vertical and horizontal hydraulic conductivities
k_s	horizontal hydraulic conductivity within the smear zone
K	elastic bulk modulus
K_a, K_p	active and passive earth pressure coefficients

K_r, K_θ	radial and circumferential earth pressure coefficients
m_v	oedometric compressibility of soil
M	slope of critical state line in $p : q$ plane
n	stress concentration factor
N	viscosity ratio
N	location of isotropic normal compression line in $v : \ln p'$ plane
OCR	overconsolidation ratio in terms of vertical effective stress
p	pressure, average mean stress
p'	average mean effective stress
$p'_t extrmy$	reference size of yeld locus for Modified Cam Clay
p_{lim}	cavity limit pressure
p_{up}	upheaval pressure
P_i	injection pressure
q	deviator stress
r	radial coordinate
r_p	radius of the pastic region
r_c	radius of the critical state region
R	isotropic overconsolidation ratio
R_avg	average radius of low pressure jet grouting column
R_S	substitution ratio
s_u	undrained shear strength
S	drain spacing
t	time
u	pore pressure
$U\%$	degree of consolidation
v	specific volume $= 1 + e$
V	volume
V	total volume
V_s	volume of solids
V_v	volume of voids
V_g	grout bulb volume
z	depth
α	parameter for post CPR stress calculation

β	volume fraction of reinforcement
γ	unit weight
γ_w	unit weight of water
Γ	location of critical state line in compression plane
$\epsilon, \dot{\epsilon}$	strain, strain rate
ϵ_p	volumetric strain
ϵ_q	deviatoric strain
ϵ_r	radial strain
ϵ_{sh}	volume loss ratio due to shrinkage of grout
ϵ_z	vertical strain
ϵ_θ	circumferential strain
η	stress ratio $= q/p'$
η	grout compensation efficiency
κ	slope of unloading-reloading line in $v : \ln p'$ plane
λ	slope of virgin compression line in $v : \ln p'$ plane
λ_c	volume loss ratio due to consolidation
Λ	$(\lambda - \kappa)/\lambda$
μ	settlement reduction factor
μ	diameter ratio $= D/d_e$
ν	Poisson's ratio
ν'	Poisson's ratio in terms of effective stress
ρ	settlement
σ	total stress
σ'	effective stress
σ_r	radial stress
σ_z	vertical stress
σ_θ	circumferential stress
τ	shear stress
ϕ	friction angle
ψ	dilatancy angle

Introduzione

Il CPR Grouting, acronimo di *Consolidação Profunda Radial*, che in portoghese significa Consolidazione Profonda Radiale, viene utilizzato con successo in Brasile per ridurre i cedimenti dei rilevati costruiti su terreni (argillosi) molli, per accorciare i tempi di consolidazione, ma anche per aumentare la resistenza non drenata di terreni interessati da scavi senza opere di sostegno. A grandi linee, consiste nella disposizione di un sistema di dreni verticali e nell'esecuzione di una serie di iniezioni con malta cementizia secondo una griglia regolare. Utilizzando una miscela altamente viscosa, si riescono a creare dei corpi abbastanza uniformi, detti bulbi di compressione, che espandendosi migliorano la consistenza del terreno.

Nonostante la tecnica sia concettualmente molto semplice, il suo studio teorico e numerico si rivela estremamente complesso, in quanto presenta una serie di problematiche non di poco conto durante la modellazione geotecnica, le quali rendono difficile il consolidamento di un modello teorico. Le difficoltá iniziano giá a partire dalla modellazione del processo di iniezione utilizzando la teoria di espansione di cavità, giacché è necessario tenere in considerazione le varie direzioni di sollecitazione, l'esecuzione multipla e sequenzia delle iniezioni, assieme alla successiva consolidazione che viene promossa, radialmente, dai dreni. Inoltre, dopo la presa, la malta esibisce un comportamento meccanico molto differente dal geomateriale circostante, rappresentando un elemento estraneo che deve essere correttamente modellato.

Questa molteplicità di fattori suggerisce di analizzare il problema con metodi numerici, che paiono essere particolarmente adatti per prevedere il comportamento meccanico dei terreni dopo il trattamento. Eppure, essi non sono privi di difficoltà, essendo il problema accoppiato e in grandi deformazioni. Queste ultime possono provocare, utilizzando gli elementi finiti, distorsioni molto grandi nella mesh, portando alla non convergenza del problema o a instabilità numeriche. Inoltre, la modellazione costitutiva dovrebbe essere capace di riprodurre la perdita di struttura (rimaneggiamento) che eventualmente potrebbe avvenire a causa del processo di espansione di cavità. Il

grande numero di variabili coinvolte comporta, quindi, un grande numero di parametri nel modello. Alla complessità di calcolo si aggiunge, quindi, la difficoltà nel conferire un adeguato valore ai parametri del modello. Tutto ciò rende infattibile la progettazione del CPR Grouting a livello pratico, dato che nella si eseguono comunemente le investigazioni geotecniche di campo e laboratorio classiche, le quali non offrono parametri avanzati necessari per una corretta modellazione. È anche vero che, in generale, i professionisti richiedono modelli semplici, anche a costo dell'accuretezza dei risultati, pur di poter avere una risposta rapida alle questioni progettuali di carattere non solamente preliminare.

Il presente studio si prefigge lo scopo di fornire agli ingegneri progettisti un metodo pratico per stimare il guadagno che si ottiene sia in termini di resistenza, sia in termini di rigidezza, quando si usa il CPR Grouting. A tal uopo, si utilizza la teoria dell'espansione di cavità per intendere meglio il processo di formazione dei bulbi. Le soluzioni proposte nel capitolo 3 si riferiscono al caso di espansione profonda in argilla, in condizioni non drenate. Il problema dell'espansione di cavità sferica, in un mezzo omogeneo, isotropo, incompressibile e infinito, soggetto ad uno stato uniforme di sforzo (idrostatico), comincia adottando un modello costitutivo elastico perfettamente plastico, con criterio di rottura di Tresca. L'analisi viene quindi condotta in sforzi totali, impiegando la coesione non drenata e disinteressandosi delle pressioni neutre in eccesso. In maniera più approfondita, lo stesso problema è studiato considerando il modello Cam Clay Modificato, con il quale è possibile ricostruire l'andamento degli sforzi efficaci, le pressioni neutre in eccesso e i percorsi tensionali. Si identificano in questo caso tre zone attorno alla cavità: una più esterna, in cui il terreno si comporta ancora elasticamente, una intermedia, in cui la plasticizzazione è cominciata, e una interna, a contatto con la cavità, in cui lo stato critico è stato praticamente raggiunto.

Nel capitolo 4 è stata condotta un'ampia ricerca bibliografica sulle tecniche di *grouting* più utilizzate in argilla, tra cui si annoverano il compensation e il compaction grouting, con la quale si è potuto adattare, per mezzo di confronti, il concetto di cella unitaria al CPR Grouting, così come si è ottenuta una semplice equazione per la previsione dell'indice dei vuoti medio post trattamento, basata sul concetto di rapporto di sostituzione (*substitution ratio*). Per dedurla, al modello classico bifasico (vuoti, solidi) si è aggiunta un'altra fase, il geogrout. Tale diminuzione è stata relazionata al guadagno di resistenza non drenata secondo la teoria dello stato critico.

Successivamente, con l'obiettivo di ricostruire lo stato di sforzo indotto dal CPR

Grouting, ritenendosi opportuno utilizzare un approccio analitico, si è dedotta un'e-quazione il cui risultato consiste in un intervallo di possibili stati di sforzo. Le princi-pali ipotesi esemplificative rimangono l'aver assunto lo sforzo verticale poco variabile a seguito del trattamento e l'assialsimmetria. L'espressione offre, comunque, la pos-sibilità di stimare le tensioni aggiuntive (radiali e circonferenziali) che si instaurano dopo la dissipazione delle pressioni neutre in eccesso, avendo la possibilità di relazio-nare l'aumento degli sforzi efficaci con il guadagno di rigidezza, attraverso espressioni adatte.

Nei capitolo successivo, lo studio verte sul comportamento della massa di terreno sottoposto al trattamento. Il problema del flusso é stato ricondotto ad un'analisi uni-dimensionale, attraverso semplici espressioni di trasformazione, che tengono in conto la presenza del sistema di drenaggio. La formulazione include il dreno sacrificato in corrispondenza del punto di iniezione, non considerando, però, l'effetto della resisten-za idraulica di drenaggio. Quest'ultima necessita ancora di ulteriori approfondimenti, dato che é una conseguenza diretta dello strangolamento e della perdita di verticalità dei dreni a cui si incorre durante l'espansione di cavità.

Con l'uso di modelli di omogeneizzazione del modulo elastico, nello stesso capi-tolo ci si occupa di dare un'espressione valida per stimare la rigidezza dell'insieme terra–bulbi. In tale approccio, si ammette che i bulbi rappresentino l'inclusione ri-gida dispersa all'interno del terreno, trattato come matrice. Ammettendo che i due materiali coesistano nel formare un continuo isotropo e omogeneo alla macroscala, delle semplici espressioni basate su un volume elementare rappresentativo cubico. Dedotta quindi la compressibilità alla macroscala, viene calcolato un coefficiente di consolidazione fittizio attraverso la sua definizione.

Nel penultimo capitolo, si è affrontato un caso reale, consistito nell'esecuzione di due rilevati di forma quadrata e di altezza di due metri. Uno poggiava su un terreno avente unicamente un sistema di drenaggio. L'altro, invece, era stato alloggiato su un terreno precedemente trattato con CPR Grouting. I cedimenti sono stati monitorati per all'incirca 150 giorni. Ne è risultato che il rilevato costruito sul terreno migliorato ha mostrato un cedimento inferiore. I tempi di consolidazione sono comunque rimasti simili nei due casi. Sulla base di queste osservazioni, il modello di calcolo semplificato è stato calibrato mediante analisi agli elementi finiti.

Nel capitolo finale si è delineato un confronto con la tecnica DJM-PVD combinata (Dry Jet Mixing con dreni verticali prefabbricati), per certi versi simile, per altri

molto differente dal CPR Grouting. Entrambe lavorano con un sistema di drenaggio artificiale, tuttavia, il CPR Grouting non promuove la formazione di rinforzi colunnari, dato che il contatto e l'allineamento tra i bulbi non può essere garantito.

In conclusione, l'approccio progettuale consiste in un metodo semplificato, ma comunque basato su considerazioni di carattere teorico, che rende possibile prevedere il comportamento meccanico dei terreni migliorati con il CPR Gouting, utilizzando quelli che sono i parametri comunemente adottati nella pratica geotecnica.

Introduction

In this thesis a theoretical study of the CPR$^{®}$ technique will be carried out in order to establish a practical method for design purposes. Although the technique is conceptually very simple, its theoretical and numerical study proves to be extremely complex because it involves a number of problems in geotechnical modelling that complicate the establishment of a theoretical model. The difficulties begin in modeling the generation process of the bubls through the cavity expansion theory, since it is necessary to take into account the loading in multiple directions, the multiple and sequential injections, along with the subsequent radial consolidation due to the presence of drains.

Due to the complexity of the problem, the numerical analysis seem to be the most appropriate tools for predicting the behavior of the soil after the treatment. However, they are not exempt of complications because of the problem being coupled and in large deformations. For example, the deformation may generate greatly distorted elements in the mesh, leading to non-convergence or numerical instability. In addition, the constitutive model used should have the capability of representing the loss of structure (remoulding) of the clay that occurs after the expansion process. The large number of variables requires a large number of parameters in the numerical model. This is unfeasible for design purposes, since in geotechical practice are only performed the field investigations and classic laboratory tests, which provide at most the parameters of compressibility and resistance.

The scope of this work is therefore to provide engineers with a practical method to estimate the gain in undrained strength and stiffness in soils treated with CPR Grouting. To this aim, the theory of the cavity to expansion is used to better understand the process of forming the grout blubls. A large literature review on the compensation and compaction grouting techniques in clays is conducted in order to establish a theoretical model due to their similarity with the present technique. Finally, the treated soil is considered a composite medium, whose rigidity is estimated

using some models of homogenization based on the elasticity theory. The final result is a simply approach to the problem, but theoretically founded, which makes possible to predict the mechanical behavior of soils subjected to CPR Grouting employing the parameters conventionally used in geotechnical practice.

Part I

Introduction to grouting techniques

1 Soft ground improvement

1.1 Methods of improving soft soils

In this section, the general principles of the methods of improving the engineering properties of soft clay are briefly reviewed, with the purpose of carrying out a comparison with the CPR Grouting in the next chapters. The engineer needs to consider whether the soil properties can be economically improved, for this reason, he has to analyse the optimal use and limitations of each method. This section deals with the several methods available for the improvement of the engineering properties of soft clays, especially those popular in Brazil. The methods are:

1. Vertical drains in conjunction with preloading embankment or vacuum.
2. Columnar inclusions, among which Stone columns, Jet grouting and Soil Mixing.
3. Electro-osmosis, Heat and Chemical treatment.

1.1.1 Drains, preloading and vacuum

In case of low permeability soils, to achieved the desired settlement may take too long. The use of vertical drains accelerates the rate of primary consolidation, since the drainage path is shortened from the thickness of the soil layer to the radius of the drain influence zone. When drains are coupled with a temporary load, the time for settlement stabilization is even shortened. Generally, a surcharge consists of a soil embankment and is placed with standard earthmoving equipment (trucks, dozers, etc). Often the site surface is soft and wet, requiring low ground pressure equipment. As shown in Figure 1.1, the solid curve indicates the consolidation process under the design load in case overloading is not utilised, while the dotted line represents the settlement occurring when using a temporary surcharge. It is evident that embankment with preloading has its consolidation time reduced and its post-construction settlement stabilized. Least, the process improves the soil by compressing it, increas-

ing its stiffness and shear strength. Consolidation time with a vacuum applied is substantially reduced too and lateral displacement curtailed, and if sufficient vacuum pressure is sustained, the thickness of the surcharge fill required may be reduced by several metres (Indraratna et al., 2010).

Various types of vertical drains have been used to accelerate the rate of primary consolidation, both natural and made artificially. A geotextile or geosynthetic works usually as jacket material, preventing clogging. The core can be sand or a plastic profile.

Soft clays usually have a low bearing capacity, consequently, there may be a need of reinforcing the ground surface, for example by means of geotextile, in order to enable the machinery for drain installation to enter the site without danger. The drainage layer should be at least 0.3-0.5 m in thickness. The material in the drainage blanket shall have good drainage properties, in order to avoid a delay in the consolidation process (Hansbo, 1994).

Vertical drains are often used in conjunction with this method. The advantages of the vacuum method are (G. Pilot apud Brand and Brenner (1981)):

1. there are no problems of embankment stability to consider,

2. it eliminates the need for backfill material which is usually expensive and often unavailable, and

3. the installation and removal of the means of applying the preload are readily accomplished.

1.1.2 Columnar inclusions

Various methods use columnar elements to reinforce the soil. The most popular methods are listed below:

1. the so-called stone columns and sand compaction piles. Among the installation methods utilised, the cased borehole method, the Japanese vibro-composer method and vibro-replacement method are the most common ones (Hansbo, 1994),

2. geosynthetic encased stone columns, when the soft soil does not provide enough lateral support,

3. prefabricated (driven) or cast in place displacement piles (jacked in or screwed piles), with pile caps and geosynthetic layers often included for the embankment
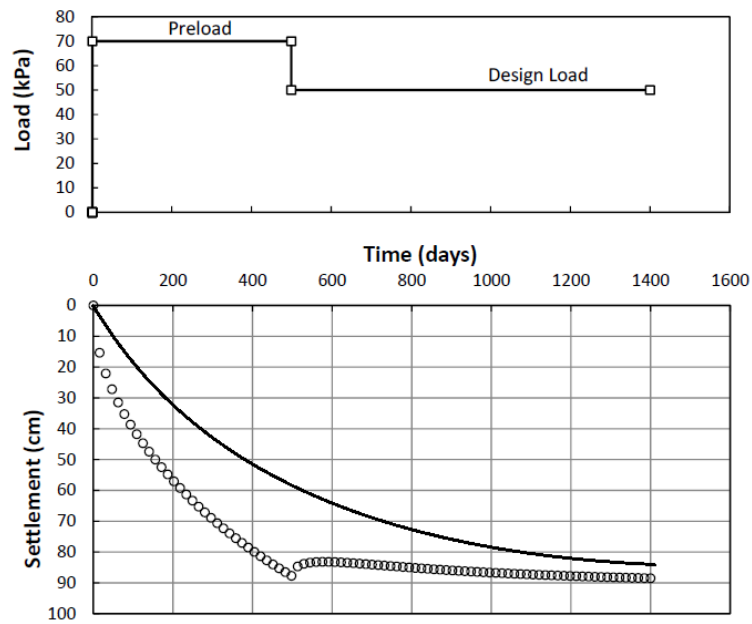
Figure 1.1: Settlement curves comparison in case of preloading (dotted line) and in case of overloading is not utilised (solid line).

reinforcement,

4. Jet grouting, soil mixing (wet or dry) etc.

All the aforementioned methods result in fact in the formation of columnar inclusions in soil which are made of stiffer and stronger material. The columns are also regularly spaced and their diameter is small, compared to the foundation size. This allows to considered the treated soil as a homogeneous but anisotropic continuum. Consequently, a unified mathematical approach for settlement computation can be used.

Design principles

Most of the design methods is based on the concept of unit cell, in which the soil surrounding the column is approximated by an equivalent circular area. The area replacement factor is defined as the ratio of the column area over the whole area of the equivalent cylindrical unit, expressed as:

$$a_c = \frac{A_c}{A_c + A_s} \tag{1.1}$$

where A_c and A_s are the cross sectional areas of the column and surrounding soil, respectively. Obviously, $A = A_c + A_s$. Because of equilibrium, at any time the soil and the columns carry the applied load, hence:

$$\int_{A_s} \sigma_s \, dA + \int_{A_c} \sigma_c \, dA = \int_A \sigma dA \qquad (1.2)$$

In terms of average stresses, the above equation can be rewritten as:

$$\sigma = \sigma_c a_c + \sigma_s (1 - a_c) \qquad (1.3)$$

where σ_c and σ_s are the average total stresses within the column and the surrounding soil. Introducing the stress concentration factor, defined as:

$$n = \frac{\sigma_c}{\sigma_s} \qquad (1.4)$$

Hence, the average stresses can be expressed as follows (see for example Almeida and Marques (2010)):

$$\sigma_s = \frac{1}{1 + (n-1)a_c} \, \sigma \qquad (1.5)$$

$$\sigma_c = \frac{n}{1 + (n-1)a_c} \, \sigma \qquad (1.6)$$

Finally, the last important parameter used for designing a stone column system is the settlement reduction ratio, which is defined as the ratio of the settlement without reinforcement over the settlement of the treated soil:

$$\mu = \frac{\Delta h_{untreated}}{\Delta h_{treated}} = 1 + (n-1)a_c \qquad (1.7)$$

The above equation suggests that in order to estimate the settlement of the column reinforced soil under embankment load, it is necessary to determine the stress concentration factor. The calculation of stress concentration factor depends primarily on the assumptions made about the column behavior. At the present time, a number of different consolidation theories for composite foundations exist (Balaam and Booker, 1981; Priebe, 1995; Lorenzo and Bergado, 2003; Zhang et al., 2006; Castro and Sagaseta, 2009; Ye et al., 2012). These theories have made a great contribution

to the design and assessment of column-reinforced soils.

1.1.3 Electrochemical stabilization

By means of experimentation, it was established that an electric current flowing through a moist soil caused the pore water to flow from the positive pole (anode) to the negative pole (cathode); at the same time, electrolysis occurred, with the anions and cations of the dissolved salts moving towards the anode and cathode respectively. This process is known as electro-osmosis. The part of the electro-mosis process by which the pore water moves under the influence of an electric potential is known as electro-drainage, and its effect on fine-grained soil is to decrease the water content and, hence, to bring about consolidation and increased undrained shear strength. This technique is most commonly employed where the desired soil improvement is "local" in nature, e.g. to improve the stability of cuts and trenches, and to increase the bearing capacity of piles (used as anode in the process). A local increase in water content is also sometimes intentionally brought about to decrease the resistance to the extraction of temporary sheet piles; in such cases, the piles are used as cathode in the electro-osmosis. Electro-osmosis may also be employed as a means of carrying out chemical injection in a soil which is of too low a permeability for injection by conventional means to be feasible. This aspect of electro-osmosis, by which the ions migrate under the electric potential, is termed electro-injection or electrochemical treatment. The anode either dissolves or is fed with the appropriate ion solution to bring about a chemical change in the soil (and a strength increase) without alteration of the soil volume or structure. This provides a means for the in-situ strengthening of the soil beneath existing structures built on the ground surface which must not be disturbed.

1.2 CPR Grouting

The CPR Grouting (portuguese acronym for "Consolidação Profunda Radial", meaning deep radial consolidation) is a brazilian method for the improvement of the engineering properties of soft clays. It is a patented invention of the Engegraut Company, which is headquartered in Rio de Janeiro, Brazil. It has been used with success in mitigating and accelerating the settlement of embankments on soft soils and in improving the undrained shear strength for unsupported excavations purposes. Actually, it is an evolution of compaction grouting applied to clayey soils.

The CPR Grouting Grouting is a specific technique for modifying clay soft soils, as well as the Compaction Grouting is only appropriate to reinforce sandy soils and Jet Grouting is concrete columns maker. Improving soft clays with CPR Grouting starts with the formation of artificial drainage system, followed by the grouting phase, during which cavities are expanded by injecting a grout mix, inducing soil consolidation and increasing its resistance. The excess of pore pressure created during this stage is dissipated by means of the drainage system and, simultaneously, a high confining horinzontal pressure is established, promoting the subsequent soil hardening. The gain of stiffness is a characteristic of the final soil composite.

1.2.1 Execution procedure

In this section, the construction stages are briefly presented in order to understand the stress history under which the treated clay is submitted. In general, the CPR Grouting is applied in extremely soft to soft clays, however, there are some cases in which the method was applied in loose sands or silts, with or without the use of geodrains.

When a site is totally virgin (i.e. there is no pre-existing anthropic construction or building), it is necessary to "conquest" the area disposing a geotextiles covered by a drainage layer, called *pioneer layer*. After the construction of the pioneer layer, that permits the transit of heavy machinery, a grid of prefabricated vertical drains is installed throughout the depth of the saturated soft soil. Typically, two patterns are used: the square and the triangular one. The grout injection points are then placed on a grid spaced twice (typically spaced at 3–4 m) the spacing of the PVDs system (1.5–2 m).

The technique generally utilizes a single pass system (ie. drill down, grout up) in which the first stage grouting commences from the bottom of the pre-drilled hole and continues until a predetermined grout pressure is achieved (from 500 to 1000 kPa) or when a predetermined amount of grout is injected (800–1000 litres). Upon achieving one of these criteria, the grout pipe is raised to the next stage by a constant step, typically 1 meter. The grouting process continues in discrete stages till the top of the improvement zone is reached. The grout used in these injections is mortar, a sand–silt–cement mixture in proportions of around 80:15:5 respectively. Figure 1.2 resume briefly the features of the method.
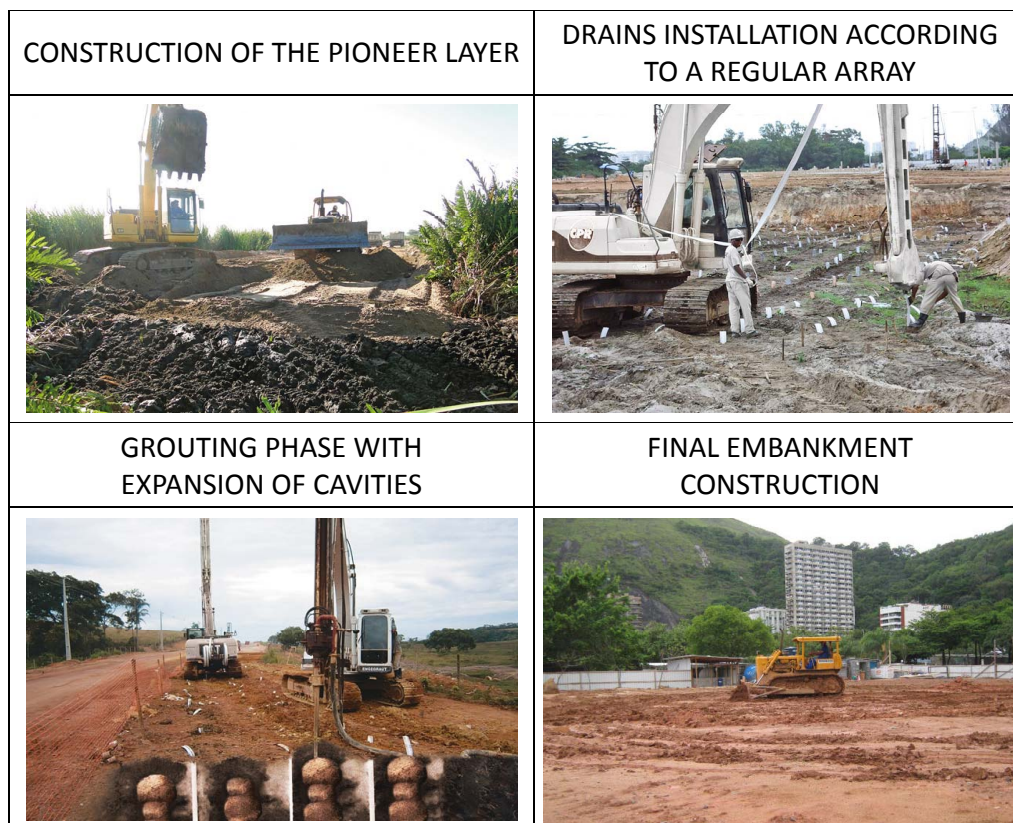
Figure 1.2: Construction stages of CPR Grouting.

1.2.2 Quality controls

For the CPR Grouting the quality control consists in a set of field and laboratory tests, including field monitoring that is always performed during embankment construction works and after, for months, until settlements stabilization is reached. The tests regard both soil and grout, but in an individual form. Although, they are intended to check either the stiffness or the strength of the treated soil, all geotechnical field tests are not capable to measure the parameters of the ensamble. Indeed, all have the defect of testing an area of limited extent, which is not representative at all. As a matter fact, depending on the position, a test will give results concerning the grout or the soil, in mutually exclusive form.

The slump test is used to ensure uniformity for different batches of grout mix under field condition. It is used to determine the workability (or pumpability) of the grout mix. The slump generally ranges from 8 to 12 cm. In some cases, several samples are

collected and cured for 28 days to carry out compression tests. Data obtained in 2014 during the Leduca Construction are presented in Figure 1.3, where it also reported a statistical analysis of the data set referring the compressive strength of the grout. The tests were carried out according to brazilian standars NBR 5739/2007. The statistical analysis of test results showed a mean value of the comrpessive strength of 3.72 MPa, which is less than that reported by de Mello (2013), who obtained an average strength 5.6 MPa. The same author also determined the grout unit weight, $\gamma = 17.8$ kN/m^3, and the secant Young modulus, $E_g = 6.6$ MPa, corresponding to a stress in the stress-strain curve equal to 1/3 the compressive strength.

Pressuremeter tests are ordinarily executed for assessing the effectiveness of the treatement. Riccio et al. (2013) pointed out the analogy that exists between the ground treatment and Ménard pressuremeter tests. Indeed, in both cases a radial stress is applied into the gound. For this reason, according to them the test should be particularly suitable. The deformation analyses made by pressuremeter test must confirm that the undrained strength increased after application of the technique. In general, after a certain time, the improved clay deposit exhibites much higher values of pressuremeter modulus and undrained shear strength than those encountered before the treatment. If the pressuremeter shows no evident improvement, the CPR Grouting is performed again.

Compressive strength of grout

age at testing: 28 days

Descriptive statistics (Resume)	
Mean	3,718
Standard Error	0,202
Median	3,60
Mode	3,40
Standard Deviation	1,179
Sample Variance	1,389
Kurtosis	-0,50425
Skewness	-0,07368
Range	4,7
Minimum	1,2
Maximum	5,9
Sum	126,4
Count	34
Values are in MPa	

SLUMP TEST

Average daily value
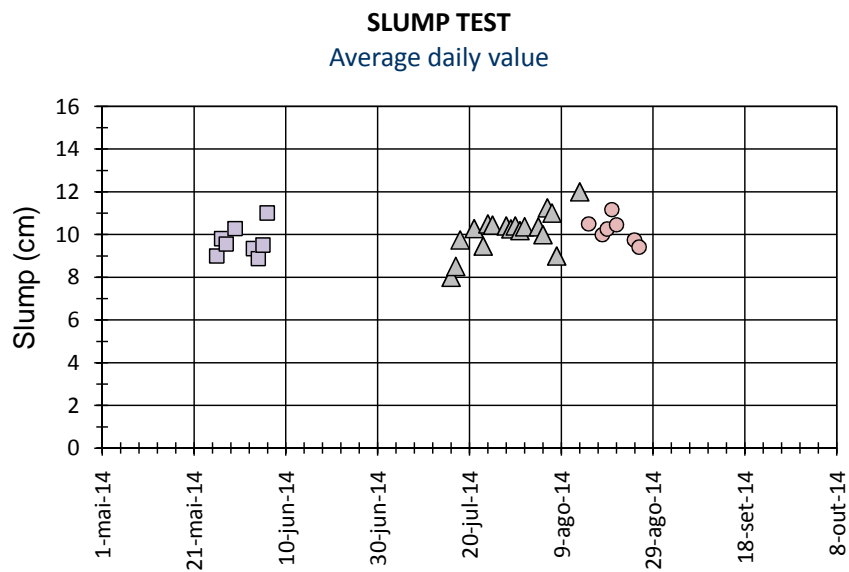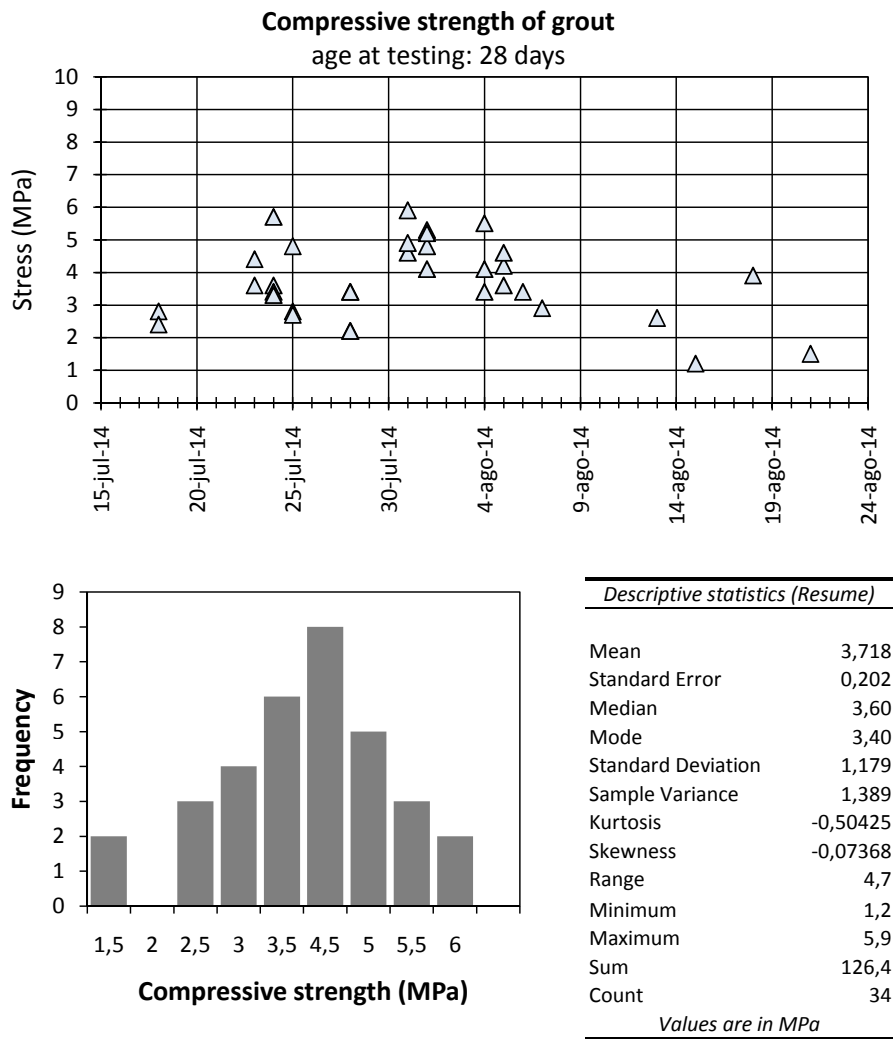
Figure 1.3: Compressive strength and slump of grout mix used in CPR Grouting.

2 General aspects of grouting loose soils

2.1 Grouting mode and shape of the grout body

In this section a literature review is presented, in order to study the factors affecting the grout body shape and grouting mode. For clarity, the following list resumes the most important parameters controlling the grouting process:

1. Soil characteristics:
   - stiffness and undrained strength;
   - permeability;
   - stress field (overburden pressure and K_0 condition);
2. Grouting characteristics:
   - viscosity of the grout;
   - injection pressure and rate;
   - nozzle diameter;

2.1.1 Grouting mode

Chen et al. (2014) reproduced numerically three different types of grouting, i.e. permeation grouting, compaction grouting and fracture grouting, by adjusting the elastic modulus and the coefficient of permeability of the soil. A qualitative overview of their results is summarized in Table 2.1.

Permeation grouting occurs when the permeability of the soil to the grout is as high as 10^{-5} cm/s, no matter what is the value of the soil modulus. For intermediate values of permeability and higher values of the soil modulus, fracture grouting generally occurs. Before any fracture develops, compaction grouting also occurs, however, as fractures open, several thin an long grout vein are generated.

Table 2.1: Different forms of grouting depending on material properties. Qualitative classification.

Soil stiffness	Soil permeability		
	Low	Medium	High
Soft	Compaction grouting	Compaction grouting	Permeation grouting
Medium	Fracture grouting	Compaction grouting	Permeation grouting
Hard	Fracture grouting	Fracture grouting	Permeation grouting

Au et al. (2003) are credited of having emphasized the importance of the viscosity of the grout mortar on the grouting mode. They presented a conceptual modelling of compensation grouting in clays that is reported in Figure 2.1. According to them, when a grout with high viscosity is used, the grout would not able to penetrate into fractures and the grout ball simply continues to expand. On the other hand, low viscosity grout will intrude into planes of weakness developing grout-filled fractures. This conceptual modelling is also supported by laboratory tests injections with different w/c (water/cement) ratio grouts. Indeed, as the w/c ratio increases, the viscosity of the grout decreases. Figure 2.2 shows sectioned samples with different OCRs and w/c ratio grouts. A thick localized spherical ball was encountered in the OCR=1 sample with $w/c = 0.6$. On the other hand, for the same grout, in the OCR=5 sample a horizontal fracture was formed. Finally, the low-visosity grout in OCR=1 sample promoted the formation and the propagation of a fracture.

2.1.2 Shape of the grout body

The grout bulb final shape is influenced by several factors. Researchers have conducted experiments in order to examine the factors affecting the grout bulb development. The main results will be discussed in this section.

As instance, Nichols and Goodings (2000) performed a series of small-scale model compaction grouting centrifuge tests to examine the effects of grout composition and injection rate on grout take and grout bulb development. They showed that the bulbs are not spherical, but they tend to develop in one of two shapes, either cylindrical
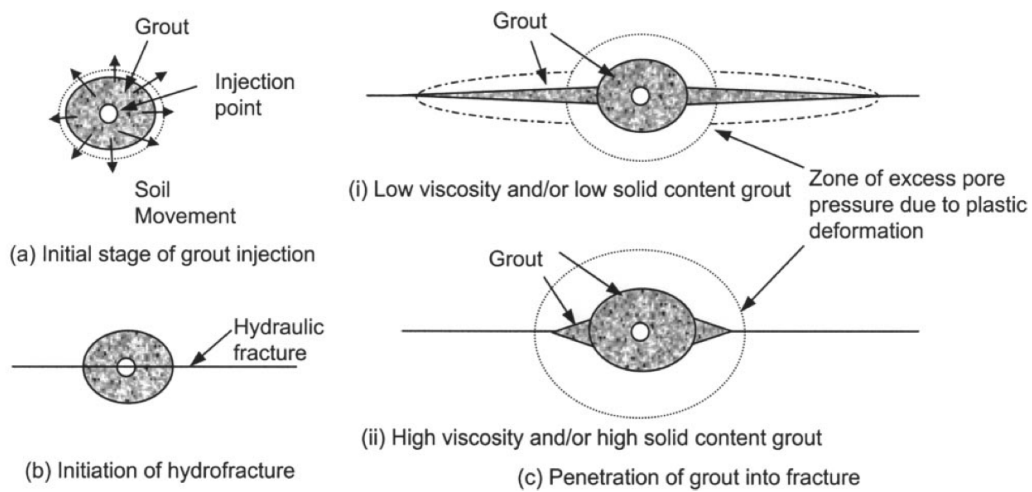
Figure 2.1: Influence of the grout viscosity on grouting mode (Au et al., 2003).
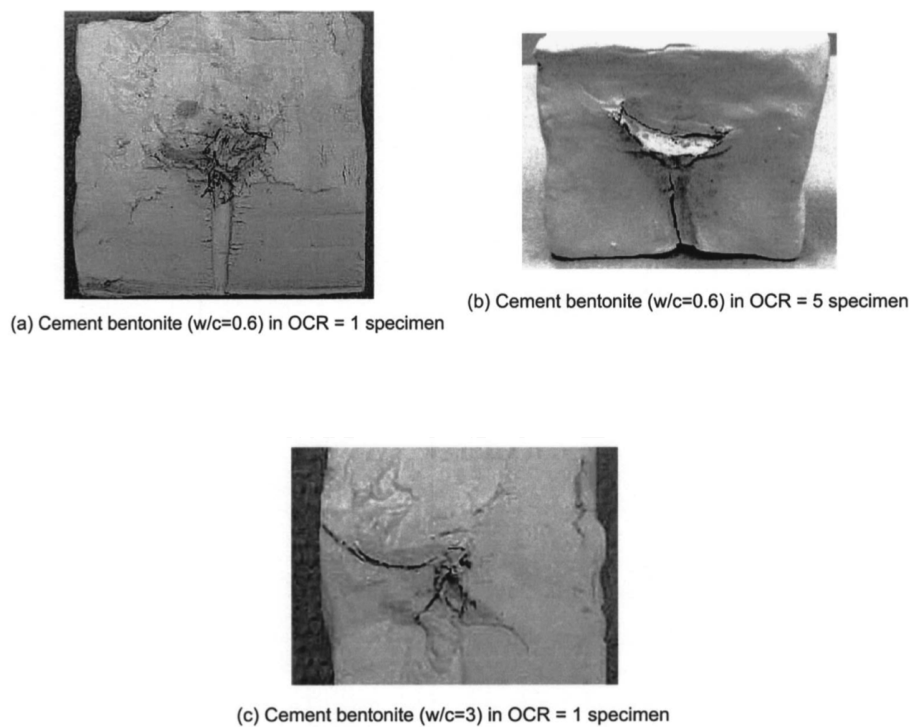
Figure 2.2: Visual examination of sectioned samples after injections, from Au et al. (2003).

or teardrop. To distinguish the grout geometries, they introduce a shape factor, $S_\psi = L/B$ defined as the ratio of the overall length of the bulb, L to its diameter, B, identifying as cylindrical bulbs those with shape factor greater than $S_\psi > 1.5$. According to them, at greater overburden pressures teardrop shaped grout bulbs are developed more easily. For this reason, they identified a transition depth between teardrop (deeper) and cylindrical (shallower) shaped grout bulbs. It was observed that this depth increases with the clay content of the grout. In fact, grout with 10% clay ran up the side of the grout tube at much lower depths and injection pressures.

Chew and Bharati (2016) designed a grouting apparatus to allow the experiment to be conducted for different values of the withdrawal rate, injection pressure, nozzle diameter, undrained shear strength of the clay and grout viscosity. They investigated the low pressure jet grouting in clays, using injection pressure lower than 3.0 MPa, being the laboratory apparatus designed for a maximum grouting pressure of 3.0 MPa. They experimentally deduced that the average radius of the grout column could be predicted by the following expression:

$$\frac{R_{\mathrm{avg}}}{d_n} = \frac{a_1}{N^{0.5}} \frac{P_i}{s_u} + a_2 \tag{2.1}$$

where d_n is the nozzle diameter, P_i is the injection pressure, s_u is the undrained shear strength of the clay, N is the viscosity ratio (kinematic viscosity of grout slurry/kinematic velocity of water ratio) and A and B are coefficient for different combinations of withdrawal rate and rotational speed.

Concluding, for fracture grouting, Au et al. (2003) observed horizontal fractures in normally consolidated samples and vertical fractures in overconsolidated samples. Indeed, cracks are generally oriented in the direction of the major principal stress.

2.2 Collapse nearby the ground surface

The compaction grout bulb is modelled here as an expanding spherical cavity in an isotropic elastic-plastic continuum, yielding with Tresca's criterion. In an ideal situation, at the start of injection, the radius of the bulb, or cavity, is the drilling radius a_0 and the soil has an isotropic effective stress p_0. When a uniformly distributed internal pressure at the grout-soil interface, or cavity wall, is increased to p_{lim}, the grout bulb radius expands in all the directions to a, and a spherical zone of radius r_p

around the grout bulb will pass into the state of plastic equilibrium. The theoretical solution for cavity expansion may be written in the following form:

$$p_{lim} = p_0 + \frac{4}{3}s_u \left\{ 1 + \ln \frac{G}{s_u} + \ln \left[1 - \left(\frac{a_0}{a} \right)^3 \right] \right\} \qquad (2.2)$$

that is the Gibson and Anderson (1961) solution where s_u is the undrained strength of the soil, G its shear modulus and a_0/a is the cavity ratio – see for example Yu (2000).

According to El-Kelesh et al. (2001), in the case of shallow injections, the grouting process follows a cavity expansion model until a failure mechanism develops under the influence of the free surface. It is reasonable to assume that, at failure, the upward force exerted by grout bulb pressure equals the total downward force resulting from the weight of the collapsed soil above the bulb plus the downward shearing resistance along the lateral surface. Considering these assumptions, a relationship between the grout bulb radius a and the pressure at the grout-soil interface p_{up}, which satisfies the ground surface upheave, could be obtained. Based on similar assumptions for cohesionless soils, Wong (1974), *apud* El-Kelesh et al. (2001), proposed a model governing the upward force exerted by the grouted mass at the condition of conical failure above the grout bulb. El-Kelesh et al. (2001) take into account the effect of the overlying structure by increasing the initial ground stress at the specified injection depth. In their case, the depth considered in the model is an equivalent depth, assuming free ground surface, which results in the same ground stress as that in the case of the overlying structure at the actual injection depth.

In our case, a relationship will be obtained for the case of a pure cohesive soil. It is assumed that the failure mechanism is a cylinder with a radius equal to that of the cavity. The shearing resistance along the lateral surface is given by the undrained strength of the soil. A distributed load on the surface will represent, eventually, structures and embankments. Referring to Figure 2.3, let us consider the expansion of a cavity of a radius a at a depth, z, and a surface load q. As introduced before, the failure mechanism will be a cylinder, whose volume can be expressed as:

$$V = \pi a^2 z - \frac{2}{3}\pi a^3 \qquad (2.3)$$
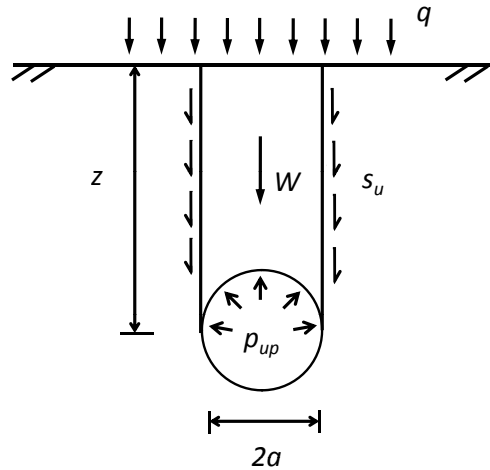
Figure 2.3: Cylindrical failure above expanding cavity in cohesive soil.

The lateral surface along which the undrained resistance is mobilized is:

$$A_L = 2\pi a z \tag{2.4}$$

Finally, we impose the vertical equilibrium to obtain the limit pressure:

$$(p_{up} - q)\,\pi a^2 - \gamma V - s_u A_L = 0 \tag{2.5}$$

Therefore, the limit pressure for injections at shallow depths is:

$$p_{up} = \gamma(z - \frac{2}{3}a) + s_u \frac{2z}{a} + q \tag{2.6}$$

This pressure value is defined as the upheaval pressure p_{up} which is the onset pressure of ground surface uplift.

The model given by Eq. 2.2 is assumed to represent the mechanics and soil response during injection, while that given by Eq. 2.6 represents the at failure condition. In modelling the compaction grouting technique, it is assumed that the injection process continues until reaching a limiting condition, but in most cases, ground surface uplift is the limiting condition. Figure 2.4 shows the representation of these two equations constituting the proposed model. As introduced before, the grouting process starts with the expansion of a cavity. For the case shown in Figure 2.4, the inner pressure
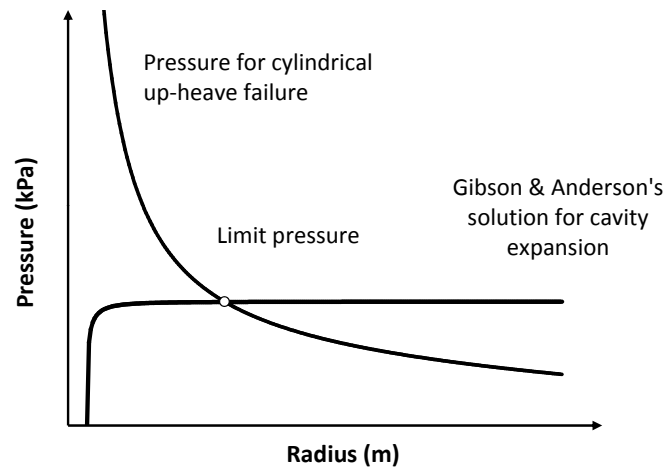
Figure 2.4: Curves representing the two mechanisms (cavity expansion and cylindrical upheave) that occur during the grouting process.

reaches rapidly a constant value, typically when the radius of the cavity becomes twice the initial one, i.e. $a = 2a_0$. As the radius of the cavity increases, the second mechanism is activated. The intersection point, identified as "limit pressure", determines the maximum bulb radius that can be expanded without surface collapse.

Part II

Cavity Expansion Solutions

3 Cavity Expansion Solutions

In this chapter the analytical solutions are well suited to the present case.

3.1 Systems of coordinates

We give here, for reference, the corresponding formulae which express the components of the strain tensor in terms of derivatives of the components of the displacement vector in the same coordinates, and the equilibrium equations which are useful to formulate the cavity expansion problem. Suggested references are Fung and Tong (2001) and Landau and Lifshitz (1970). All equations can be found in other texts on the same topic.

3.1.1 Spherical Coordinates

Let the components of the displacement vector be written as $\mathbf{u} = (u_r, u_\varphi, u_\theta)$. Thus, referring to the notation adopted in Figure 3.1, the components of the strain tensor in spherical coordinates are:

$$
\begin{aligned}
\epsilon_r &= \frac{\partial u_r}{\partial r} & \gamma_{\varphi\theta} &= \frac{1}{r\sin\varphi}\frac{\partial u_\varphi}{\partial\theta} + \frac{1}{r}\frac{\partial u_\theta}{\partial\varphi} - \frac{u_\theta}{r}\cot\varphi \\
\epsilon_\theta &= \frac{1}{r\sin\varphi}\frac{\partial u_\theta}{\partial\theta} + \frac{u_r}{r} + \frac{u_\varphi}{r}\cot\varphi & \gamma_{r\varphi} &= \frac{1}{r}\frac{\partial u_r}{\partial\varphi} + \frac{\partial u_\varphi}{\partial r} - \frac{u_\varphi}{r} \\
\epsilon_\varphi &= \frac{1}{r}\frac{\partial u_\varphi}{\partial\varphi} + \frac{u_r}{r} & \gamma_{\theta r} &= \frac{1}{r\sin\varphi}\frac{\partial u_r}{\partial\theta} + \frac{\partial u_\theta}{\partial r} - \frac{u_\theta}{r}
\end{aligned}
\tag{3.1}
$$

The equations of equilibrium now become, with F_r, F_φ, F_θ denoting the physical
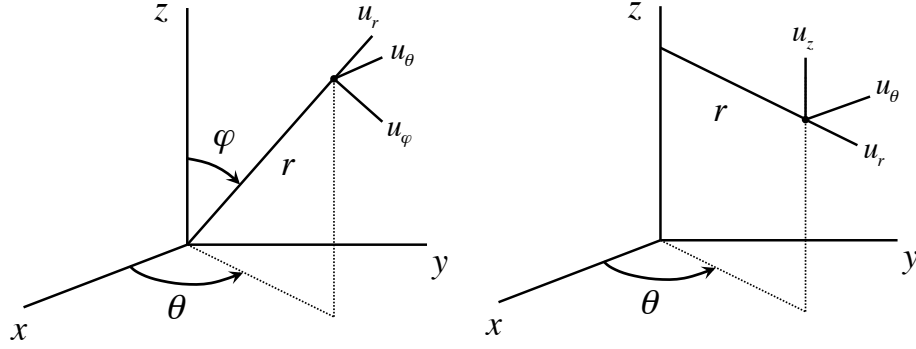
Figure 3.1: Spherical (r, φ, θ) and cylindrical (r, θ, z) coordinate systems and components of a displacement vector for each case.

components of the body force vector:

$$\frac{1}{r^2} \frac{\partial}{\partial r}(r^2 \sigma_r) + \frac{1}{r \sin \varphi} \frac{\partial}{\partial \varphi}(\tau_{r\varphi} \sin \varphi) + \frac{1}{r \sin \varphi} \frac{\partial \tau_{r\theta}}{\partial \theta} - \frac{1}{r}(\sigma_\theta + \sigma_\varphi) + F_r = 0$$

$$\frac{1}{r^3} \frac{\partial}{\partial r}(\tau_{r\varphi} r^3) + \frac{1}{r \sin \varphi} \frac{\partial}{\partial \varphi}(\sigma_\varphi \sin \varphi) + \frac{1}{r \sin \varphi} \frac{\partial \tau_{\theta\varphi}}{\partial \theta} - \frac{\sigma_\theta}{r} \cot \varphi + F_\varphi = 0 \qquad (3.2)$$

$$\frac{1}{r^3} \frac{\partial}{\partial r}(\tau_{\theta r} r^3) + \frac{1}{r \sin^2 \varphi} \frac{\partial}{\partial \varphi}(\sigma_{\theta\varphi} \sin^2 \varphi) + \frac{1}{r \sin \varphi} \frac{\partial \sigma_\theta}{\partial \theta} + F_\theta = 0$$

3.1.2 Cylindrical Polar Coordinates

The components of the displacement vector are $\mathbf{u} = (u_r, u_\theta, u_z)$. Referring to the notation adopted in Figure 3.1, in cylindrical coordinates the components of the strain tensor are:

$$\begin{aligned}
\epsilon_r &= \frac{\partial u_r}{\partial r} & \gamma_{r\theta} &= \frac{1}{r} \frac{\partial u_r}{\partial \theta} + \frac{\partial u_\theta}{\partial r} - \frac{u_\theta}{r} \\
\epsilon_\theta &= \frac{1}{r} \frac{\partial u_\theta}{\partial \theta} + \frac{u_r}{r} & \gamma_{rz} &= \frac{\partial u_r}{\partial z} + \frac{\partial u_z}{\partial r} \\
\epsilon_z &= \frac{\partial u_z}{\partial r} & \gamma_{\theta z} &= \frac{1}{r} \frac{\partial u_z}{\partial \theta} + \frac{\partial u_\theta}{\partial z}
\end{aligned} \qquad (3.3)$$

Let F_r, F_θ, F_z denote the physical components of the body force vector, hence the
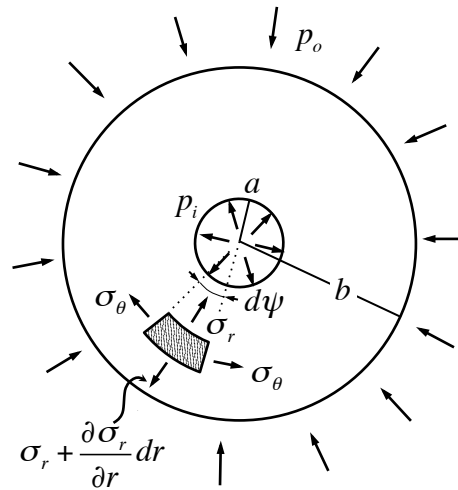
Figure 3.2: Spherical container submitted to the action of internal and external uniform pressures. Adapted from Timoshenko and Goodier (1951).

equilibrium:

$$
\frac{\partial \sigma_r}{\partial r} + \frac{1}{r}\frac{\partial \tau_{r\theta}}{\partial \theta} + \frac{\partial \tau_{rz}}{\partial z} + \frac{\sigma_r - \sigma_\theta}{r} + F_r = 0
$$

$$
\frac{\partial \tau_{r\theta}}{\partial r} + \frac{1}{r}\frac{\partial \sigma_\theta}{\partial \theta} + \frac{\partial \tau_{\theta z}}{\partial z} + \frac{2\tau_{r\theta}}{r} + F_\theta = 0 \tag{3.4}
$$

$$
\frac{\partial \tau_{rz}}{\partial r} + \frac{1}{r}\frac{\partial \tau_{\theta z}}{\partial \theta} + \frac{\partial \sigma_z}{\partial z} + \frac{\tau_{rz}}{r} + F_z = 0
$$

3.2 Expansion of a spherical cavity in elastic-perfectly plastic medium

We shall analyse the expansion of a spherical cavity in an incompressible isotropic elastic-perfectly plastic medium of infinite extent subjected to an uniform pressure. Because of the spherical symmetry the shears $\gamma_{\varphi\theta}, \gamma_{r\varphi}, \gamma_{\theta r}$ and the tangential stresses $\tau_{\varphi\theta}, \tau_{r\varphi}, \tau_{\theta r}$ are zero and $\epsilon_\theta = \epsilon_\varphi$, $\sigma_\theta = \sigma_\varphi$. As shown in Figure 3.2, let a and b denote the inner and outer radii of a spherical thick-walled shell, and p_i and p_o the internal and external uniform pressures. As the internal pressure become greater than p_o the internal sphere expands. At initial stage, the shell will deform elastically. In Timoshenko and Goodier (1951) [pag. 359, Eqs. 197, 198] can be found the elastic

solution for the stress components in spherical polar coordinates:

$$\sigma_r = \frac{p_o\, b^3(r^3 - a^3)}{r^3(a^3 - b^3)} + \frac{p_i\, a^3(b^3 - r^3)}{r^3(a^3 - b^3)}$$

$$\sigma_\theta = \frac{p_o\, b^3(2r^3 + a^3)}{2r^3(a^3 - b^3)} - \frac{p_i\, a^3(2r^3 + b^3)}{2r^3(a^3 - b^3)}$$

Where the stresses are taken to be positive in traction. We have to express the above relationships taking the stresses positive in compression, as usually done in soil mechanics. Moreover, in the extreme case when the outer radius is taken indefinitely large (i.e. $b \to \infty$) we have to do with the formation of a spherical cavity in an infinite solid medium, then:

$$\sigma_r = p_o + (p_i - p_o)\frac{a^3}{r^3}$$
$$\sigma_\theta = p_o - (p_i - p_o)\frac{a^3}{2r^3}$$

(3.5)

According to Hill (1950), with increasing the internal pressure a plastic region spreads into the medium. Because the internal pressure is greater than the external, the yielding will begin on the inner surface. For reason of symmetry the plastic boundary in a homogeneous material must be a spherical surface; its radius will be denoted with r_p. It is easy to verify from Equations 3.5 that the relation:

$$\sigma_r + 2\sigma_\theta = 3p_o$$

(3.6)

holds everywhere in the elastic region, while in the plastic region the yield criterion is assumed to be:

$$\sigma_r - \sigma_\theta = 2s_u$$

(3.7)

Bringing together Equation 3.6 and 3.7, on the plastic boundary the radial stress will be $\sigma_r = p_\mathrm{p}$, which is equal to:

$$p_\mathrm{p} = p_o + \frac{4}{3}s_u$$

We assume the internal pressure sufficiently large to generate a plastic region, that is true if the internal pressure is greater than p_p. Consequently, on the elastic region

the stress distribution is therefore:

$$\left.\begin{aligned} \sigma_r &= p_o + (p_{\mathrm{p}} - p_o)\frac{r_{\mathrm{p}}^3}{r^3} \\ \sigma_\theta &= p_o - (p_{\mathrm{p}} - p_o)\frac{r_{\mathrm{p}}^3}{2r^3} \end{aligned}\right\} \quad (r \geq r_{\mathrm{p}}) \tag{3.8}$$

From the condition of equilibrium of an element cut out from the medium by the two concentric spheres of radii r and $r + dr$ and by a circular cone with a small angle $d\psi$ (Figure 3.2) we find:

$$\sigma_\theta \frac{\pi r}{2}\, dr\,(d\psi)^2 = \frac{d\sigma_r}{dr}\frac{\pi r^2}{4}\, dr\,(d\psi)^2 + \sigma_r \frac{\pi r}{2}\, dr\,(d\psi)^2$$

from which we have the equilibrium equation (Timoshenko and Goodier, 1951):

$$\frac{\partial \sigma_r}{\partial r} + 2\,\frac{\sigma_r - \sigma_\theta}{r} = 0 \tag{3.9}$$

Combining the equilibrium equation (Equation 3.9) with the yielding criterion (Equation 3.7) immediately follows:

$$\sigma_r = -4s_u \ln r + B$$

where B is a integration constant.

Since σ_r must be continuous across the inner sphere and across the plastic boundary, we will find the two remaining unknown r_{p} and B by considerations of equilibrium. On the inner surface we impose $\sigma_r(R = a) = p_i$, hence $B = p_i + 4\,s_u \ln a$. We express the stresses in the plastic region taking into account the yield criterion (Equation 3.7):

$$\left.\begin{aligned} \sigma_r &= p_i - 4s_u \ln(r/a) \\ \sigma_\theta &= p_i - 2s_u[1 + 2\ln(r/a)] \end{aligned}\right\} \quad (a \leq r < r_{\mathrm{p}}) \tag{3.10}$$

Now we may express the plastic radius r_{p} by imposing the equilibrium across the plastic boundary, i.e. $\sigma_r(r = r_{\mathrm{p}}) = p_{\mathrm{p}}$, then:

$$r_{\mathrm{p}} = a \, \exp\left(\frac{p_i - p_{\mathrm{p}}}{4s_u}\right) \tag{3.11}$$

If the displacement of the inner surface are quite small, the approximation $a \simeq a_0$

will be valid,[1] and the stress distribution completely determined. But if the internal displacement is large, then the pressure-expansion relation will require a complete solution as pointed out by Hill (1950), who proposed the following expression for the case in exam:

$$\frac{r_{\mathrm{p}}}{a} = \left(\frac{E}{3s_u}\right)^{\frac{1}{3}} = \left(\frac{G}{s_u}\right)^{\frac{1}{3}} \tag{3.12}$$

the equation suggests that is impossible to expand a cavity in a medium from zero radius to a without generating a plastic region around it and moreover it indicates that the ratio r_{p}/a remains constant and depends on the *Rigidity Index* $I_r = G/s_u$. Furthermore, it is obvious that

$$a = \sqrt[3]{\frac{3V_i}{4\pi}}$$

represents the radius of the cavity related to its volume V_i. Another important consequence derives from equating Equation 3.11 and 3.12:

$$p_i = p_{\mathrm{p}} + \frac{4s_u}{3} \ln\left(\frac{G}{s_u}\right) \tag{3.13}$$

in other words, the internal pressure p_i is constant during the expansion. The stress distribution in the elastic-plastic state is shown in Figure 3.3.

3.2.1 Kinematics of cavity expansion

Recalling that the analysis considers a homogeneous, isotropic and incompressible soil initially subjected to an isotropic state of stress, we can express the strain rates as a function of the volume rate increment of the cavity:[2]

$$\begin{aligned}
\dot{\epsilon}_r &= \frac{\dot{V}_i}{2\pi r^3} \\
\dot{\epsilon}_\theta &= -\frac{\dot{V}_i}{4\pi r^3}
\end{aligned} \tag{3.14}$$

---

[1]In which a_0 is the initial inner radius of the cavity.

[2]Let us consider an inner spherical surface and an external spherical surface of radius r. If the cavity expands, it will displace the surrounding soil, which will move with a velocity $\dot{u}_r$. And if we neglect volume deformation, then we may write:

$$\int_0^t \int_S \dot{u}_r \, dS \, dt = \int_0^t \dot{V}_i \, dt$$

The equation must hold for every t and because of symmetry $\dot{u}_r$ must be constant on the whole control surface. Thus, the velocity field is $\dot{u}_r = \dot{V}_i/S$, where $S = 4\pi r^2$.
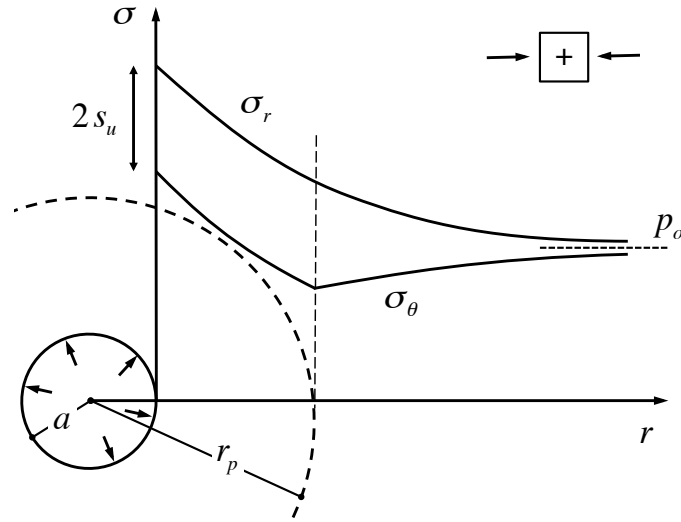
Figure 3.3: Stresses around a spherical cavity expanded from zero radius in a homogeneous, isotropic and incompressible elastic perfectly plastic medium subjected to an uniform pressure and yielding with Tresca's criterion.

where $\dot{V}_i = 4\pi a^2 \dot{a}$ is the volume rate increment of the cavity and $\dot{a}$ the rate increment of its radius. The equation states that the soil deformations are fully determined without the need to know the shearing behaviour of the soil. As a consequence, the problem is totally strain-controlled and, for any given constitutive relation, *exact* stress and pore pressure fields can be simply computed and equilibrium directly satisfied. The approach is known as Strain Path Method (Baligh, 1985). The strain rates in Equation 3.14 are:

$$\dot{\epsilon}_r = -\frac{\partial \dot{u}_r}{\partial r}, \quad \dot{\epsilon}_\theta = -\frac{\dot{u}_r}{r} \tag{3.15}$$

where

$$\dot{u}_r = \frac{a^2}{r^2}\dot{a} \tag{3.16}$$

represents the displacement rate. From them we can derive an useful compatibility equation:

$$\frac{\dot{\epsilon}_r - \dot{\epsilon}_\theta}{r} = \frac{\partial \dot{\epsilon}_\theta}{\partial r} \tag{3.17}$$

The constitutive relations for elastic and plastic response are the last equations we need. To take into account the soil incompressibility we put $\nu = 0.5$ in the following

elastic constitutive relations written in incremental form:

$$\begin{aligned}
\dot{\epsilon}_r^{\text{e}} &= \frac{1}{E}\left(\dot{\sigma}_r - \dot{\sigma}_\theta\right)\\
\dot{\epsilon}_\theta^{\text{e}} &= \frac{1}{2E}\left(\dot{\sigma}_\theta - \dot{\sigma}_r\right)
\end{aligned} \tag{3.18}$$

where $\dot{\epsilon}_r^{\text{e}} = \dot{\epsilon}_r - \dot{\epsilon}_r^{\text{p}}$ and $\dot{\epsilon}_\theta^{\text{e}} = \dot{\epsilon}_\theta - \dot{\epsilon}_\theta^{\text{p}}$. Recalling that the incremental form of the yield criterion is $\dot{\sigma}_\theta = \dot{\sigma}_r$, the above equations indicate no elastic strains developing in the plastic region during plastic expansion. At this point, to close the solution it is necessary to choose a plastic flow rule. We assume no volumetric plastic strains:

$$\dot{\epsilon}_r^{\text{p}} + 2\dot{\epsilon}_\theta^{\text{p}} = 0 \tag{3.19}$$

Finally, combining Equations 3.14, 3.17 and 3.19 we obtain the plastic strain rates:

$$\begin{aligned}
\dot{\epsilon}_r^{\text{p}} &= \frac{2r}{3}\frac{\partial \dot{\epsilon}_\theta}{\partial r} = \frac{\dot{V}_i}{2\pi r^3}\\
\dot{\epsilon}_\theta^{\text{p}} &= -\frac{r}{3}\frac{\partial \dot{\epsilon}_\theta}{\partial r} = -\frac{\dot{V}_i}{4\pi r^3}
\end{aligned} \tag{3.20}$$

In conclusion, we shall analyse the radius of the plastic region around the cavity by determining its radius r_{p}. When a cavity is expanded at constant volume rate, the volume of the cavity will be $V_i = \dot{V}_i t$ at any time. Thus, using Equations 3.7, 3.14 and 3.18, the circumferential strain at which the yielding occurs is:

$$-\epsilon_{ty} = \frac{s_u}{E} = \frac{V_i}{4\pi r_{\text{p}}^3} = \frac{a^3}{3r_{\text{p}}^3}$$

which is equivalent to:

$$\frac{r_{\text{p}}}{a} = \left(\frac{E}{3s_u}\right)^{\frac{1}{3}}$$

The equation coincides with Hill's solution (Equation 3.12) and it confirms again that the ratio r_{p}/a depends only on the strain at which the yielding begins.

3.3 Cavity Expansion in Modified Cam Clay

In the present section, the solution for the undrained cavity expansion in Modified Cam Clay is used to predict the limit pressure, the radius of the plastic region, the

stresses and the pore water pressure field induced by the grouting injection. The problem is formulated in small strain in the elastic zone and large strain in the plastic zone. The analysis is based on recent critical state solutions that have been proposed by Collins and Yu (1996), Yu (2000), Cao et al. (2001) and Silvestri and Abou-Samra (2011).

3.3.1 Preliminary considerations

The expansion problem needs to identify which definition of strain is used in the analysis. Under the undrained condition the soil is considered incompressible. Hence, the conservation of volume condition gives the following relation between r, the current radius of a material element, which was initially at r_0, and the current and initial rardii of the cavity, a and a_0, respectively (Hill, 1950):

$$r^3 - r_0^3 = a^3 - a_0^3 \tag{3.21}$$

The strain rates have been presented in the previous section, they are:

$$\dot{\epsilon}_r \quad = \frac{\partial \dot{u}_r}{\partial r} = \frac{2a^2}{r^3}\dot{a} \tag{3.22}$$

$$\dot{\epsilon}_\theta \quad = \frac{\dot{u}_r}{r} = -\frac{a^2}{r^3}\dot{a} \tag{3.23}$$

Using Equation 3.21 the radial strain rate can be written as:

$$\dot{\epsilon}_r = \frac{2a^2}{r_0^3 + a^3 - a_0^3}\dot{a} \tag{3.24}$$

Since r_0 is fixed for a given particle, the strain rate can be integrated to obtain its finite form:

$$\epsilon_r = \frac{2}{3}\ln\left(\frac{r_0^3 + a^3 - a_0^3}{r_0^3}\right) \tag{3.25}$$

associated with the particle originally located al r_0. This relation can be now be rewritten in terms of the current coordinate r:

$$\epsilon_r = -\frac{2}{3}\ln\left(1 - \frac{a^3 - a_0^3}{r^3}\right) \tag{3.26}$$

At the cavity wall the strain is:

$$\epsilon_r(r = a) = 2\ln\left(\frac{a}{a_0}\right) \tag{3.27}$$

which is infinite when the initial radius of the cavity is zero. Finally, it should be noted that the incompressibility condition written in terms of Cauchy infinitesimal strain is:

$$(1 + \epsilon_r^*)(1 + \epsilon_\theta^*)^2 = 0 \tag{3.28}$$

when strain are small, we have the usual approximate form $\epsilon_r^* + 2\epsilon_\theta^* = 0$. Since by definition $\epsilon_r = \ln(1 + \epsilon_r^*)$ and $\epsilon_\theta = \ln(1 + \epsilon_\theta^*)$, however, in natural or logarithmic strain the incompressibility condition reduces to the exact relation:

$$\epsilon_r + 2\epsilon_\theta = 0 \tag{3.29}$$

Stress and strain invariants

We use the conventional terminology used in critical state soil mechanics (Wood, 1990):

$$p = \frac{1}{3}(\sigma_1 + \sigma_2 + \sigma_3) \tag{3.30}$$

$$p' = \frac{1}{3}(\sigma_1' + \sigma_2' + \sigma_3') = p - u \tag{3.31}$$

$$q = \frac{1}{\sqrt{2}}[(\sigma_1' - \sigma_2')^2 + (\sigma_2' - \sigma_3')^2 + (\sigma_3' - \sigma_1')^2]^{1/2} \tag{3.32}$$

$$d\epsilon_p = d\epsilon_1 + d\epsilon_2 + d\epsilon_3 \tag{3.33}$$

$$d\epsilon_q = \frac{\sqrt{2}}{3}[(d\epsilon_1 - d\epsilon_2)^2 + (d\epsilon_2 - d\epsilon_3)^2 + (d\epsilon_3 - d\epsilon_1)^2]^{1/2} \tag{3.34}$$

The excess of pore pressure Δu may be expressed as:

$$\Delta u = u - u_0 = (p - p_0) - (p' - p_0') \tag{3.35}$$

The total strain increments are the sum of elastic and plastic components:

$$d\epsilon_p = d\epsilon_p^{\mathrm{e}} + d\epsilon_p^{\mathrm{p}} \tag{3.36}$$

$$d\epsilon_q = d\epsilon_q^{\mathrm{e}} + d\epsilon_q^{\mathrm{p}} \tag{3.37}$$

For the expansion of a spherical cavity the following equivalences hold:

$$\sigma_r = \sigma_1, \; \sigma_\theta = \sigma_\varphi = \sigma_2 = \sigma_3 \tag{3.38}$$

$$\epsilon_r = \epsilon_1, \; \epsilon_\theta = \epsilon_\varphi = \epsilon_2 = \epsilon_3 \tag{3.39}$$

Hence the stress strain invariants become:

$$p = \frac{1}{3}(\sigma_r + 2\sigma_\theta) \tag{3.40}$$

$$p' = \frac{1}{3}(\sigma_r' + 2\sigma_\theta') \tag{3.41}$$

$$q = \sigma_r - \sigma_\theta = \sigma_r' - \sigma_\theta' \tag{3.42}$$

$$d\epsilon_p = d\epsilon_r + 2d\epsilon_\theta = 0 \tag{3.43}$$

$$d\epsilon_q = \frac{2}{3}(d\epsilon_r - d\epsilon_\theta) \tag{3.44}$$

Due the incompressibility condition $d\epsilon_p = 0$ follows that:

$$d\epsilon_r = -2d\epsilon_\theta \tag{3.45}$$

$$d\epsilon_q = d\epsilon_r = -2d\epsilon_\theta \tag{3.46}$$

Elastic analysis

The stress field in the elastic zone is still represented by the Equations 3.8. In the undrained condition there is no volume change, i.e. $dv = 0$, thus:

$$d\epsilon_p = -\kappa \frac{dp'}{vp'} = 0$$

which indicates that the mean effective stress is constant, since κ is non-zero. But also the mean total stress is constant because $\sigma_r + 2\sigma_\theta = 3p_0$. Hence, as pointed out by Cao et al. (2001) no excess of pore pressure would be generated in the elastic zone. Another consequence is that the elastic bulk modulus K_0' also remains constant at its initial value:

$$K_0' = \frac{vp_0'}{\kappa} \tag{3.47}$$

The initial value of the shear modulus can be deduced from the bulk modulus and a assumed Poisson's ratio (Wood, 1990):

$$G_0' = K_0' \frac{3(1 - 2\nu')}{2(1 + \nu')} = \frac{3}{2} \frac{v p_0'(1 - 2\nu')}{\kappa(1 + \nu')} \tag{3.48}$$

which leads to a shear modulus dependent on the mean effective stress assuming a constant Poisson's ration, this assumption may result in an unconservative model (Zytynski et al., 1978). In the present context both variable and constant shear modulus cases will be considered. However, in the elastic zone, since there is no variation in mean effective stress, the initial shear modulus remains constant in any case.

Plastic analysis

For the MMC model the yield criterion is represented by the equation (Wood, 1990):

$$q - Mp' \left(\frac{p_y'}{p'} - 1 \right)^{1/2} = 0 \tag{3.49}$$

Hence, recalling that the mean effective stress in the elastic region is constant, the deviator stress at the elastic-plastic boundary is:

$$q_p = Mp_0' \sqrt{R - 1} \tag{3.50}$$

where R is the initial isotropic overconsolidation ratio, defined as p_{yo}'/p_0', which is different from the conventional overconsolidation ratio OCR defined in terms of the effective vertical stress. Then, at the plastic boundary the total stresses σ_r and σ_θ are (Cao et al., 2001):

$$\begin{cases} \sigma_r = p_0 + \dfrac{2}{3} q_p \\ \sigma_\theta = p_0 - \dfrac{1}{3} q_p \end{cases} \tag{3.51}$$

The effective stress path followed in the undrained cavity expansion is the same of the undrained triaxial test. Indeed, we can be derived it by considering the incompressibility condition (the overall increment in volume is zero, i.e. $d\epsilon_p = 0$), which

implies that $d\epsilon_p^e = -d\epsilon_p^p$:

$$\kappa \frac{dp'}{vp'} = -(\lambda - \kappa)\frac{dp'_y}{vp'_y} \tag{3.52}$$

and combining it with the yield criterion (Eq. 3.49) gives the effective stress path (ESP):

$$q = Mp' \left[R \left(\frac{p'}{p'_0} \right)^{-1/\Lambda} - 1 \right]^{1/2} \tag{3.53}$$

where $\Lambda = (\lambda - \kappa)/\lambda$ is the plastic volumetric strain ratio. According to Wood (1990) it can be estimated as $(C_c - C_s)/C_c$, where C_c and C_s are respectively the compression and the swelling index. The rupture will occur when soil reaches the critical state, i.e. $q = Mp'$, in which the effective stress invariants remains constant and have the values (Cao et al., 2001):

$$p'_u = p'_0 (R/2)^\Lambda \tag{3.54}$$

$$q_u = Mp'_0 (R/2)^\Lambda \tag{3.55}$$

The deviator stress at the critical state can be related to the undrained strenght $2s_u = q_u$. If the soil is heavily overconsolidated it will exhibit a softening behaviour. More precisely, the deviator stress will increase to a maximum value q_m and then decrease to the ultimate value q_u. According to Cao et al. (2001) we distinguish the following cases:

1. If $R \geq 2\Lambda/(2\Lambda - 1)$

$$q_m = \frac{Mp'_0}{\sqrt{2\Lambda - 1}} \left(\frac{2\Lambda - 1}{2\Lambda} R \right)^\Lambda \tag{3.56}$$

2. If $2 \leq R \leq 2\Lambda/(2\Lambda - 1)$

$$q_m = q_p \tag{3.57}$$

3. If $R < 2$ no softening will be observed and the maximum value is equal to the ultimate deviator stress, i.e. $q_m = q_u$.

Strains

The relationship between effective stresses and radial distance from the cavity centre can be established from the expression for the deviatoric strain. The total deviatoric strain includes the recoverable elastic component ϵ_q^e and the plastic irrecoverable

component ϵ_q^{p}. Recalling the plastic flow rule for MCC model Wood (1990):

$$\frac{d\epsilon_p^{\mathrm{p}}}{d\epsilon_q^{\mathrm{p}}} = \frac{M^2 - (q/p')^2}{2(q/p')} \tag{3.58}$$

it gives the plastic deviatoric strain increment (Silvestri and Abou-Samra, 2011):

$$d\epsilon_q^{\mathrm{p}} = -\frac{\kappa}{v}\frac{dp'}{p'}\frac{2(q/p')}{M^2 - (q/p')^2} \tag{3.59}$$

Combining Equation 3.59 with Equation 3.53 gives:

$$d\epsilon_q^{\mathrm{p}} = -\frac{2\kappa}{vM}\frac{\left[R\left(\frac{p'}{p_0'}\right)^{-1/\Lambda} - 1\right]^{1/2}}{2 - R\left(\frac{p'}{p_0'}\right)^{-1/\Lambda}}\frac{dp'}{p'} \tag{3.60}$$

The integration of this equation is facilitated with introducing an auxiliary variable $y = R(p'/p_0')^{-1/\Lambda}$, then $dp'/p' = -\Lambda\,dy/y$. The integration of right-hand side of Equation 3.60 is then in the form:

$$\int_R^y \frac{\sqrt{y-1}}{2y-y^2}\,dy = \frac{1}{2}\ln\left[\frac{1+\sqrt{y-1}}{1-\sqrt{y-1}}\cdot\frac{1-\sqrt{R-1}}{1+\sqrt{R-1}}\right] - \tan^{-1}\sqrt{y-1} + \tan^{-1}\sqrt{R-1}$$

This allows the determination of the deviatoric plastic strain:

$$\epsilon_q^{\mathrm{p}} = \frac{2\kappa\Lambda}{vM}\left\{\frac{1}{2}\ln\left[\frac{1+\sqrt{y-1}}{1-\sqrt{y-1}}\cdot\frac{1-\sqrt{R-1}}{1+\sqrt{R-1}}\right] - \tan^{-1}\sqrt{y-1} + \tan^{-1}\sqrt{R-1}\right\} \tag{3.61}$$

where, for clarity, the auxiliary variable is:

$$y = R\left(\frac{p'}{p_0'}\right)^{-1/\Lambda} \tag{3.62}$$

The same expression was obtained by Cao et al. (2001). The deviatoric elastic strain considering a constant shear modulus is simply:

$$\epsilon_q^{\mathrm{e}} = \frac{q}{3G_0'} \tag{3.63}$$

where G_0' is as expressed in Equation 3.48. The increment in deviatoric elastic strain

considering a variable shear modulus can be expressed as found in Silvestri and Abou-Samra (2011):

$$d\epsilon_q^e = \frac{dq}{3G'} = \frac{2\kappa(1+\nu')}{9v(1-2\nu')}\frac{dq}{p'} \tag{3.64}$$

An expression for dq is provided by differentiating Equation 3.53:

$$dq = M\left\{\left[R\left(\frac{p'}{p_0'}\right)^{-1/\Lambda} - 1\right]^{1/2} - \frac{R}{2\Lambda}\left(\frac{p'}{p_0'}\right)^{-1/\Lambda}\left[R\left(\frac{p'}{p_0'}\right)^{-1/\Lambda} - 1\right]^{-1/2}\right\}dp' \tag{3.65}$$

Again, into Equation 3.64 we introduce the auxiliary variable $y = R(p'/p_0')^{-1/\Lambda}$ and the integration of right-hand side is in the form:

$$\int_R^y -\Lambda\frac{\sqrt{y-1}}{y} + \frac{1}{2\sqrt{y-1}}dy = (1-2\Lambda)(\sqrt{y-1} - \sqrt{R-1}) + \dots$$
$$+ 2\Lambda(\tan^{-1}\sqrt{y-1} - \tan^{-1}\sqrt{R-1}) \tag{3.66}$$

Finally, the elastic deviatoric strain for a variable shear modulus is:

$$\epsilon_q^e = \frac{2\kappa(1+\nu')M}{9v(1-2\nu')}\left\{(1-2\Lambda)(\sqrt{y-1} - \sqrt{R-1}) + 2\Lambda(\tan^{-1}\sqrt{y-1} - \tan^{-1}\sqrt{R-1})\right\} \tag{3.67}$$

3.3.2 Closure of the problem

From Equation 3.26 the radial natural strain is obtained since the current radius a of the cavity is known. And due the incompressibility condition it follows that $\epsilon_q = \epsilon_r = -2\epsilon_\theta$. Thus, the solution of the problem is in the following implicit form:

$$\frac{2}{3}\ln\left(1 - \frac{a^3 - a_0^3}{r^3}\right) = -(\epsilon_q^e + \epsilon_q^p) \tag{3.68}$$

from which we can deduce the relationship between the effective mean stress p' and the radial distance from the center of the cavity for the plastic region. As illustrated before, ϵ_q^p can be expressed with Equation 3.61, while ϵ_q^e can be expressed with Equation 3.63 for a constant shear modulus or with Equation 3.67 for a variable shear modulus. The deviator stress q can be then calculated from Equation 3.53. The position of the plastic boundary can be related to the current cavity radius with the

following relationship:

$$\ln\left(1 - \frac{a^3 - a_0^3}{r_p^3}\right) = -\frac{q_p}{2G_0'} \tag{3.69}$$

where q_p is defined in Equation 3.50. Under the hypothesis of small strains we may use the following approximation:

$$\frac{r_p^3}{a^3 - a_0^3} = \frac{2G_0'}{q_p} \tag{3.70}$$

If the cavity is expanded from zero radius, or if the cavity continues to expand indefinitely (i.e. $a \gg a_0$), then:

$$\frac{r_p}{a} = \left(\frac{2G_0'}{q_p}\right)^{1/3} \tag{3.71}$$

Finally, the total mean stress p and, consequently, the pore water pressure excess can be evaluated by integrating the equilibrium equation in spherical symmetry. Indeed, using the definition of the stress invariants we can express $\sigma_r - \sigma_\theta = q$ and $\sigma_r = p + 2/3q$, thus the equilibrium equation can be rewritten in the following form:

$$\frac{\partial p}{\partial r} + \frac{2}{3}\frac{\partial q}{\partial r} + 2\frac{q}{r} = 0 \tag{3.72}$$

that is solvable, for example, with the finite difference method. Finally, the pore water pressure excess is obtained from Equation 3.35.

3.3.3 Results

In this section some selected results for the stress paths and the effective stress and pore pressure distributions will be presented for the undrained expansion of a spherical cavity. The parameters of the modified Cam Clay model used for the example analyses are listed in Table 3.1. It is assumed a constant shear modulus. Three different values of $R = 1.001$, 2.005 and 8 are considered to investigate the impact of OCR on the stress paths and distributions surrounding the cavity. The analysis are carried out considering an initial isotropic stress state in which the initial mean effective stress is the same for all cases and is equal to $p_0' = 40$ kPa. The value $R = 1.001$ is chosen to avoid an infinite plastic radius, indeed, according to Equation 3.71 when $R = 1$ the plastic zone coincides with with the entire infinite medium. The value $R = 2.005$ is chosen because the mean effective stress has been selected as the independent variable.

The difference between effective (ESP) and total (TSP) stress paths gives the excess pore pressure Δu because the initial pore pressure is set to zero. Figures 3.5, 3.7 and 3.9 show that for a given initial effective mean stress p'_0 the limit mean total stress increases with the OCR, but the ratio p_u/s_u decreases as shown in Table 3.2.

Figures 3.6, 3.8 and 3.10 show the variations of the normalised radial and tangential effective stresses, σ'_r/s_u and σ'_θ/s_u, and the normalized excess pore pressure, $\Delta u/s_u$, with the normalised abscissa r/a (where a is the current cavity radius) for the cases $R = 1.001$, 2.005 and 8. The results show that generally three zones – the external elastic zone, the intermediate plastic zone, and the internal critical state failure zone – may coexist around the cavity as shown in Figure 3.4. No excess pore pressure is generated in the elastic zone, as a consequence, it develops only within the plastic boundary. When $R = 2$ the behaviour is elastic-perfectly plastic and the critical state region coincides with the plastic one, i.e. $r_c = r_p$. It is found that within the critical state region the effective stresses are practically constant. The extension of the critical state region can be estimated by setting the auxiliary variable y, as in Equation 3.62, equal to 1.995. Another way may be graphically by means of the inspection of the effective stress distribution, identifying the critical state region in the portion of the curve where the effective stresses are constant.

It is seen that the soil with lower value of R develops higher limiting normalized excess pore pressure. However, for heavily overconsolidated soil, negative excess pore pressure could be generated away from the cavity. On the basis of this finding Cao et al. (2001) assert the possiblity of using the excess pore pressure to estimate the in-situ overconsolidation ratio. Furthermore, as shown in Figure 3.10, for heavily overconsolidated soils the effective tangential stress could reach a negative value, leading to possible tension cracks.

Approximate analysis

In order to obtain a simple closed form for describing the total stresses during a cavity expansion, Cao et al. (2001) assumed the deviator stress constant in both plastic and critical zones and equal to the ultimate deviator stress, $q_u = 2s_u$. In this manner, they obtained the approximate expression for the ultimate cavity pressure in a form equal to the elastic-perfeclty plastic case (Eq. 3.13 – Gibson and Anderson's solution) as follows:

$$\sigma_u = p_0 + \frac{2}{3}Mp'_0(R/2)^\Lambda \left(1 + \ln \frac{2G'_0}{Mp'_0(R/2)^\Lambda}\right) \tag{3.73}$$
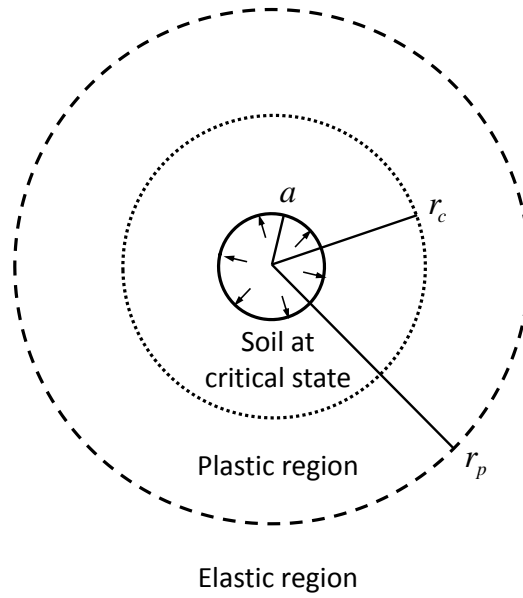
Figure 3.4: Undrained spherical cavity expansion in critical state model soil. Three region are now distinguishable.

where it is important to recal that $Mp'_0(R/2)^\Lambda = 2s_u$ and $\sigma_u = p_u + 2/3q_u$. Thus, corresponding to the ultimate total stress, the ultimate pore pressure excess at the cavity wall Δu_a is:

$$\Delta u_a = p'_0(R/2)^\Lambda \left(\frac{2}{3}M \ln \frac{G'_0}{s_u} - 1 \right) + p'_0 \tag{3.74}$$

For a normally consolidated soil, i.e. for $R = 1.001$., the approximation gives a ultimate cavity pressure $\sigma_u = 121.2$ kPa, a value very close to $\sigma_u = 116.74$ kPa calculated with the exact solution. However, for overconsolidated soils the approximation is even better. Indeed, for $R = 2.005$ the difference becomes very little, being $\sigma_u = 169.81$ kPa the value obtained from Equation 3.73 and $\sigma_u = 169.49$ kPa the exact value. Similarly, for $R = 8$ the approximate cavity limit pressure is $\sigma_u = 339.97$ kPa and the exact value is $\sigma_u = 340.05$ kPa.
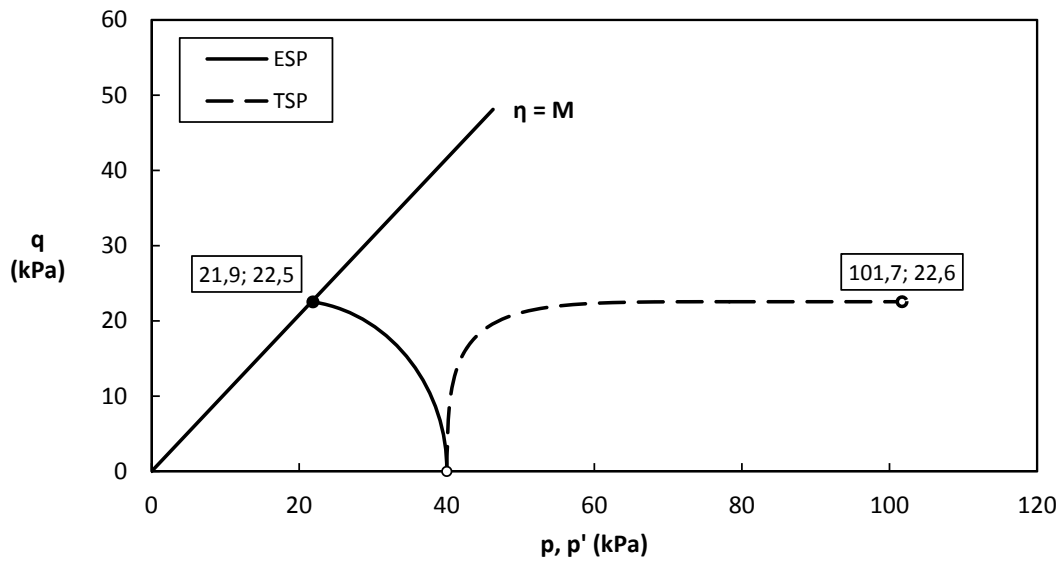
Figure 3.5: Stress paths at cavity wall for normally consolidated soil, $R = 1.001$.
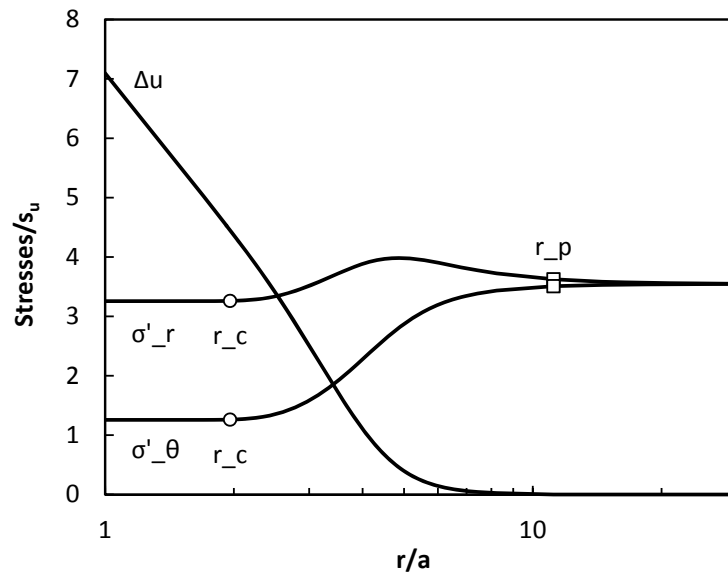
Figure 3.6: Effective radial, tangential and excess pore pressure distributions around the cavity for normally consolidated soil, $R = 1.001$.
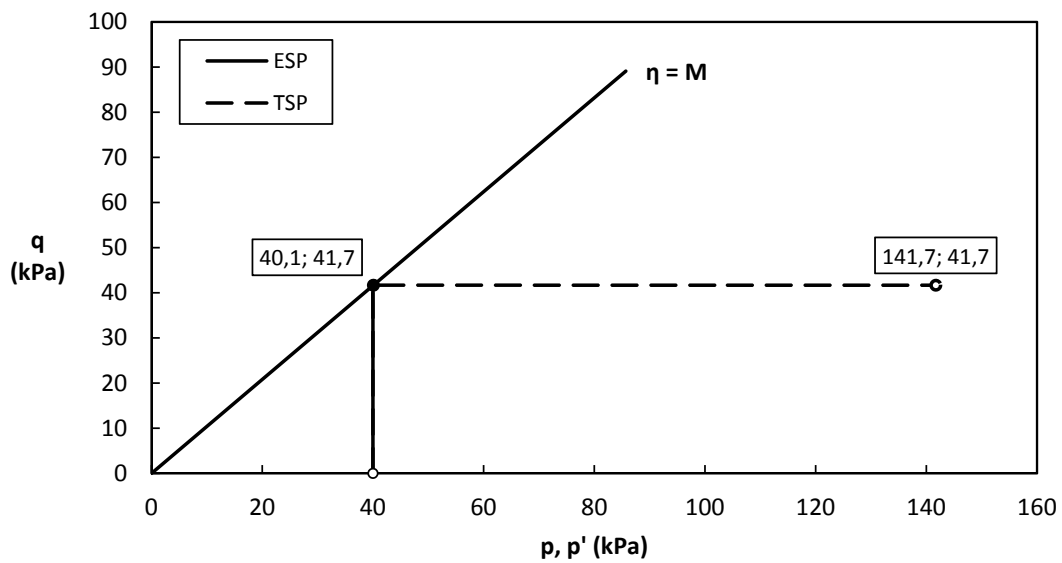
Figure 3.7: Stress paths at cavity wall for overconsolidated soil, $R = 2.005$.
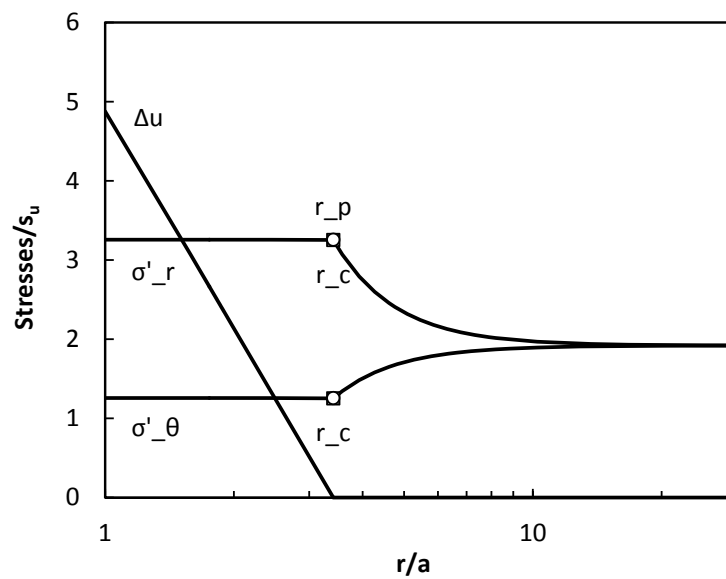
Figure 3.8: Effective radial, tangential and excess pore pressure distributions around the cavity for overconsolidated soil, $R = 2.005$.
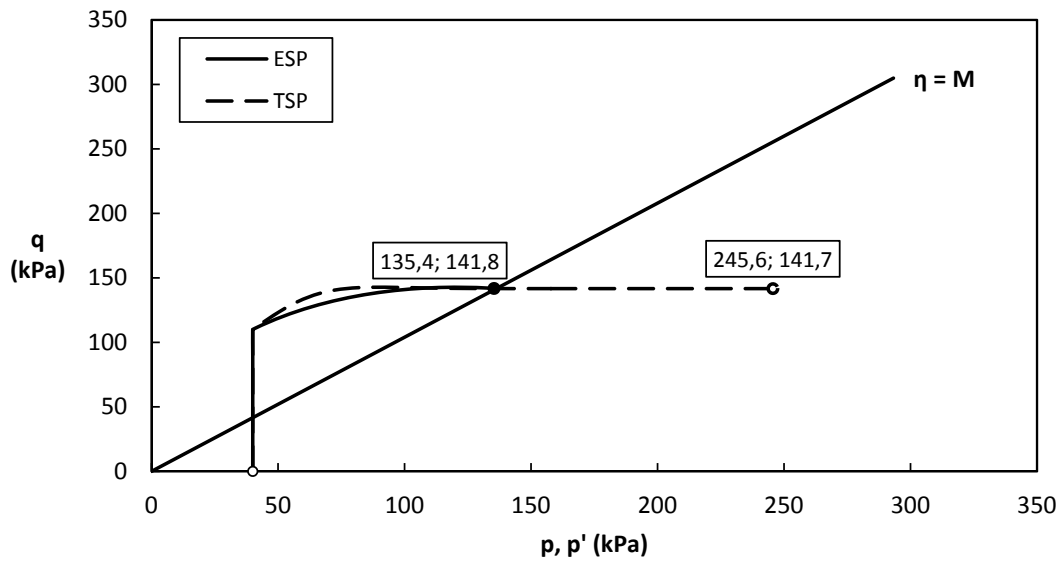
Figure 3.9: Stress paths at cavity wall for heavily overconsolidated soil, $R = 8$.
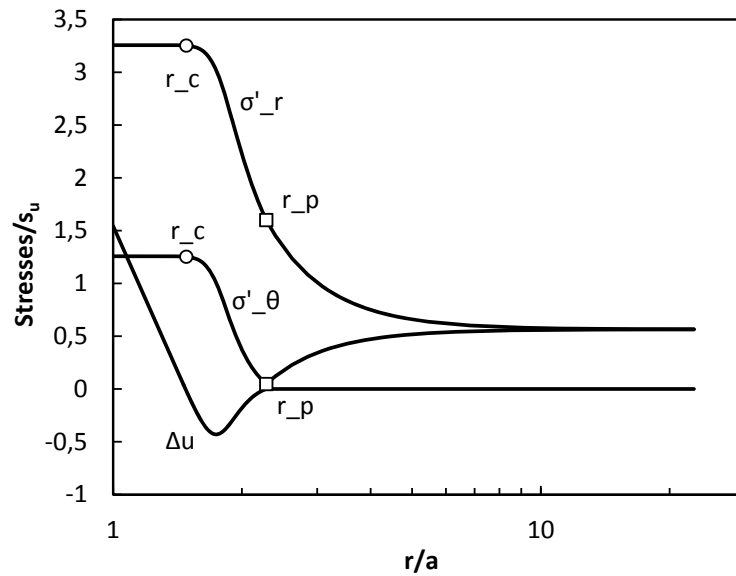
Figure 3.10: Effective radial, tangential and excess pore pressure distributions around the cavity for heavily overconsolidated soil, $R = 8$.

Table 3.1: Parameters of the modified Cam Clay model for a brazilian soft clay from Santa Cruz Industrial Zone. Adapted from Campos (2007).

λ	κ	Λ	Γ	N	ϕ'	M	ν'
0.825	0.096	0.884	7.28	7.79	26.3°	1.04	0.3

Table 3.2: Results for three different values of $R = 1.001$, 2.005 and 8. The initial mean effective stress is the same for all cases and is equal to $p'_0 = 40$ kPa

R	v_0	G'_0 (kPa)	s_u (kPa)	p_u (kPa)	p_u/s_u	r_c/a	r_p/a
1.001	4.75	917.8	11.28	101.7	9.02	1.96	11.18
2.005	4.24	819.3	20.84	141.7	6.80	3.41	3.40
8	3,23	624.1	70.84	245.6	3.47	1.48	2.25

3.4 Dissipation of pore pressure excess

The solution of the consolidation around a cavity during and after the expansion has been provided via finite element method by Carter et al. (1979) in the case of a cylinder. They employed the Modified Cam Clay model, a Biot coupled consolidation analysis and made the assumption of plane strain and axisymmetric deformation. After the expansion, the final radius of the cavity was mantained constant and a pore pressure decrease was observed and the effective radial stress increased but, significantly the total radial stress decreased. The stress paths are represented in Figure 3.11, which shows that the effective mean stress increases while the total mean stress decreases during the dissipation of the pore pressure excess. They observed that the dissipation of pore pressures with time is relatively unaffected by the choice of the consitutive soil model, since a good estimate can be obtained assuming a linear elastic behaviour. Hovever, the prediction of the stress distribution is much more dependent.

In this section a semi-analytical method is derived for the consolidation around a spherical cavity and the validation of the results is made by using the finite element method. To this aim, we shall recall the governing equations:
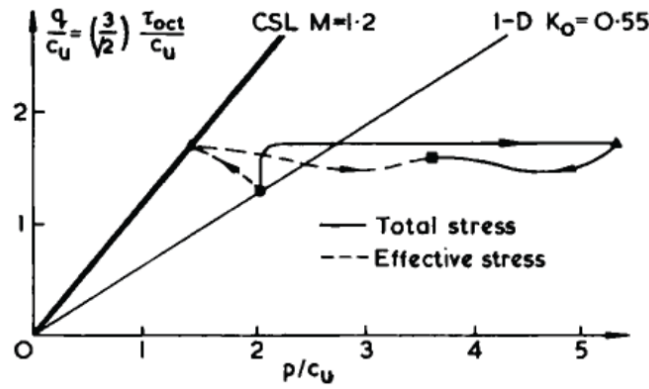
Figure 3.11: Stress paths during a cylindrical cavity expansion and reconsolidation at the cavity interface. (Carter et al., 1979)

1. $\dfrac{dp'}{p'} + \dfrac{2\eta}{M^2 + \eta^2}\, d\eta = \dfrac{dp'_y}{p'_y}$ (yield criterion)

2. $dq = \eta\, dp' + p'\, d\eta$ $\eta = q/p'$

3. $d\epsilon_p^{\mathrm{p}} = (\lambda - \kappa)\dfrac{dp'_y}{vp'_y}$ volumetric plastic strains

4. $\dfrac{d\epsilon_p^{\mathrm{p}}}{d\epsilon_q^{\mathrm{p}}} = \dfrac{M^2 - \eta^2}{2\eta}$ (flow rule)

5. $d\epsilon_q = \dfrac{2}{3}\, d\epsilon_p$ hypothesis on displacement field

The above equations allow to write down the constitutive relationships in the form:

$$
\begin{cases}
d\epsilon_q = \dfrac{dq}{3G'} + \dfrac{2\eta}{M^2 - \eta^2}(\lambda - \kappa)\dfrac{dp'_y}{vp'_y} \\[2ex]
d\epsilon_p = \kappa\dfrac{dp'}{vp'} + (\lambda - \kappa)\dfrac{dp'_y}{vp'_y}
\end{cases}
\tag{3.75}
$$

Making the hypothesis that only vertical displacements occur, the only non-zero strain is $\epsilon_z = du_z/dz$, from which the deviatoric and the volumetric strain can be derived, i.e. $d\epsilon_p = d\epsilon_z$ and $d\epsilon_q = \frac{2}{3}d\epsilon_z$. Thus, Equation 3.75 can be rewritten as:

$$
\dfrac{dq}{2G'} + \dfrac{3\eta}{M^2 - \eta^2}(\lambda - \kappa)\dfrac{dp'_y}{vp'_y} = \kappa\dfrac{dp'}{vp'} + (\lambda - \kappa)\dfrac{dp'_y}{vp'_y}
$$

Combining it with the differential forms of the yield criterion and of the deviator stress q yields:

$$\frac{\eta\,dp' + p'\,d\eta}{2G'} + \frac{3\eta}{M^2 - \eta^2}\frac{(\lambda - \kappa)}{v}\left[\frac{dp'}{p'} + \frac{2\eta}{M^2 + \eta^2}d\eta\right] = \kappa\frac{dp'}{vp'} + \frac{(\lambda - \kappa)}{v}\left[\frac{dp'}{p'} + \frac{2\eta}{M^2 + \eta^2}d\eta\right]$$

That can be rearranged as:

$$\left[\frac{p'}{2G'} + \frac{\lambda - \kappa}{v}\frac{2\eta}{M^2 + \eta^2}\left(\frac{3\eta}{M^2 - \eta^2} - 1\right)\right]d\eta = \left[\frac{\lambda}{vp'} - \frac{(\lambda - \kappa)}{vp'}\frac{3\eta}{M^2 - \eta^2} - \frac{\eta}{2G'}\right]dp'$$
(3.76)

The last equation is in the form:

$$dp' = \frac{f(p', \eta, v, G')}{g(p', \eta, v, G')}d\eta, \quad g(p', \eta, v, G') \neq 0$$

The solution can be obtained numerically by imposing a negative increment $d\eta$ to obtain the corresponding increment dp' at each step. Equation 3.76 provides the effective stress path under the hypothesis introduced before in the domain $\eta \in (M, \eta_a)$, η_a is the value for which $g = 0$. The value of η_a can be found easily assuming a variable shear modulus:

$$G' = \frac{3}{2}\frac{vp'}{\kappa}\frac{1 - 2\nu'}{1 + \nu'}$$

That simplifies the Equation 3.76 in the form:

$$dp' = \frac{f^*(\eta)}{g^*(\eta)}p'd\eta, \quad g^*(\eta) \neq 0$$

Hence, η_a is the real root of the following cubic equation:

$$\rho\eta^3 - \eta^2 - (3\Lambda + \rho M^2)\eta + M^2 = 0$$
(3.77)

where the following coefficients have been introduced:

- $\Lambda = \dfrac{\lambda - \kappa}{\lambda}$

- $\rho = \dfrac{\kappa}{\lambda}\dfrac{1 + \nu'}{3(1 - 2\nu')}$

Since $\rho << 1$ the cubic term may be neglected in order to solve a quadratic equation.

Thus, with a good order of approximation it follows:

$$\eta_a \approx \frac{1}{2}\left[\sqrt{(3\Lambda + \rho M^2)^2 + 4M^2} - (3\Lambda + \rho M^2)\right] \tag{3.78}$$

3.4.1 Comparison with FEM analysis

Calculations are carried out in order to validate the proposed method. Comparison will be made with the results obtained with a FEM axisymmetric analysis. The constitutive properties of the clay used are: $e_0 = 3.5$ (initial void ratio), $\phi' = 22°$, $C_c = 0.69$ (compression index), $C_s = 0.09$ (swelling index), $\nu' = 0.25$, $R = 1$ (isotropic overconsolidation ratio) and $K_0 = 1$. The soil parameters for the MCC model are: $\lambda = C_c/\ln 10 = 0.300$, $\kappa = C_s/\ln 10 = 0.039$, $\lambda^* = \lambda/(1 + e_0) = 0.0638$, $\kappa^* = \kappa/(1 + e_0) = 0,0083$, $M = 6\sin\phi'/(3 - \sin\phi') = 0.856$, $\Lambda = (\lambda - \kappa)/\lambda = 0.870$, $\rho = 0.007$. In the model a sphere is expanded from a radius of 0.5 m to a final value of 0.55 m applying a volumetric strain in three different consolidation strages, i.e. $+1\%$, $+5\%$ $+25\%$ with a time interval of 100 s. The grout is modelled as a non-porous elastic medium with $E = 15$ MPa and $\nu = 0.3$. In the last stage the volume of the sphere is held constant and the pore pressure is allowed to dissipate.

Table 3.3: Data resume from FEM analysis

Point	x (m)	y (m)	p'_0 (kPa)	p'_u (kPa)	p'_a (kPa)	η_a
A	0.17	5.48	22.62	12.39	27.20	0.266
B	0.40	5.30	23.50	12.84	28.31	0.268
C	0.51	5.05	24.76	13.58	30.11	0.251

Table 3.4: Results from proposed analytical method

Point	p'_0 (kPa)	p'_u (kPa)	p'_a (kPa)	η_a
A	22.62	12.38	27.01	0.255
B	23.50	12.86	28.06	0.255
C	24.76	13.55	29.56	0.255
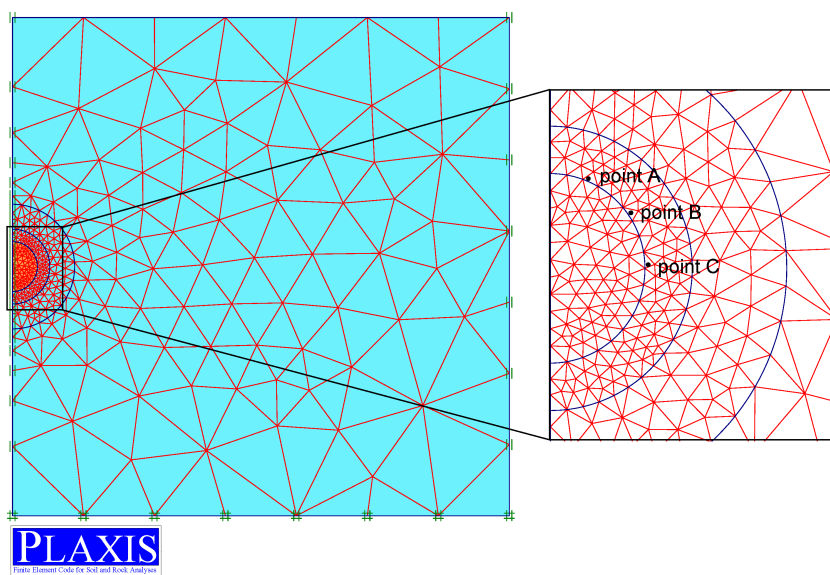
Figure 3.12: Mesh used for the finite element analysis with PLAXIS. Points A, B and C are the gauss points nearest to the cavity.
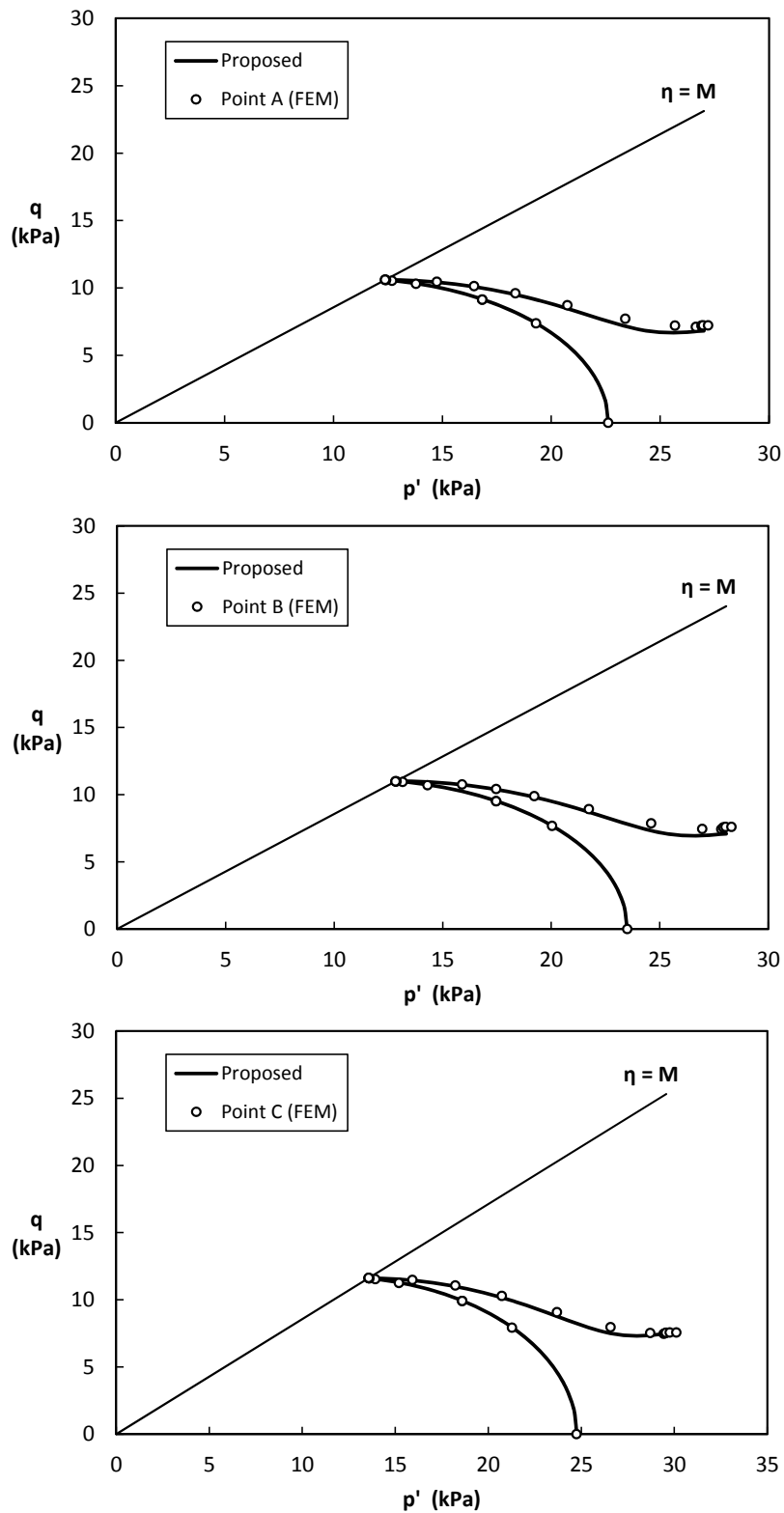
Figure 3.13: Comparison of proposed semi-analytical method with finite element analysis with PLAXIS.

Part III

Geotechnical Modelling

4 Unit cell

4.1 Rigid boundary hypothesis

The pattern of grout injection points can be adjusted to achieve the required engineering performance of the soil. Typically, two patterns are used in the CPR Grouting: the square and the triangular one. As shown in Figure 4.1, for both it is possible to define a *unit cell* as the representative control volume delimited by a well-defined drainage rigid boundary.[1] For instance, if a triangular array is used, the boundary will be a hexagon, which can be approximated as an equivalent circle, whose diameter can be evaluated as $D = \sqrt{4A/\pi}$, where A is the area of the cross section of the unit cell. As instance, identifying with S the drain spacing, the unit cell area equals to $A = 3S^2/\cos 30°$ for triangular array or $A = 4S^2$ for square one. The rigid boundary hypothesis was introduced by Soga et al. (2004) and represents a useful exemplification for geotechnical modelling. If the hypothesis is correct, a multiple injection can be simulated by a single injection confined within an equivalent radial fixed boundary. In particular, Soga et al. (2004) conducted a series of laboratory experiments concluding that the hypothesis is practically correct for simultaneous injection (see Fig. 4.3). However, they encountered differences between simultaneous and sequential injection. Actually, for normally consolidated clays the ground heave due to the grouting process is dependent on the waiting period between injections, as shown in Figure 4.4. They suggested that the partial consolidation occurring between each injection could be the cause of different degrees of consolidation created by different waiting periods. In this way, non-simultaneous injections create large stress concentrations around the injection points, leading to a larger soil consolidation. A relevant fact is that this was not observed for heavily overconsolidated clays, whose behaviour seemed to be irrespective of waiting period.

---

[1] Actually, in real-life applications, there would not be a well-defined physical boundary to soil deformation.
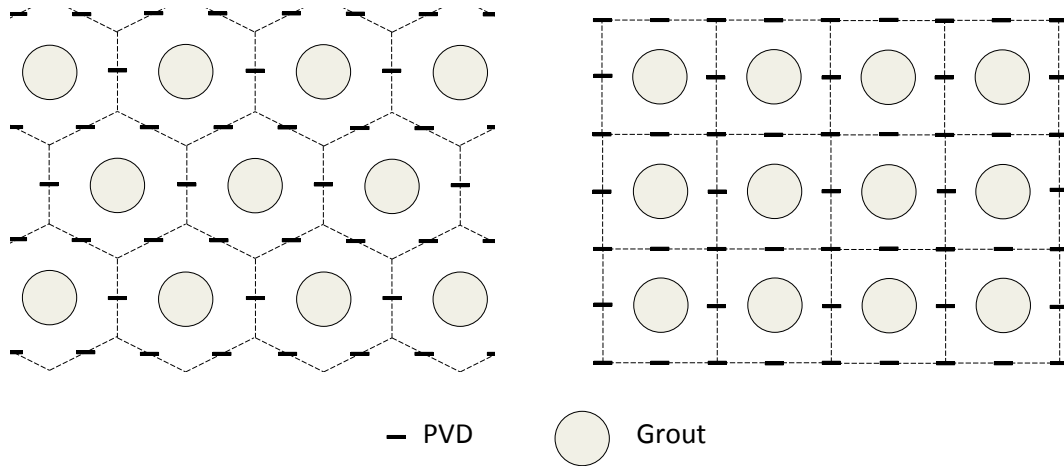
Figure 4.1: Triangular and square patterns: the unit cell is a hexagon or a square.

4.2 Substitution ratio

The design of the CPR Grouting consists in the choice of a suitable distance between drains and an amount of injected grout. These informations can be summarized by introducing the *substitution ratio R_S*, defined as *the volume of grout injected in an undeformed unit cell*. As shown in Figure 4.2, the initial volume of a unit cell depends on the distance S between drains and on its height, which is equal to the height of the improved soft clay layer. The CPR Grouting generally utilizes a single pass system (ie. drill down, grout up) in which the first stage grouting commences from the bottom of the pre-drilled hole and continues until a predetermined grout pressure is achieved or when a predetermined amount of grout is injected. Upon achieving one of these criteria, the grout pipe is raised to the next stage by a constant step, typically 1 meter. The grouting process continues in discrete stages till the top of the improvement zone is reached. Keeping in mind these considerations, we can express the substitution ratio with the following equation:

$$R_S = \frac{\sum\limits_{i=1}^{N} V_{g_i}}{A\,Nh} \tag{4.1}$$

where V_{g_i} is the amount of grout injected at the *i-th* stage, A is the area of the horizontal cross section of the unit cell, N is the number of stages, i.e. the number of injection points along the hole, and h is the vertical raising step. If we make the
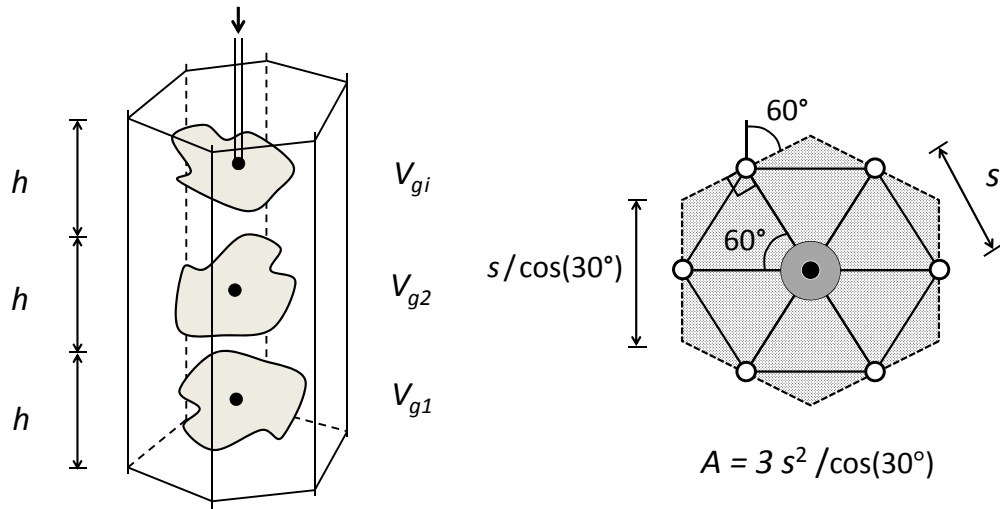
Figure 4.2: Unit cell and injection points vertically spaced by a constant amount.

hypothesis that the amount of injected grout is constant for each stage and equal to V_g, then the substitution ratio becomes:

$$R_S = \frac{V_g}{Ah} \tag{4.2}$$

for instance, for a triangular array with $S = 1.5$ m, $h = 1$ m and $V_g = 900$ l as design parameters, it follows that $R_S = 11.55\%$.

A similar concept has been proposed by Soga et al. (2004) who introduced a dimensionless *radial boundary ratio* n_r defined as:

$$n_r = \frac{D}{2a} \tag{4.3}$$

where D is the diameter of the rigid boundary (i.e. the equivalent diameter of the unit cell) and a is the equivalent radius of the expanded cavity, given by:

$$a = \sqrt[3]{\frac{3V_g}{4\pi}} \tag{4.4}$$

where V_g is the injected grout volume. When n_r is small, the spacing between the injections is close, on the other hand a single injection in an infinite space is at $n_r = \infty$.

4.2.1 Grout efficiency

The use of a concept derived from the compensation grouting technique is necessary for a better comprehension of the topic presented in the next section. The effectiveness of compensation is often evaluated with the *grout efficiency*, η, defined as *the amount of soil heave (or of volume compensated) for a given injected grout volume* (Komiya et al., 2001). Ideally, if soil deformation is occurring in the undrained condition and there are no horizontal displacements, the heave volume is equal to the injected volume, i.e. $\eta = 1$. However, this is not what happens in the field. As a matter of fact, the grout efficiency decreases with time, since surface settlements occur due to soil consolidation. Moreover, horizontal displacements are unavoidable and the grout is subjected to the "bleeding" phenomenon. In order to take into account the loss due to (a) dissipation of the excess pore pressure and (b) shrinkage of the grout itself, Komiya et al. (2001) proposed the following expression for the grout efficiency:

$$\eta = \frac{\text{Heaved volume}}{\text{Injected volume}} = \frac{V_g - V_c - V_{sh}}{V_g} = 1 - \lambda_c - \epsilon_{sh} \tag{4.5}$$

where V_g is the injected volume, V_c is the decrease in volume due to consolidation, and V_{sh} is the decrease in volume due to shrinkage of the grout. The volume loss ratios of consolidation effect and shrinkage are defined as $\lambda_c = V_c/V_g$ and $\epsilon_{sh} = V_{sh}/V_g$ respectively.

A large number of laboratory experiments have been carried out in order to study the factors affecting the grout efficiency. The results are summarized below:

- **Bleeding and solid penetration:** grout after hardening can loose 30% of its original volume. The addition of a chemical hardener can reduce ϵ_{sh} to 0.07 (Komiya et al., 2001). To avoid the influence of bleeding a balloon expansion test can be carried out.

- **OCR:** for normally consolidated clay a negative grout efficiency can be observed (Au et al., 2003). In general, better compensation efficiencies are achieved in stiff clays, in fact overconsolidated samples show a grout efficiency close to 1 (Komiya et al., 2001; Au et al., 2003).

- **Substitution ratio** R_S**:** for NC clays, for small injection volumes there is a large loss due to soil consolidation ($\lambda_c = 0.65$). As the injection volume increases, for a given radius of the radial boundary, λ_c decreased to a value of approximately 0.10. (Komiya et al., 2001). Soga et al. (2004) observed a similar

trend within the range OCR=1-2, pointing out that the final grout efficiency is strongly dependent on R_S, although this is not so obvious for OC clays.

- **Injection rate:** when the injection rate is slow the consolidation that occurs is not negligible – i.e. the expansion is under partially drained conditions – and the maximum (peak) heave induced is lesser than the one obtained by a rapid injection. The heave increases linearly with time at a constant expansion rate (Au et al., 2006). However, the average rate of consolidation is as independent of the cavity expansion rate as the long-term efficiency (Au et al., 2007).

- **Multiple injections:** the consolidation behaviour is very similar for both single and multiple simultaneous injections for NC or OC clays. However, the grout efficiency decreases when injections are performed sequentially in normally consolidated clays with increase in the waiting period between injections (Soga et al., 2004).

- K_0 **condition:** although this condition was not investigated for clays, it has been observed for residual soils that the ground heave increases when lateral earth pressure coefficient K_0 increases (Wang et al., 2010).

4.3 Estimation of void ratio change

In this section a simple approach will be provided to demonstrate that the introduction of grout material in the soil mass results in a diminution of its void ratio. As shown in Figure 4.5, let us consider a unit cell before the treatment, its initial volume will be denoted as $V_0 = V_s + V_{v0}$, where V_s is the volume of solids, V_{v0} is the initial volume of voids.[2] Let us denote with $e_0 = V_{v0}/V_s$ the initial void ratio, then $V_0 = V_s(1 + e_0)$. The amount of grout to be injected is predetermined and its value is $V_g = R_S V_0$. The grouting will induce enormous strain in the surrounding soil, as a result a variation of the control volume will be observed. Since the radial boundary is rigid, only a ground heave will occur. Thus, recalling the concept of *grout efficiency*, the final volume of the unit cell can be expressed as $V = V_0 + \eta V_g$, where η is the grout efficiency as defined in Eq. 4.5. Assuming the solids incompressible, the final volume of the unit cell can be expressed also as $V = V_s + V_v + V_g(1 - \epsilon_{sh})$, in which ϵ_{sh} is the volume loss factor due to shrinkage, bleeding and solid penetration.

---

[2]Actually, the cavity is expanded by injecting the grout with a pipe driven in a pre-drilled borehole. In the analysis, its volume is assumed negligible.
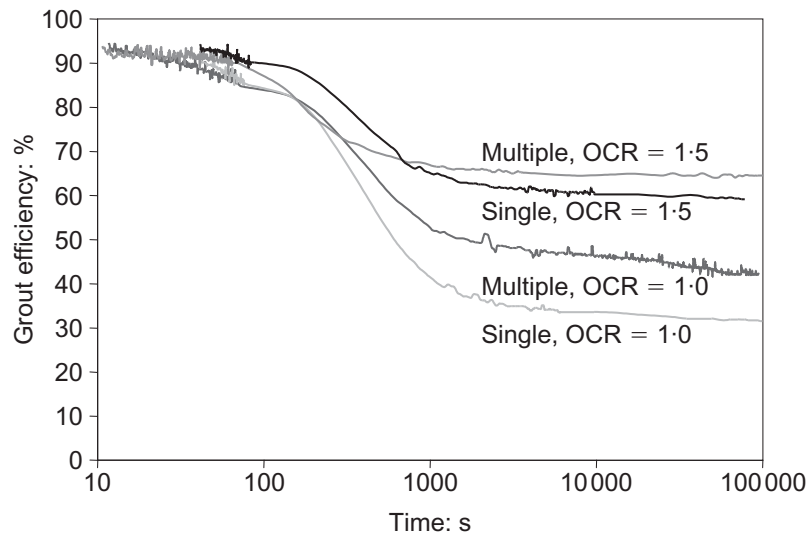
Figure 4.3: Grout efficiency of single and multiple simultaneous balloon expansion tests (Soga et al., 2004). The response is similar.
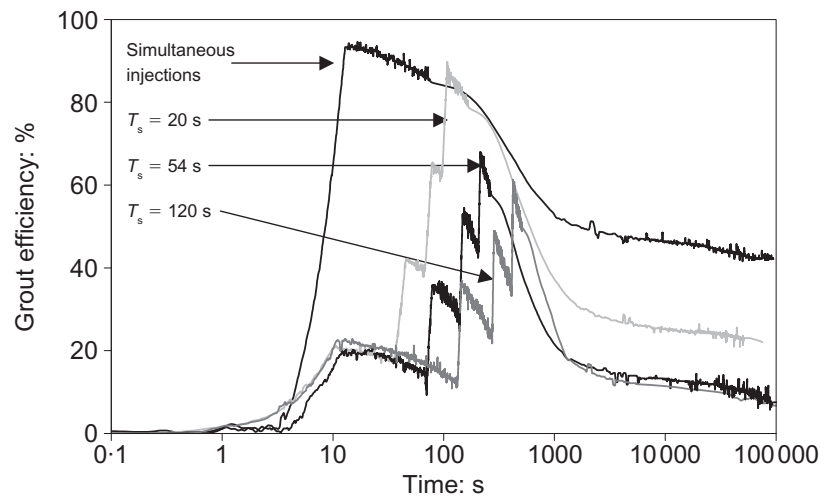
Figure 4.4: Effect of waiting period (T_s) on grouting efficiency. The efficiency decreases with the waiting period because the soil consolidates at each waiting period (Soga et al., 2004).
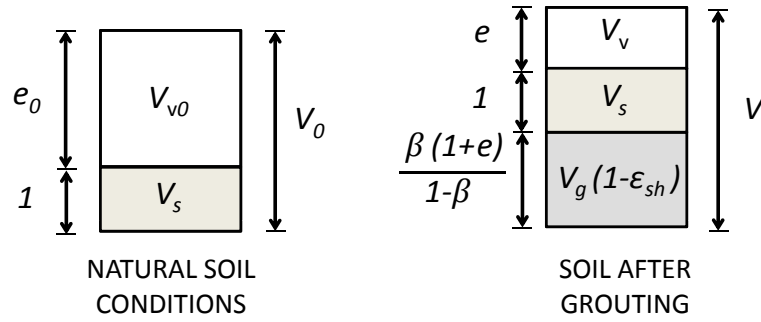
Figure 4.5: Multiphase model. Schematic representation of a unit cell volume pre- and post-treatment. A volume is associated to each phase.

Thus the volume change of the unit cell is:

$$\Delta V = V - V_0 = (V_{\mathrm{v}} - V_{\mathrm{v}0}) + V_g(1 - \epsilon_{sh}) \tag{4.6}$$

Dividing by $V_0 = V_s(1 + e_0 + b_0)$ both sides yields:

$$\frac{\Delta V}{V_0} = \frac{e - e_0}{1 + e_0} + R_S(1 - \epsilon_{sh}) \tag{4.7}$$

in which $\Delta V / V_0$ is the volumetric strain that the unit cell undergoes because of the injection. Noting that $\Delta V / V_0 = \eta R_S$, Eq. 4.7 can be rewritten as:

$$\eta R_S = \frac{e - e_0}{1 + e_0} + R_S(1 - \epsilon_{sh}) \tag{4.8}$$

Finally, we add $+1$ to both sides of the equation to get:

$$e = (1 - \lambda_c R_S)(1 + e_0) - 1 \tag{4.9}$$

The above equation provides a good estimation for the final void ratio, since the volume loss ratio due to consolidation, $\lambda_c = 1 - \eta - \epsilon_{sh}$, is known. Obviously, for small amounts of injected grout volume, at a first approximation we can make the trivial assumptions that no volumetric strain of the unit cell occurs due to the treatment, in other words the final grout efficiency is zero, i.e. $\eta = 0$, and no bleeding effect takes

place, i.e. $\epsilon_{sh} = 0$, then the final void ratio can be estimated as:

$$e = (1 - R_S)(1 + e_0) - 1 \qquad (4.10)$$

For example, for a initial void ratio[3] $e_0 = 3.5$ and a substitution ratio $R_S = 11.55$ % the final void ratio is $e = 2.98$ that corresponds to a diminution of 14.86%.

This value has to be considered as an average diminution of the void index within the the unit cell. As a matter of fact, the void ratio importantly decreases just near the injection zone, being the clay compacted in the vicinity of the bulb by the increased radial stress arisen after grouting and dissipation of pore water pressure excess. It leads to the conclusion that the variation of void ratio is less appreciable as the radial distance increases. Weber et al. (2010) have observed that the region of soil that is affected by a stone column installation process appears to reach to a distance of about 2.5 times the nominal column radius.[4] They reported the change in porosity depending on the distance from the stone column axis (see Figure 4.6) and they fitted the data points with a hyperbolic function in the form:

$$y = \frac{a_1}{r + a_2} + a_3 \qquad (4.11)$$

We shall introduce another parameter to improve our formulation. Let us denote with $\beta = V_g(1 - \epsilon_{sh})/V$ the grouting volume ratio after the treatment, then it can easily shown that:

$$\beta = \frac{R_S(1 - \epsilon_{sh})}{1 + \eta R_S} \qquad (4.12)$$

Actually, in general $\beta \neq R_S$ depending on the values assumed by the volume loss ratios ϵ_{sh} and η.

Experimental setup and procedure

Laboratory testes can be carried out to evaluate λ_c for different soils using a balloon expansion test. The shrinkage volume loss ratio can be assumed as property of the grout utilized for the treatment. Finally, η can be estimated by means of Eq. 4.5.

---

[3]Almeida and Marques (2010) suggest for brazilian soft and very soft clays from Barra da Tijuca - Area 3 a void ratio between 2.2 and 4.7.

[4]Their problem can be idealized as a cylindrical cavity expansion, which is quite similar to the present one.
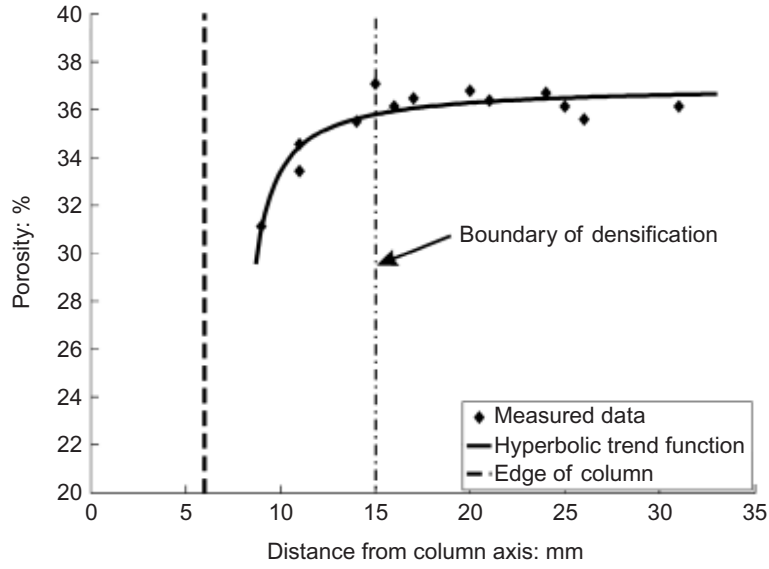
Figure 4.6: Measurements from mercury intrusion porosimetry – porosity as a function of distance from the stone column axis. (Weber et al., 2010)

4.3.1 Change in the undrained shear strength

The change in the undrained shear strength of soil can be described by the average shear strength enhancement ratio, which is defined as the ratio of the average undrained shear strength of soil after expansion and consolidation, s_u, to the initial undrained shear strength of the soil, s_{u0}, that is (Au et al., 2007):

$$\frac{s_u}{s_{u0}} = \exp\left(\frac{e_0 - e}{\lambda}\right) \tag{4.13}$$

where e_0 is the initial void ratio of the soil, e is the void ratio after the treatment and $\lambda = C_c / \ln 10$ is the slope of the virgin compression line in the plane $e - \ln p'$. Equation 4.13 suggest that any decrease in the average void ratio will result in an increase in the average undrained shear strength of the soil specimen. Under the assumption that the volume of the borehole is negligible, i.e. $b_0 \simeq 0$, the average shear strength enhancement ratio can be calculated by means of Eq. 4.9 obtaining:

$$\frac{s_u}{s_{u0}} = \exp\left(2.3\, \lambda_c\, R_S\, \frac{1 + e_0}{C_c}\right) \tag{4.14}$$

Table 4.1: Results obtained by the proposed simplified method compared with measured enhancement in undrained shear strength by pressuremeter tests.

S (m)	A (m^2)	R_S	Depth (m)	e_0	C_c	e	λ	α (Riccio et al., 2013)	α (by Eq 4.13)
1.5	9	10%	1	6.64	2.9	5.88	1.261	2.10	1.83
			3	5.12	2.4	4.51	1.087	1.65	1.75
			5	0.84	0.6	0.66	0.365	2.08	1.64
			7	2.33	0.5	2.00	0.208	1.16	4.89

Thus, the change in the undrained shear strength can be easily estimated knowing the compression ratio $CR = C_c/(1 + e_0)$, the substitution ratio R_S and the volume loss factor of consolidation effect λ_c. For a normally consolidated soil we can make the trivial assumption that $\lambda_c = 1$, then, as instance, for a soft clay with $C_c = 1.5$, $e_0 = 5$ and $R_S = 11.55\%$, follows that $s_u/s_{u0} = 2.89$, which means a gain of 189% in undrained shear strength.

By means of pressuremeter tests Riccio et al. (2013) evaluated the improvement of stiffness and strength of a soft clay from Athletes' Park in Barra da Tijuca, Rio de Janeiro, reporting that for the clay at a depth of 3 m, with parameters $C_c = 2.4$ and $e_0 = 5 : 12$, the increase in undrained strength was found to be about 1.65. The improvement consisted in CPR Grouting with 1.5 m spaced drains in square array. The designed volume of bulb was 900 liters per meter depth. From this information it can be estimated by Equations 4.2, 4.10 and 4.14 the substitution ratio, R_S, the post-CPR Grouting void ratio and the undrained strength increment, α, respectively. The results are summarized in Table 4.1. The increase in undrained strength calculated by the proposed method is very close to that measured by Riccio et al. (2013), confirming that with a very simple approach one can quickly estimate the average shear strength enhancement ratio for soils improved with CPR Grouting.

5 Stress field modelling after grouting

For the purpose of geotechnical modelling of the CPR Grouting, the soil conditions after the treatment must be predicted by introducing some hypothesis for the stress field within the *unit cell*. In order to do this some remarks are necessary. Firstly, the lateral earth pressure theory provides the minimum (K_a) and maximum (K_p) stress ratio between the major (σ_1') and minor (σ_3') principal stress for the case of cohesionless soils. Actually, it is physically impossible that $\sigma_3' < K_a\,\sigma_1'$, or equivalently, $\sigma_1' > K_p\,\sigma_3'$. Secondly, if σ_r, σ_θ and σ_z are principal stresses in axisymmetric condition, let us introduce the radial earth pressure coefficient:

$$K_r = \frac{\sigma_r'}{\sigma_z'} \tag{5.1}$$

which may differ from the circumferential earth pressure coefficient, defined as:

$$K_\theta = \frac{\sigma_\theta'}{\sigma_z'} \tag{5.2}$$

As introduced before, these values cannot be greater than the passive earth pressure coefficient or smaller than the active one. However, if we assume $K_r > K_\theta$, even the ratio K_r/K_θ cannot exceed the passive earth pressure coefficient K_p. This can be understood referring to the Mohr's circle shown in Fig. 5.1, in which the radial stress σ_r' is assumed to be the major principal stress, the circumferential stress σ_θ' the minor principal stress and the vertical effective stress σ_z' is assumed to the intermediate principal stress. Hence, by using the definitions given in Eqs 5.1 and 5.2, we can express:

$$\frac{K_r}{K_\theta} \leq K_p, \quad \text{or} \quad \frac{K_\theta}{K_r} \geq K_a \tag{5.3}$$

Accordingly, we can define a domain Ω such that:

$$K_\theta, K_r \in \Omega, \quad \Omega = \{K_a \leq K_\theta \leq K_p,\ K_\theta \leq K_r \leq K_p K_\theta,\ K_r \leq K_p\} \tag{5.4}$$
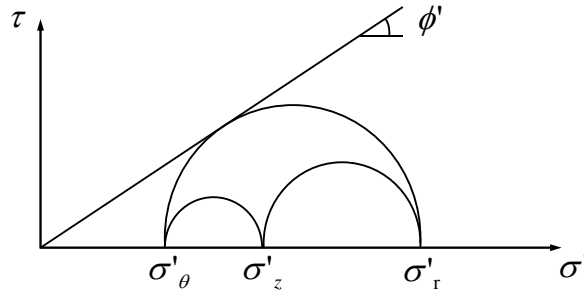
Figure 5.1: Mohr's circle at failure.

where:

$$K_a = \frac{1 - \sin \phi'}{1 + \sin \phi'} = \frac{1}{K_p} \tag{5.5}$$

5.0.2 Stress invariants

Considering the coefficients expressed in the Eqs. 5.1 and 5.2, under the hypothesis that σ_r, σ_θ and σ_z are principal stresses, for the Modified Cam Clay it is possible to define the stress invariants p', q as a function of the earth pressure coefficients K_r and K_θ in the following manner:

$$p' = \sigma'_z \frac{1 + K_r + K_\theta}{3} \tag{5.6}$$

$$q = \sigma'_z \frac{1}{\sqrt{2}} \left[(K_r - K_\theta)^2 + (K_r - 1)^2 + (K_\theta - 1)^2 \right]^{1/2} \tag{5.7}$$

from which follows the stress ratio:

$$\eta = \frac{q}{p'} = \frac{3}{\sqrt{2}} \frac{\left[(K_r - K_\theta)^2 + (K_r - 1)^2 + (K_\theta - 1)^2 \right]^{1/2}}{1 + K_r + K_\theta} \tag{5.8}$$

5.0.3 Compression lines at constant stress ratio

According to Wood (1990), in the plane $v - \ln p'$ any stress ratio η defines a geometrical line which is parallel to the isotropic compression line (iso-NCL) identified by the
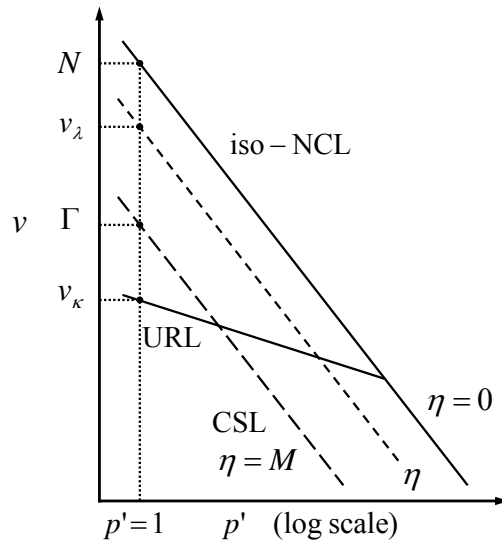
Figure 5.2: Modified Cam Clay. Adapted from Wood (1990).

equation $v = N - \lambda \ln p'$. Each of these lines ha an equation of the form:

$$v = v_\lambda - \lambda \ln p' \tag{5.9}$$

where v_λ is the specific volume at a unit effective mean stress. The value of v_λ that corresponds to a given value of η can be obtained from the following expression provided by Wood (1990) [cap.6, pag. 145, eq. 6.14]:

$$v_\lambda = N - (\lambda - \kappa) \ln \frac{M^2 + \eta^2}{M^2} \tag{5.10}$$

This expression leads to the conclusion that the value v_λ depends only on the stress ratio η. Furthermore, two particular cases can be identified:

1. $\eta = 0$: Eq. 5.10 provides the value $v_\lambda = N$, and Eq. 5.9 identifies the isotropic normal compression line (iso-NCL in Fig. 5.2);

2. $\eta = M$: Eq. 5.10 gives the specific volume at a unit effective mean stress of the critical state line:

$$v_\lambda = \Gamma = N - (\lambda - \kappa) \ln 2$$

and 5.9 gives the expression of the CSL line in Fig. 5.2.

5.1 Derivation of the stress field after treatment

The aim of this study is to provide a good estimation of the generated stress field within the unit cell after the application of the CPR Grouting to a soft soil layer. Due to the complexity of the problem (large strains, consolidation coupled analysis, boundary effects, expansion rate, multiple non-simultaneous injections etc.) some simplifications are needed in order to develop an analytical solution able to describe the in situ conditions after the treatment. In the model the following assumptions will be adopted:

1. The unit cell is approximated to an equivalent cylinder whose radius r_e is greater than the equivalent radius of the cavity a ;

2. Axisymmetric condition, considering σ_r, σ_θ and σ_z principal stresses and the excess pore pressure completely dissipated, i.e. $\Delta u = 0$;

3. K_r and K_θ as defined in Eqs. 5.1 and 5.2 are constant; as a consequence, η (as in Eq. 5.8) will be constant too;

4. The average void ratio within the unit cell can be estimated with the expression (Eq. 4.10):
$$\bar{e} = (1 - R_s)(1 + e_0) - 1$$

5. The average vertical effective stress within the unit cell is approximately equal to the in-situ vertical effective stress previous to the treatment, i.e. $\bar{\sigma}'_z \simeq \sigma'_{zo}$;

6. The *average value* $\bar{x}$ of a variable x within a domain Ω is calculated as follows:
$$\bar{x} = \frac{1}{\Omega} \int_\Omega x \, d\Omega$$

From assumptions (2) and (3) the stresses at a fixed depth depend only on the radial coordinate r and the equilibrium equation (Eq. 3.4) can be rewritten as:

$$K_r \frac{\partial \sigma'_z}{\partial r} + \sigma'_z \frac{K_r - K_\theta}{r} = 0 \qquad (5.11)$$

the integration leads to the following expression for the vertical effective stress:

$$\sigma'_z(r, z) = \frac{A_z}{r^\alpha} \qquad (5.12)$$

in which the exponent $\alpha = 1 - K_\theta/K_r$ has been introduced and A_z is an integration constant, whose value can be determined recalling assumptions (5) and (6):

$$\bar{\sigma}'_z = \frac{A_z}{\pi(D^2/4 - a^2)} \int_a^{D/2} 2\pi r^{1-\alpha} dr \tag{5.13}$$

from which it follows:

$$A_z = \sigma'_{zo} \frac{2 - \alpha}{2} \frac{D^2/4 - a^2}{(D/2)^{2-\alpha} - a^{2-\alpha}} \tag{5.14}$$

The vertical effective stress distribution is completely known given the geometry and the value of the parameter α. It is important to point out that α can strictly assume values corresponding to the pairs K_r, K_θ that come from Ω. Hence, α is defined in interval $[0, 1 - K_a]$. Consequently, the stresses decrease with the distance from the grouted region and they are at least constant within the unit cell only when $\alpha = 0$.

Finally, Eqs. 5.9 and 5.10 suggest the value of the void index at a generic point known the mean effective stress. The equation can be rewritten in terms of void index, recalling that $v = 1 + e$, Eq. 5.9 can be rewritten as:

$$e = e_\lambda - \lambda \ln p' \tag{5.15}$$

where $e_\lambda = v_\lambda - 1$ and $p' = \sigma'_z(1 + K_r + K_\theta)/3$ (see Eq. 5.6). As a matter of fact, being η constant within the unit cell, the points in the plane $e - \ln p'$ are all aligned and e_λ is constant. Thus, from hypothesis (4) and (6) we can write down an equation that relates the void index to the stress field:

$$\bar{e} = \frac{1}{\pi(D^2/4 - a^2)} \int_a^{D/2} 2\pi r \, e(r) \, dr \tag{5.16}$$

in which

$$e(r) = e_\lambda - \lambda \left[\ln \frac{A_z}{3}(1 + K_r + K_\theta) + \ln r^{-\alpha} \right]$$

The integration yields:

$$\bar{e} = e_\lambda - \lambda \ln \frac{A_z}{3}(1 + K_r + K_\theta) + \frac{\alpha\lambda}{2(D^2/4 - a^2)} \left[D^2/4(2\ln D - 2\ln 2 - 1) - a^2(2\ln a - 1) \right] \tag{5.17}$$

which is an implicit equation that allows the closure of the problem, given a value of the parameter α.

5.2 Results and discussion

A detailed study of the simulated stress field is made by means of calculations carried out using the soil parameters presented in Table 3.1 for normally consolidated soil under a overburden effective stress of $\sigma'_{z0} = 20$ kPa. A triangular pattern is chosen with a drain spacing equal to 1.7 m and a raising step of 1 m. Then, any substitution ratio is easily calculated since to $R_S = 5\%$ corresponds a grout volume $V_g = 500$ l, to $R_S = 8\%$ corresponds $V_g = 800$ l and so on. Two important features are expected: (i) the increase in lateral confining stress and (ii) the densification (i.e. the diminution of the void ratio). In addition, the influence of the substitution ratio (R_S) on the residual stresses[1] will be investigated for normally consolidated soil. Due to the dependency of the grout efficiency on the OCR, its effect on the stresses is not outlined in the present work, because for overconsolidated soils Equation 4.10 is no longer accurate. A deeper study is needed to establish a relationship between the OCR and the grout efficiency to provide a good estimation of the volume loss due to consolidation λ_c and, consequently, the variation of the void ratio.

To solve Equation 5.17, a set of values of α is considered in order to carry out a parametric study. Actually, it is necessary to enter admissible values. It is easy to note that α can strictly assume values within the range $[0, 1 - K_a)$. The condition $K_r = K_\theta$ corresponds to $\alpha = 0$, while $\alpha = 1 - K_a$ is not allowed because it corresponds to the failure condition. As shown in Figure 5.3, the radial earth pressure coefficient K_r is not very affected by α and, as expected, increases with the increase of the substitution ratio. For any α, K_r is the major principal effective stress and its value can exceed two times the vertical effective stress. On the other hand, the tangential earth pressure coefficient decreases as the parameter α increases, however, it is an obvious consequence of the definition of α itself, being $\alpha = 1 - K_\theta/K_r$.

Figures 5.4 to 5.9 show that for $\alpha = 0$ (i.e. $K_r = K_\theta$, so $\sigma'_r = \sigma_\theta$) the residual stresses within the unit cell are constant as well as the void ratio and shear modulus. In this case the tangential stress reaches its maximum value, as shown in Figure 5.6.

---

[1]The term *residual stresses* identify the stress state after the injection and complete dissipation of the pore pressure excess.

As a consequence, according to Figure 5.12 in the plane $e - \log \sigma'_z$ (oedometric plane) the soil is represented by a single point. Moreover, the average mean effective stress reaches its maximum value, which can be calculated in any case as:

$$\bar{p}' = \sigma'_{z0} \frac{1 + K_r + K_\theta}{3}$$

This equation provides a way to estimate the increase in stiffness for a treated soil if a relationship between stiffness and mean effective stress is known. As instance, the curves in Figure 5.7 have a linear relationship with the mean effective stress, because G' is calculated by means of Eq. 3.48. This suggests that the soil is stiffer after the treatment due to the increase in horizontal stresses.

As α increases the stresses distribution becomes more variable. Furthermore, the tangential stress decreases up to becoming the lowest principal stress, as shown in Figure 5.11. The points representing the soil condition in the plane $e - \log \sigma'_z$ are more scattered around the mean value ($\bar{e} - \log \sigma'_{z0}$), but they remain parallel to the virgin compression curve (Figs. 5.13 and 5.14) because they are aligned along a η-compression curve.[2]

---

[2]The cause can be traced to the assumption that the horizontal earth pressure coefficients are constant within the unit cell. Consequently, $\eta = q/p'$ is constant too.
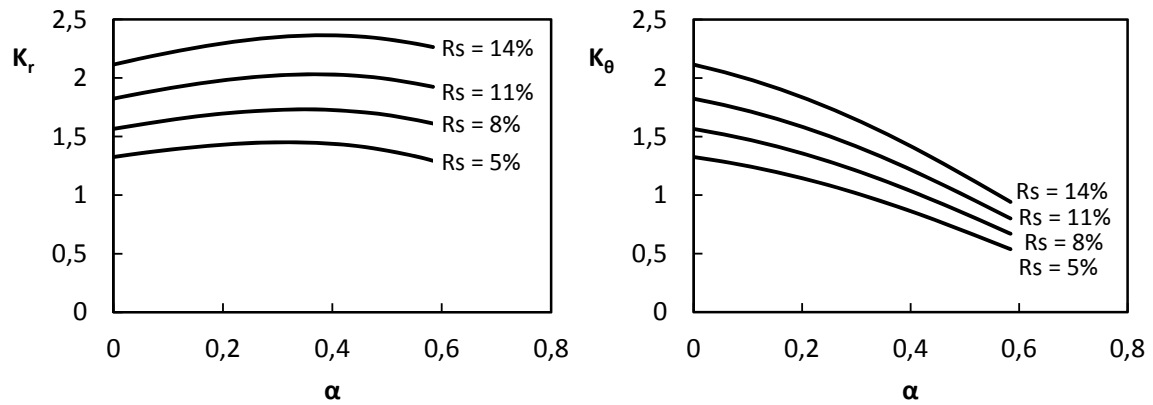
Figure 5.3: Parametric study. Radial $(K_r = \sigma'_r/\sigma'_z)$ and tangential $(K_\theta = \sigma'_\theta/\sigma'_z)$ earth pressure coefficients for different substitution ratios.
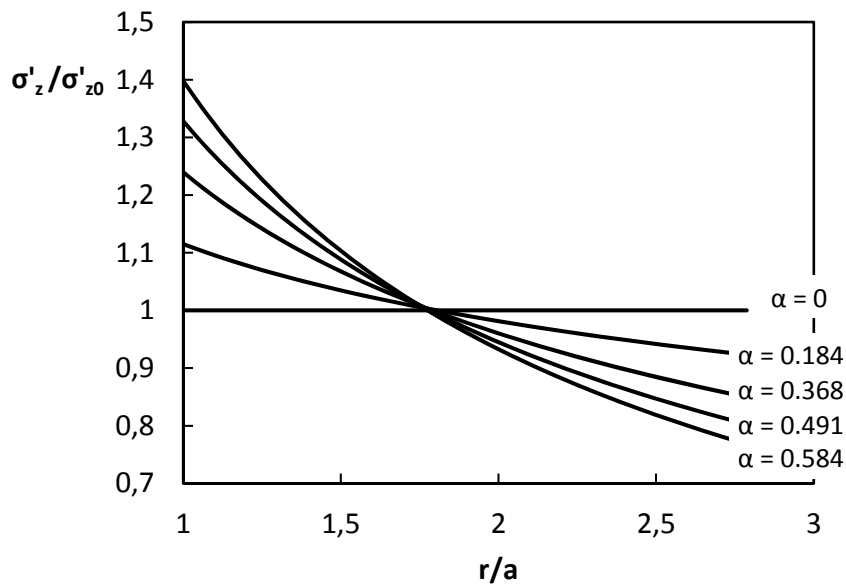
Figure 5.4: Increment in vertical effective stress depending on α within the unit cell for $R_S = 11\%$.
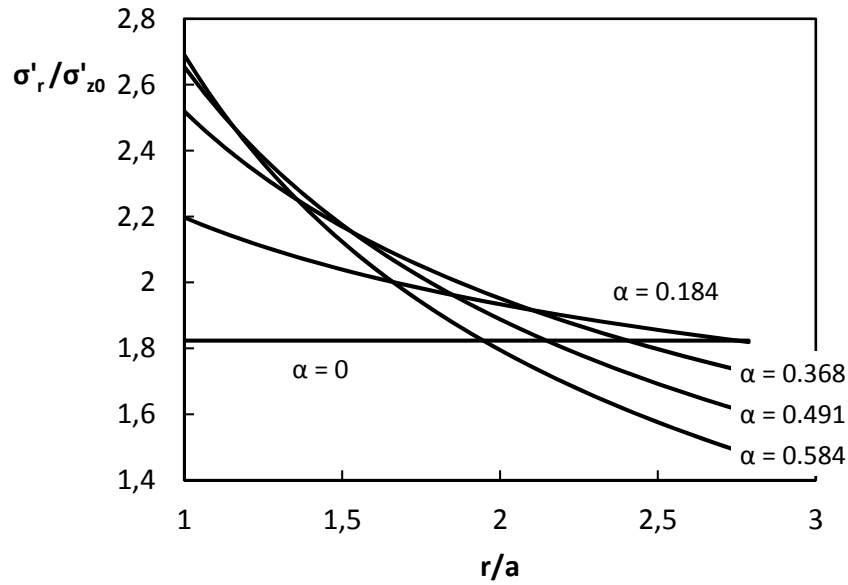
Figure 5.5: Increment in radial effective stress depending on α within the unit cell for $R_S = 11\%$.
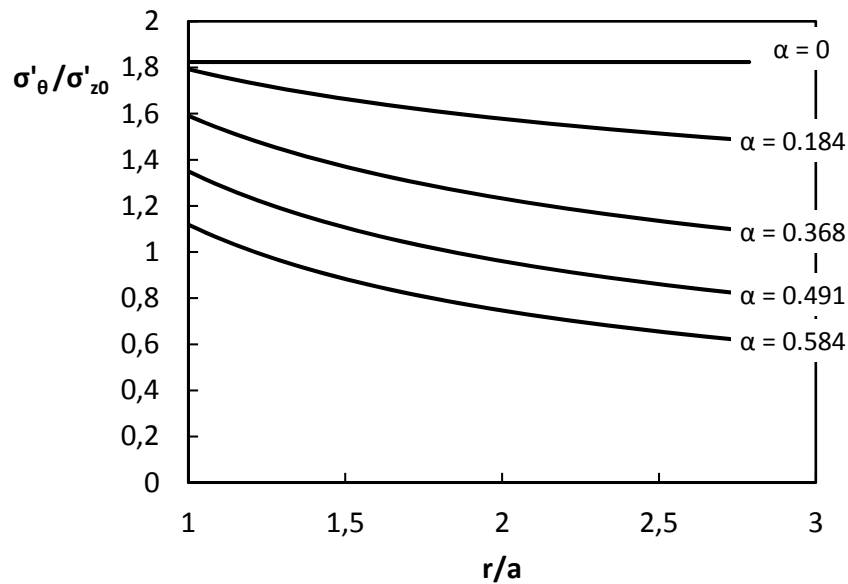
Figure 5.6: Increment in tangential effective stress depending on α within the unit cell for $R_S = 11\%$.
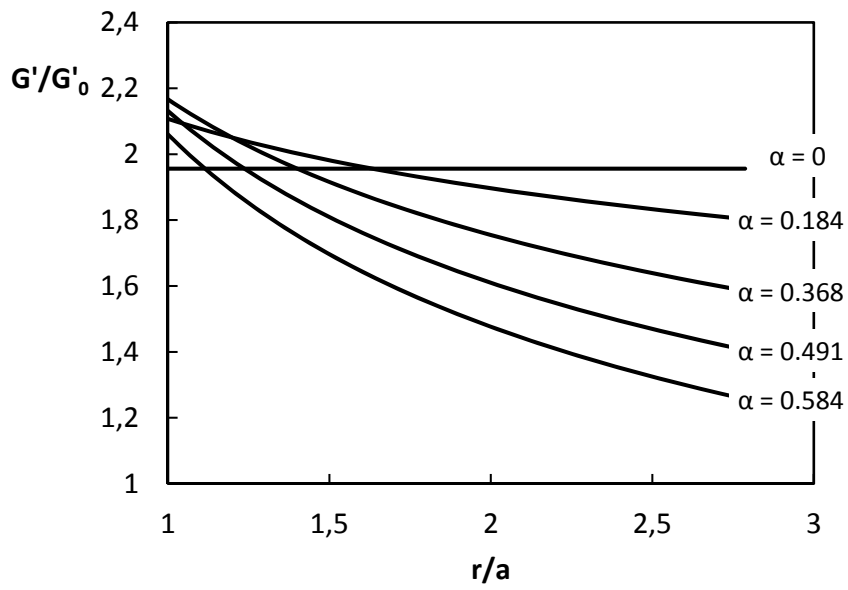
Figure 5.7: Trend of the shear modulus increment with α within the unit cell for $R_S = 11\%$.
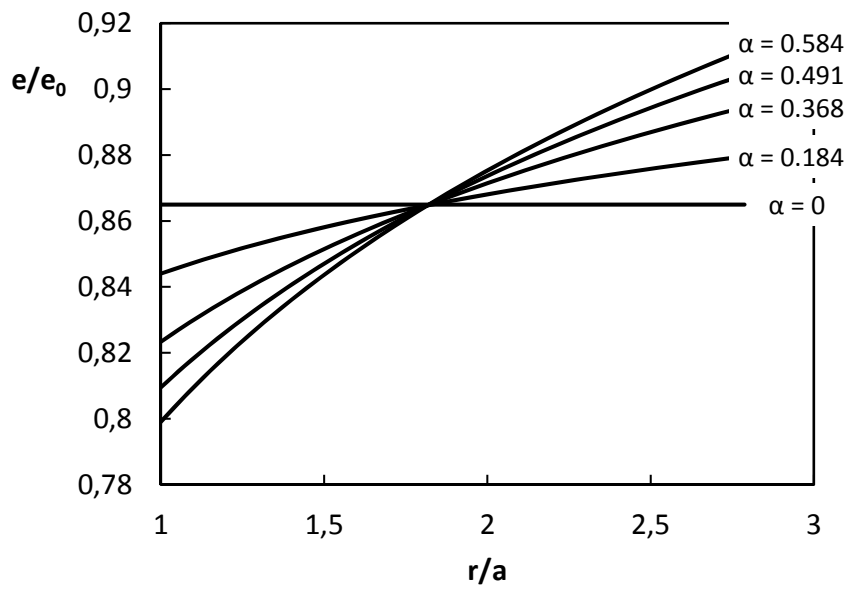
Figure 5.8: Densification profiles depending on α within the unit cell for $R_S = 11\%$.
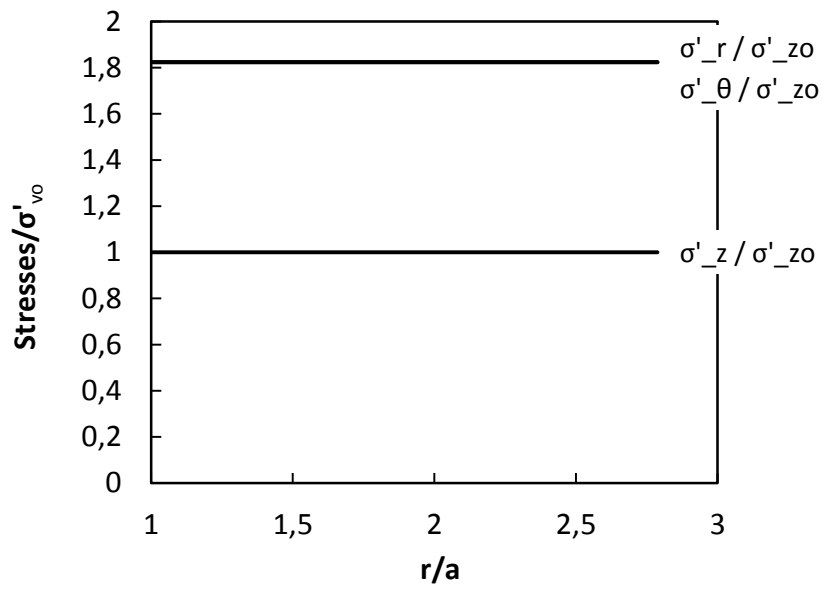
Figure 5.9: Residual stresses distribution for $\alpha = 0$.
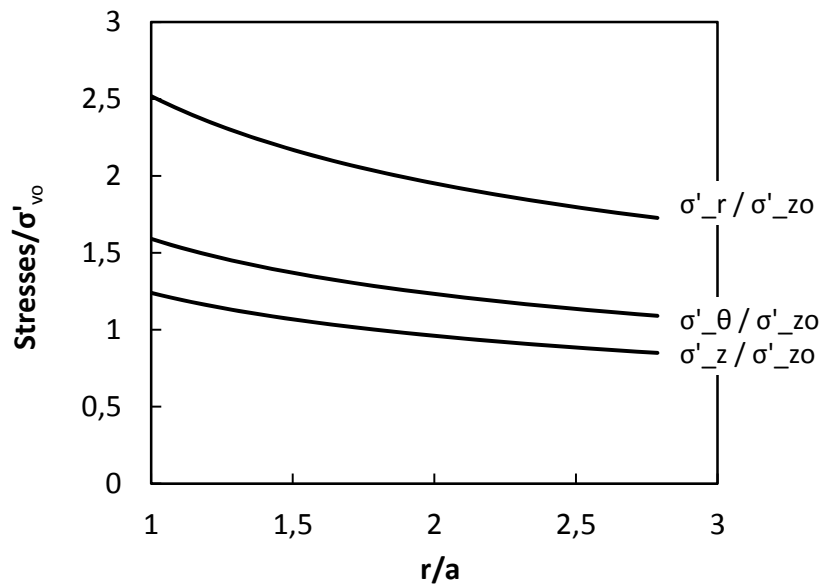
Figure 5.10: Residual stresses distribution for $\alpha = 0.368$.
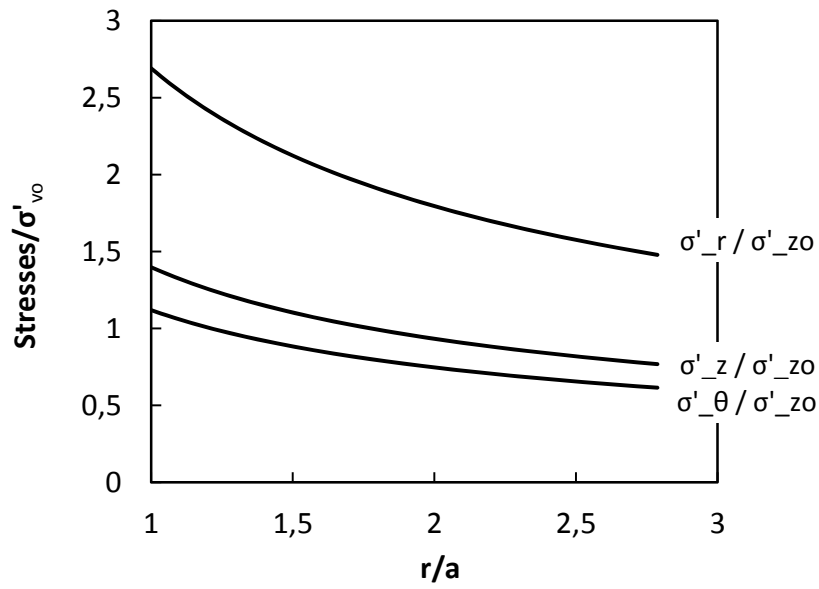
Figure 5.11: Residual stresses distribution for $\alpha = 0.584$.
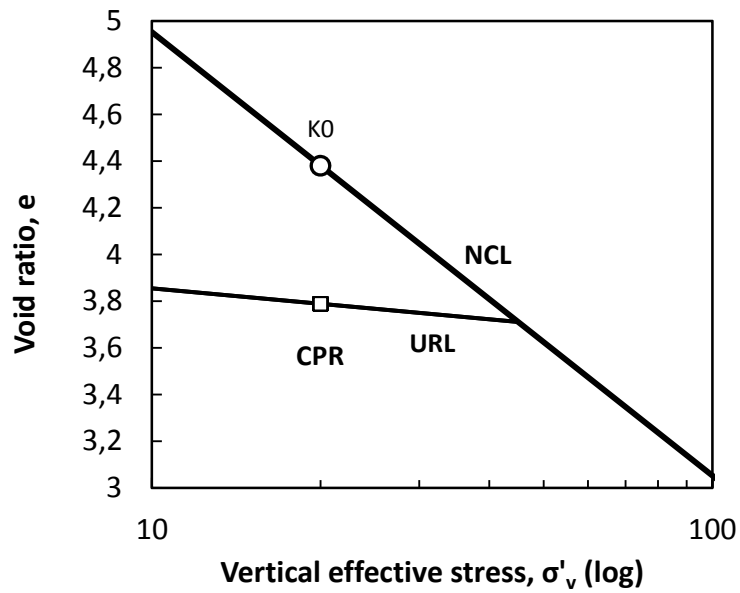
Figure 5.12: Results in the plane $e - \log \sigma'_z$ for $\alpha = 0$.
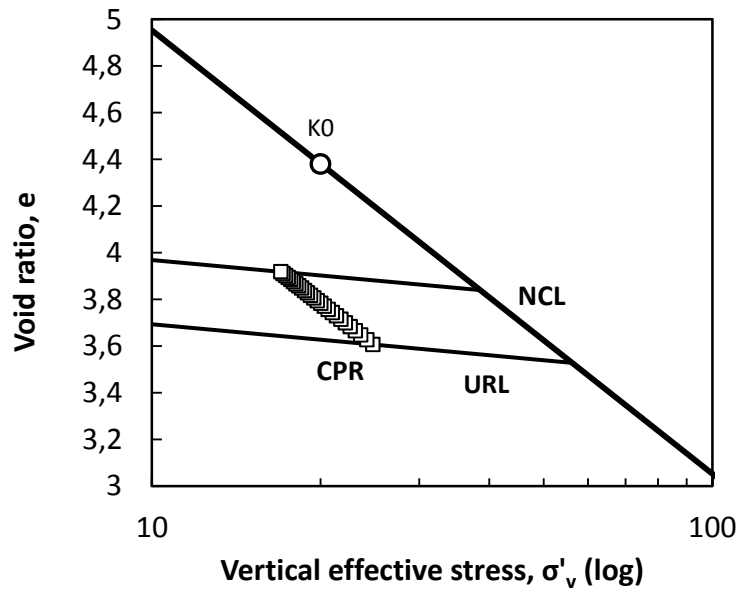
Figure 5.13: Results in the plane $e - \log \sigma'_z$ for $\alpha = 0.368$.
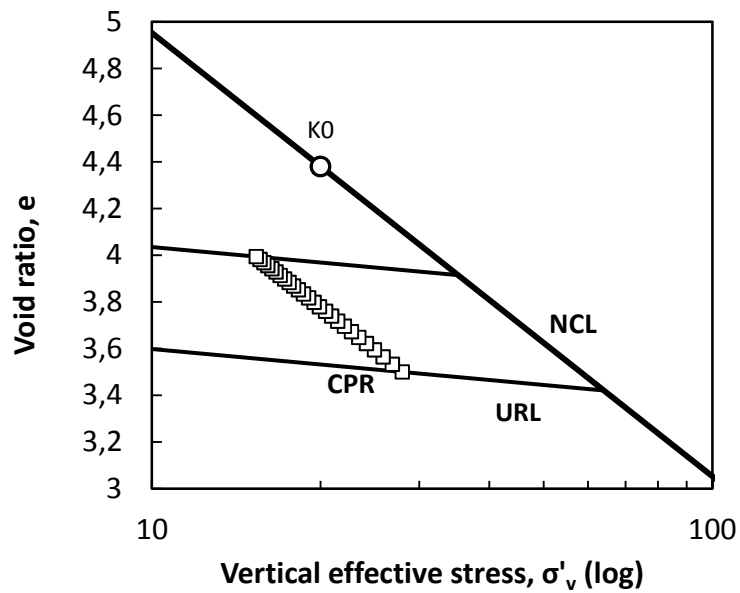
Figure 5.14: Results in the plane $e - \log \sigma'_z$ for $\alpha = 0.584$.

6 Simplified method for predicting embankment settlement

The aim of this section is to develop an analytical solution that is able to predict both settlement and degree of consolidation of soils subjected to CPRGrouting.

6.1 Consolidation with vertical drains

If a three-dimensional process of consolidation is symmetrical about an axis, it is more convenient to replace the cartesian coordinates by cylindrical polar coordinates, thus the differential equation governing the consolidation process is give as (Terzaghi, 1943):

$$\frac{\partial u}{\partial t} = c_h \left[\frac{1}{r} \frac{\partial u}{\partial r} + \frac{\partial^2 u}{\partial r^2} \right] + c_v \frac{\partial^2 u}{\partial z^2} \tag{6.1}$$

where the permeability in the radial direction is considered different from the vertical one. The two coefficients of consolidation are given by the equations:

$$c_v = \frac{k_v}{\gamma_w m_v} \quad \text{and} \quad c_h = \frac{k_h}{\gamma_w m_v} \tag{6.2}$$

If the vertical coefficient of permeability k_v is equal to n times the horizontal coefficient of permeability k_h, therefore the ratio between the two coefficient of consolidation is equal to n, i.e.:

$$\frac{k_v}{k_h} = \frac{c_v}{c_h} \tag{6.3}$$

Carrillo (1942) have shown, however, that Eq. 6.1 can be solved separating the problem into parts. The former consists in solving the radial flow in the horizontal plane, represented by the differential equation:

$$\frac{\partial u}{\partial t} = c_h \left[\frac{1}{r} \frac{\partial u}{\partial r} + \frac{\partial^2 u}{\partial r^2} \right] \tag{6.4}$$

and the latter is the one-dimensional consolidation in the vertical direction:

$$\frac{\partial u}{\partial t} = c_v \frac{\partial^2 u}{\partial z^2} \tag{6.5}$$

Finally, the overall degree of consolidation of the three-dimensional problem can be evaluated with the following expression:

$$(1 - U) = (1 - U_v)(1 - U_h) \tag{6.6}$$

in which U_r is given by solving Eq.6.4 and U_v is the average vertical degree of consolidation from Terzaghi's one-dimensional consolidation solution (Eq. 6.5).

Barron (1948) presented the first exhaustive solution of Eq. 6.4 to the problem of a soil cylinder containing a central sand drain. He assumed two types of vertical strain that might occur in the subsoil, namely: (1) uniform vertical surcharge on the ground surface ("free strain" condition), and (2) uniform vertical deformation of the surface ("equal strain" condition). The solution under assumption (2) gained popularity due to its simplicity and, however, Barron (1948) showed that the numerical value of the average degree of consolidation obtained by assuming equal strains is almost equal to the value obtained by assuming that the strains in the soil develop freely in full accordance with the rate of pore pressure dissipation (the so-called free strain condition).

Time later, Hansbo (1981) has improved Barron's solution in order to take into account the smear and the drain resistance effects. The solution is valid under the following assumptions:

- instantaneous loading,
- equal strains irrespective of the radial distance from the drain centre,
- the drain is fully penetrating and has a cylindrical shape with diameter d_w. It has limited discharge capacity $q_w = k_w A_w$,
- the installation of a drain causes a circular-cylindrical zone of smear around the drain with diameter d_s and lower permeability k_s than in the undisturbed soil,
- Darcy's law is valid, the soil is fully saturated and the water flow in the vertical direction in the soil between the drains is neglected

The radial degree of consolidation is given by the following approximate expression

(Rixner et al., 1986; Bergado et al., 1996):

$$U_h = 1 - \exp(-8T_h/F) \tag{6.7}$$

with:

$$T_h = \frac{c_h t}{d_e^2} \quad \text{(time factor)} \tag{6.8}$$

and

$$F = F(n) + F_s + F_r \tag{6.9}$$

where d_e is the diameter of the equivalent soil cylinder (see Fig. 6.1) and F is the factor that express the additive effect due to the spacing of drains, smear effect and well resistance. For this reason, in literature F is usually decomposed in three terms as shown in Eq 6.9. The spacing factor is given as:

$$F(n) = \frac{n^2}{n^2 - 1} \ln(n) - \frac{3n^2 - 1}{4n^2} \tag{6.10}$$

however, for values of the ratio $n = d_e/d_w \geq 20$, is usually approximated as:

$$F(n) = \ln \frac{d_e}{d_w} - 0.75 \tag{6.11}$$

the smear effect factor is given as:

$$F_s = \left[\frac{k_h}{k_s} - 1\right] \ln \frac{d_s}{d_w} \tag{6.12}$$

the well resistance factor is given as:

$$F_r = \pi z(2H_d - z)\frac{k_h}{q_w} \tag{6.13}$$

where d_w is the equivalent diameter of the drain, d_s is the diameter of the disturbed zone, k_h is the horizontal hydraulic conductivity in the undisturbed soil and k_s in the disturbed zone, H is the length of the drainage path (H is equal to the length of the PVD in the improved zone when drainage occurs at one end only or half of the length of the PVD when drainage occurs at both ends) and $q_w = k_w A_w$ is the discharge capacity of the drain at unit hydraulic gradient.

It can be seen that the degree of consolidation varies with depth if there is well

resistance. To calculate an average value of degree of consolidation for the entire layer, it is necessary integrating from zero to L the term $\pi z(2H_d - z)k_h/q_w$, where L is the length of the PVD drain. For the one-way drainage follows $L = H$ and an average value can be obtained as:

$$\frac{1}{H}\int_0^H \pi z(2H_d - z)\frac{k_h}{q_w}\,dz = \frac{\pi}{H}\frac{k_h}{q_w}\left[z^2 H_d - \frac{z^3}{3}\right]_0^H = \frac{2\pi H_d^2}{3}\frac{k_h}{q_w} \tag{6.14}$$

while for the two-way drainage, $L = 2H$, and the average value is:

$$\frac{1}{2H}\int_0^{2H} \pi z(2H_d - z)\frac{k_h}{q_w}\,dz = \frac{\pi}{2H}\frac{k_h}{q_w}\left[z^2 H_d - \frac{z^3}{3}\right]_0^{2H} = \frac{2\pi H_d^2}{3}\frac{k_h}{q_w} \tag{6.15}$$

Thus, the following formula can be utilized as an approximation of Eq. 6.9:

$$F = \ln\frac{d_e}{d_w} - 0.75 + \left[\frac{k_h}{k_s} - 1\right]\ln\frac{d_s}{d_w} + \frac{2\pi H_d^2}{3}\frac{k_h}{q_w} \tag{6.16}$$

From Eqs. 6.7 and 6.20, the time, t, to obtain a given degree of consolidation,U_h, at an assumed spacing of PVD, is given as follows:

$$t = F\frac{d_e^2}{8c_h}\ln\frac{1}{1 - U_h} \tag{6.17}$$

The degree of consolidation in the vertical direction U_v can be evaluated with a good order of approximation with the following formulas (Terzaghi, 1943):

$$\begin{aligned} T_v &= \frac{\pi}{4}U_v^2 & U_v \leq 52.6\% \\ T_v &= -0,085 - 0.933\log_{10}(1 - U_v) & U_v > 52.6\% \end{aligned} \tag{6.18}$$

in which the vertical time factor

$$T_v = \frac{c_v\,t}{H_d^2} \tag{6.19}$$

assumes different values depending on the drainage condition. The above equation is suitable for the present case of instantaneous loading. Finally, by means of Eqs. 6.6, 6.7 and 6.18, given the final primary consolidation settlement, ρ_∞, the settlement at any time t is calculated by:

$$\rho(t) = \rho_\infty U \tag{6.20}$$
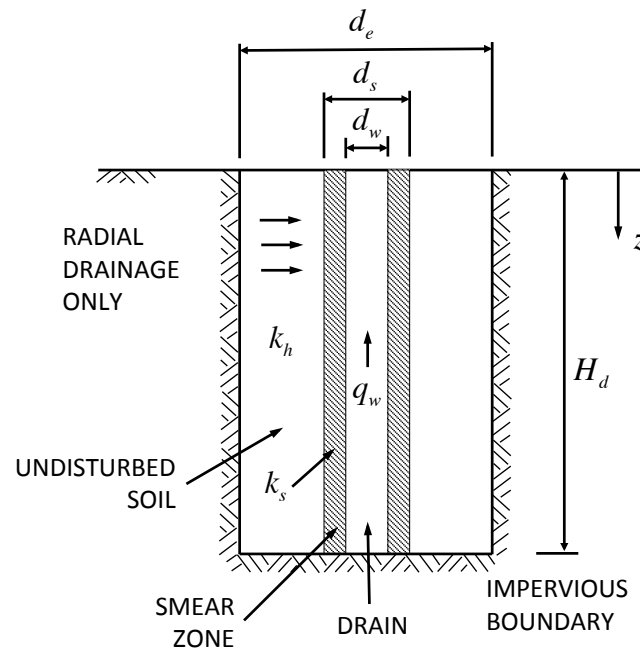
Figure 6.1: Schematic representation of a PVD unit cell with drain resistance and soil disturbance. Adapted from Rixner et al. (1986).

in this way the curve settlement versus time is constructed.

6.1.1 Simplified methods for considering vertical drains

As introduced in the previous sections, the *unit cell* in the CPR Grouting has a drainage system that can be simplified as a continuous cylindrical drain wall (see Fig. 6.2). This simplification was proposed firstly by Indraratna et al. (2008) for deriving an analytical solution of PVDs system under circular embankments and it was improved later by Ye et al. (2012) for the consolidation of soil-cement columns with PVDs. In such a transformation, within the unit cell an equivalent horizontal permeability is introduced in order to take into account the effect of the several drains present on the boundary. For clarity, the development of the analytical model is proposed below.

According to Indraratna et al. (2008) the mainly assumptions of Hansbo's solution hold, except the well resistance that is neglected. It is assumed that the cylindrical drain wall has a negligible thickness and D denotes its diameter. Let S denote the drain spacing, that is related to D depending on the pattern used. The relationship
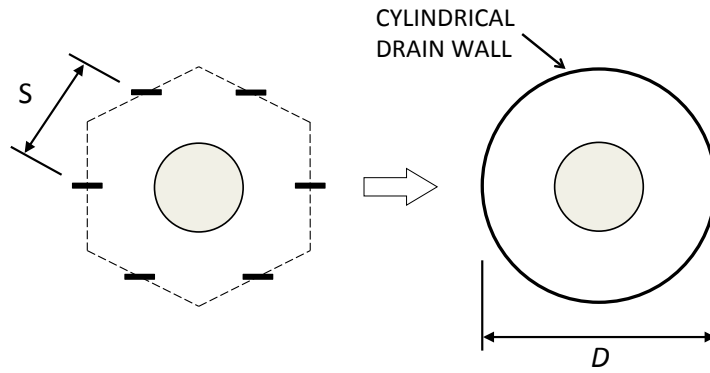
Figure 6.2: The PVDs on the boundary are transformed in a continuous drain wall.

between S and D is shown in Table 6.1 for four suitable cases. The ratio $\mu = D/d_e$ relates the equivalent diameter D of the *unit cell* with the the equivalent diameter d_e of the soil cylinder surrounding the drain as in conventional PVDs theory.

Consider a disk shape control volume of radius r and height dz. During a period Δt, the radial outflow through the lateral surface that bound the control volume is expressed by:

$$Q_{r_{\text{out}}} = -2\pi r \, \frac{k_h'}{\gamma_w} \frac{\partial u}{\partial r} \, dz \, \Delta t \tag{6.21}$$

where $u(r, z, t)$ is the excess pore pressure, k_h' is the transformed horizontal hydraulic conductivity and $2\pi r dz$ is the area of the lateral surface. Introducing the average excess pore water pressure within the horizontal cross section of the unit cell:

$$\bar{u}(z, t) = \frac{4}{\pi D^2} \int_0^{D/2} u(r, z, t) \cdot 2\pi r \, dr \tag{6.22}$$
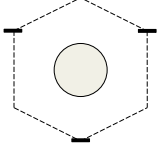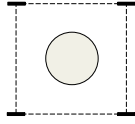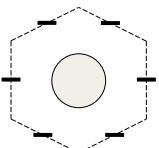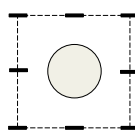
then, the vertical inflow through the bottom surface can be expressed as:

$$Q_{z_{\text{in}}} = \pi r^2 \frac{k_v}{\gamma_w} \frac{\partial}{\partial z} \left(\bar{u} + \frac{\partial \bar{u}}{\partial z} dz \right) \Delta t \tag{6.23}$$

where k_v is the real vertical hydraulic conductivity of the soil and πr^2 is the control volume base area. Note that a Taylor's expansion has been used for writing the differential form of the term $\bar{u}(z + dz, t)$. The vertical outflow is:

$$Q_{z_{\text{out}}} = \pi r^2 \frac{k_v}{\gamma_w} \frac{\partial \bar{u}}{\partial z} \Delta t \tag{6.24}$$

Table 6.1: Equivalent diameters depending on the used pattern.

Unit cell type	d_e/S	D/S	$D/d_e = \mu$
	$2\sqrt{\dfrac{\cos 30°}{\pi}}$	$2\sqrt{\dfrac{\cos 30°}{\pi}}$	1
	$\dfrac{2}{\sqrt{\pi}}$	$\dfrac{2}{\sqrt{\pi}}$	1
	$\sqrt{\dfrac{6\cos 30°}{\pi}}$	$4\sqrt{\dfrac{\cos 30°}{\pi}}$	$\dfrac{2\sqrt{6}}{3}$
	$2\sqrt{\dfrac{4}{3\pi}}$	$\dfrac{4}{\sqrt{\pi}}$	$\sqrt{3}$

$$S = \text{drain spacing}$$

Under the "equal strain" assumption the horizontal sections of the soil remain horizontal throughout the consolidation process, hence the reduction of soil volume during the same time interval is expressed as:

$$\Delta V = \pi r^2 \frac{\partial \epsilon}{\partial t} \, dz \, \Delta t \tag{6.25}$$

Due to the load being maintained constant and applied instantaneously, by means of introducing the oedometric compressibility, m_v, it follows that:

$$\frac{\partial \epsilon}{\partial t} = -m_v \frac{\partial \bar{\sigma}'_z}{\partial t} = m_v \frac{\partial \bar{u}}{\partial t} \tag{6.26}$$

Note that soil dilation is taken as positive, thus the increase of the effective stress

involves a corresponding decrease in volume. Finally, the balance of water flow is applied:

$$\Delta V = Q_{\text{in}} - Q_{\text{out}} \tag{6.27}$$

Obtaining from Eqs. 6.21, 6.23, 6.24, 6.25 and 6.26 the following partial differential equation:

$$\frac{k_v}{\gamma_w} \frac{\partial^2 \bar{u}}{\partial z^2} + \frac{k'_h}{\gamma_w} \frac{2}{r} \frac{\partial u}{\partial r} = m_v \frac{\partial \bar{u}}{\partial t} \tag{6.28}$$

or equivalently

$$c_v \frac{\partial^2 \bar{u}}{\partial z^2} + c'_h \frac{2}{r} \frac{\partial u}{\partial r} = \frac{\partial \bar{u}}{\partial t} \tag{6.29}$$

in which the consolidation coefficients c'_h and c_v have been introduced:

$$c_v = \frac{k_v}{\gamma_w m_v}, \quad c'_h = \frac{k'_h}{\gamma_w m_v} \tag{6.30}$$

A preliminary integration of Eq. 6.29 is possible because at the boundary the excess pore pressure is set to zero (since the well-resistance of the drain wall is neglected). The boundary condition is then $u = 0$ at $r = D/2$. The integration yields:

$$u = \frac{1}{4c'_h} \left(\frac{D^2}{4} - r^2 \right) \left(c_v \frac{\partial^2 \bar{u}}{\partial z^2} - \frac{\partial \bar{u}}{\partial t} \right)$$

that integrated over again according to Eq. 6.22 gives:

$$\bar{u} = \frac{D^2}{32} \frac{c_v}{c'_h} \frac{\partial^2 \bar{u}}{\partial z^2} - \frac{D^2}{32} \frac{1}{c'_h} \frac{\partial \bar{u}}{\partial t} \tag{6.31}$$

The above pde has to be solved under the following boundary and initial conditions:

$$\bar{u} = 0, \qquad z = 0 \tag{6.32}$$

$$\frac{\partial \bar{u}}{\partial z} = 0, \qquad z = H_d \tag{6.33}$$

$$\bar{u} = \bar{u}_0, \qquad t = 0 \tag{6.34}$$

Using the Fourier method of separation of variables, the average excess pore water pressure has the following form (Ye et al., 2012):

$$\bar{u} = \bar{u}_0 \sum_{i=0}^{\infty} \frac{2}{M} \sin\left(\frac{Mz}{H_d} \right) e^{-\beta_i t} \tag{6.35}$$

in which

$$M = \frac{\pi}{2}(2i + 1) \tag{6.36}$$

$$\beta_i = M^2 \frac{c_v}{H_d^2} + 32 \frac{c_h'}{D^2} \tag{6.37}$$

Equation 6.35 is formally similar to Terzaghi's solution. Actually, if we denote with $f(t, z)$ the classical solution for the one-dimensional consolidation problem (see Terzaghi (1943)), Eq. 6.35 can be rewritten as the following:

$$\bar{u} = f(z, t) \cdot \exp\left[-32 \frac{c_h'}{D^2} t\right] \tag{6.38}$$

in perfect agreement with Carrillo's (1942) separation (see Eq. 6.6). The right-hand factor of the product in the above equation can be equated to Hansbo's solution (Eq. 6.7) on the basis of equivalent average radial degree of consolidation to get the ratio between the real and equivalent horizontal hydraulic conductivities:

$$\frac{k_h'}{k_h} = \frac{c_h'}{c_h} = \frac{\mu^2}{4F} \tag{6.39}$$

where $\mu = D/d_e$ as stated above (see Tab. 6.1) and F is the factor according to Eq. 6.16, however omitting the well resistance, i.e. $q_w = \infty$.

In order to simplify the consolidation analysis, to represent the contribution of PVDs by means of solving a one-dimensional problem, Zhang et al. (2006) used an equivalent vertical hydraulic conductivity k_v' that can be obtained considering only the first term of the series in both Terzaghi's and present (Eq. 6.35) solutions. In this way, an approximate consolidation analysis is constructed adopting the following coefficient of vertical hydraulic conductivity:

$$k_v' = \left(1 + \frac{128}{\pi^2} \frac{H_d^2}{D^2} \frac{k_h'}{k_v}\right) k_v \tag{6.40}$$

Effectively, the correct transformation should take into account an equivalence that holds for all the terms of the series. The drawback of the approximation proposed by Zhang et al. (2006) is evident in Fig. 6.3, in which we can observe an accelerated consolidation process, because the coefficient of consolidation results overestimated in the middle term analysis. On the other hand, for degree of consolidation greater
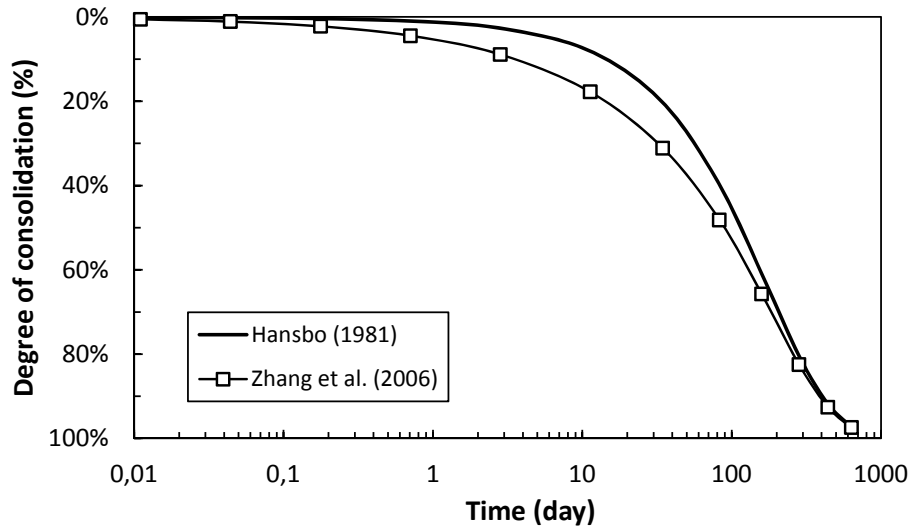
Figure 6.3: Comparison between PVDs classical approach (no well resistance) and the approximate method proposed by Zhang et al. (2006).

than 70% the approximation is notably good.

6.2 Approach to equivalent stiffness

The grouted soil can be assumed as a composite material, where the grout bulbs represent the reinforcement. In the theory of composite materials, for a fiber-reinforced material, the equivalent stiffness (or strength) is determined by means of the theory of elasticity introducing several simplifying assumptions. The most prominent is that the strain in the fiber direction is the same in the fiber as in the matrix. It allows to predict the equivalent elastic modulus in the direction of the fibers according the rule of mixtures (Voigt model). For the present case, the adjusted expression is:

$$E_1 = (1 - \beta)E_s + \beta E_g \tag{6.41}$$

where E_s is the elastic modulus of the soil, E_g is the elastic modulus of the grout bulbs and β is the volume fraction of the grout (final substitution ratio or replacement ratio). The Poisson's ratio is obtained in a manner similar to that of E_1. Several theories for a composite foundation reinforced by columns are developed on the basis that both soil

and columns undergo to the same strain, according to the equal strain assumption. From it follows that the composite modulus is derived according to Eq. 6.41, that however represents an upper bound value and it may lead to unconservative results, i.e. the stiffness can be overestimated. Moreover, when stone columns are used, the reinforcing material has an appreciable continuity that, in the case of a grouted soil, is not obvious any more. Consequently, the choice of a proper equivalent modulus is crucial.

The apparent Young's modulus in the direction transversal to the fibers is obtained by assuming that the matrix and the fibers undergo to the same transverse stress. In this way, the equivalent elastic modulus in the direction transverse to the fibers is determined by means of the inverse rule of mixtures (Reuss model):

$$\frac{1}{E_2} = \frac{1-\beta}{E_s} + \frac{\beta}{E_g} \tag{6.42}$$

On the basis of the principle of minimum complementary energy it can be proved that Eq. 6.42 is a lower bound on the apparent modulus for a composite material. On the other hand, the application of the principle of minimum potential energy leads to the upper bound on the equivalent elastic modulus, which coincides approximately with Eq. 6.41. For more details, see for example Jones (1975), whose book reports the expression for the equivalent elastic modulus of a composite material that is stiffened by dispersion of cube-shaped particles (see Figure 6.4(a)), also defined as Paul model. Considering the iso-strain condition, the expression in the case of a soil-grout composite becomes:

$$\frac{E}{E_s} = \frac{E_s + (E_g - E_s)\beta^{2/3}}{E_s + (E_g - E_s)(1 - \beta^{1/3})\beta^{2/3}} \tag{6.43}$$

According to the upper/lower bound limits, the value of E is always between E_1 and E_2. Still following Jones (1975), the value of Poisson's ratio for the composite material has been derived explicitly as:

$$\nu = \frac{(1-\nu_s-2\nu_s^2)\beta\nu_g E_g + (1-\nu_g-2\nu_g^2)(1-\beta)\nu_s E_s}{(1-\nu_s-2\nu_s^2)\beta E_g + (1-\nu_g-2\nu_g^2)(1-\beta)E_s} \tag{6.44}$$

If we assume that the grout is much stiffer than the grout, i.e. $E_g >> E_s$, Eq. 6.43

can be approximated as:

$$\frac{E}{E_s} = \frac{1}{1 - \beta^{1/3}} \tag{6.45}$$

As shown in Fig. 6.5, the approximation becomes valid when the elastic modulus of the grout is a hundred times the soil modulus. The modified Paul model consider instead a cubic inclusion a spherical particle within a cubic shaped matrix (see Figure 6.4(b)).Botas et al. (2008) give the expression for the composite elastic modulus in the following form:

$$\frac{E}{E_s} = \left[(1 - 2R) - \frac{1}{k\sqrt{R^2 - \frac{1}{k}}} \ln \left| \frac{R - \sqrt{R^2 - \frac{1}{k}}}{R - \sqrt{R^2 - \frac{1}{k}}} \right| \right]^{-1} \tag{6.46}$$

where $R = \sqrt[3]{\frac{3\beta}{4\pi}}$ is the radius of the spherical particle and $k = \pi(E_g/E_s - 1)$. As done before, assuming the grout as a rigid reinforcement, the above expression can be approximated as:

$$\frac{E}{E_s} = \frac{1}{1 - 2R} \tag{6.47}$$

which is quite similar to Eq. 6.43, but it gives greater values for the prediction of the equivalent stiffness, being $2R \approx 1.24\,\beta^{1/3}$. The sphere within the control volume behaves like an internal constraint whose dimensions cannot be exceeded by the diameter of the enclosed spherical particle. Therefore, as pointed out by Botas et al. (2008), there must exist a maximum reinforcement volume fraction value, that is:

$$\beta_{\max} = 52\%$$

High volume fractions imply a denser packing accommodation which generates a strong anisotropy (Botas et al., 2008). Hence, the particle dispersed model should be used within a low range of volume fractions, that is the case of the CPR Grouting.

If we consider that the ratios between the composite and matrix modulus does not vary much, relatively:

$$\frac{E}{E_s} \approx \frac{G}{G_s} \approx \frac{K}{K_s} \dots \text{etc.}$$

then, the oedometric compressibility of the composite material, m_v', can be estimated

(a) Paul Model

(b) Modified Paul model.
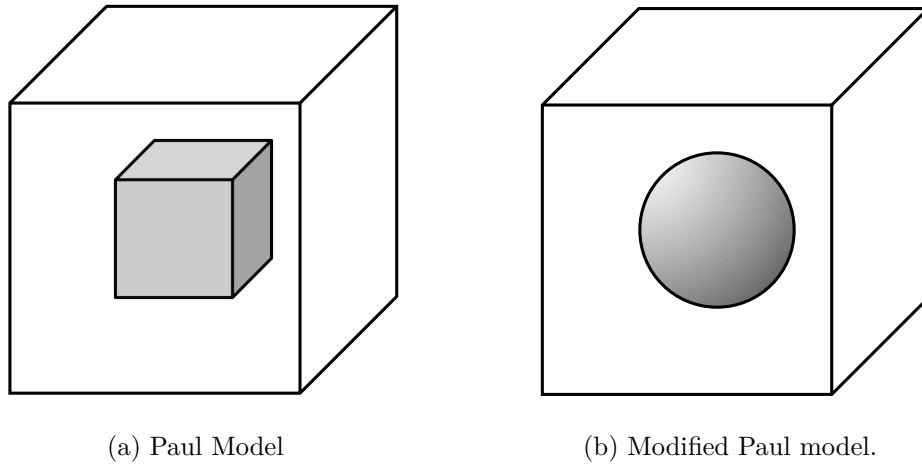
Figure 6.4: Unit cell and particle reinforcement for dispersed composite models.

as:

$$m'_v = m_v(1 - \beta^{1/3}) \qquad \text{(Paul Model)} \qquad (6.48)$$

$$m'_v = m_v(1 - 1.24\beta^{1/3}) \qquad \text{(Modified Paul Model)} \qquad (6.49)$$

where m_v is the oedometric compressibility of the soil after the treatment, which is not equal to that of the natural soil, having changed its stress field to a higher mean effective stress.

The proposed approach considers that the spatial distribution of the reinforcement is such that, at a large scale, the composite material is homogeneous and isotropic. Considering the values that β assumes in the range of interest of the technique, a comparison is made by plotting in Fig. 6.6 the results obtained from Eqs. 6.42, 6.46 and 6.47 considering $E_g = \infty$.

6.3 Proposed simplified analysis

By means of use of two transformation, the former for obtaining an equivalent vertical hydraulic conductivity, the latter for deriving an equivalent oedometric compressibility, it is possible finally to write down the equivalent coefficient of consolidation for the soil-grout composite:

$$c'_v = \frac{k'_v}{\gamma_w m'_v} \qquad (6.50)$$
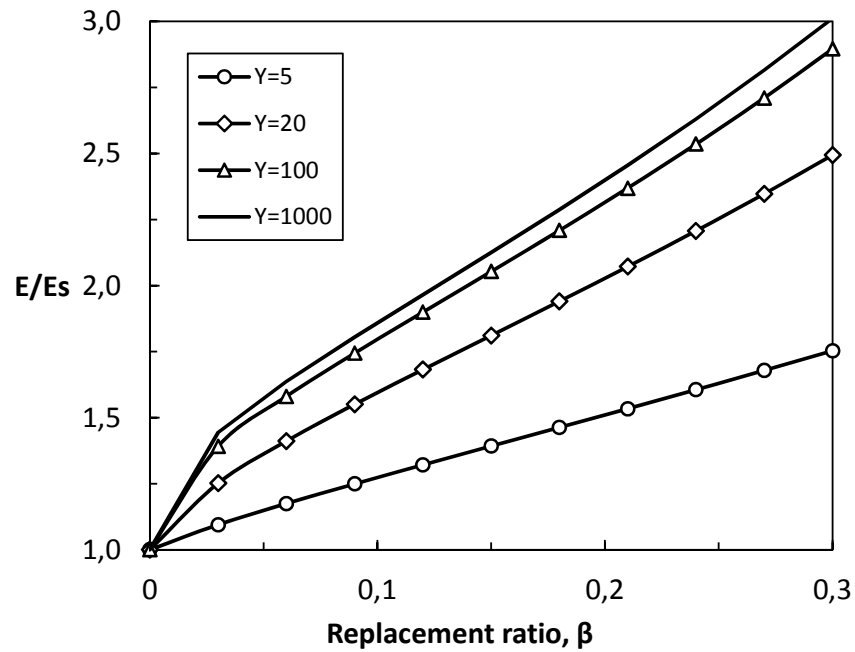
Figure 6.5: Effect of stiffness ratio $Y = E_g/E_s$ on the equivalent modulus E of the composite material.
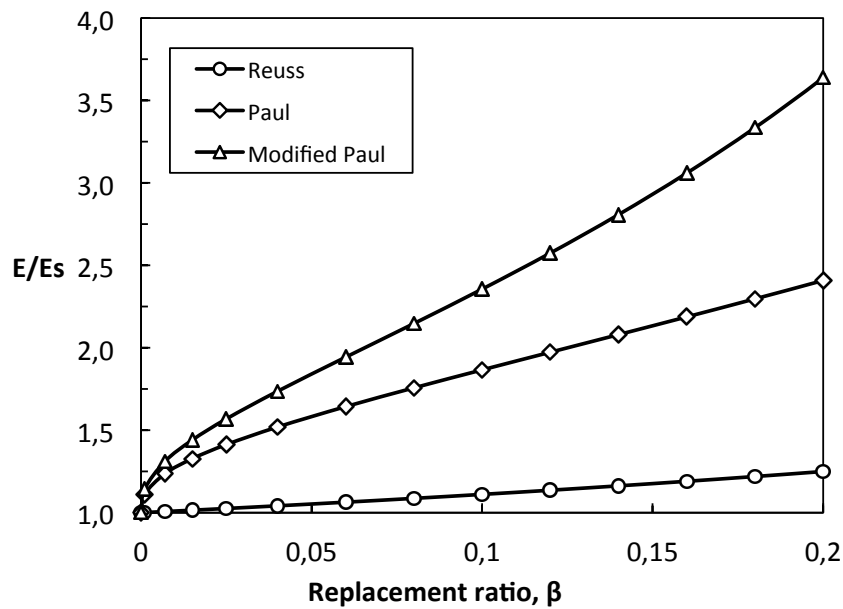
Figure 6.6: Composite stiffness for rigid inclusions.

where k'_v is the equivalent hydraulic conductivity as expressed by Eq. 6.40 (that represents the contribution of the PVD system) and m'_v is the oedometric compressibility as in Eq. 6.48 or in Eq. 6.49 (to take into account the effect of grout inclusions). In this way, denoting with $\bar{u}$ the average excess pore pressure, the analysis reduces to solving the following differential equation:

$$c'_v \frac{\partial^2 \bar{u}}{\partial z^2} = \frac{\partial \bar{u}}{\partial t} \tag{6.51}$$

which is identical to Terzaghi's 1D consolidation theory in formats, except the modified consolidation coefficient. Its solution is straightforward and quickly permits a consolidation analysis since the equivalent parameters k'_v and m'_v are estimated correctly.

Part IV

Validation and Calibration

7 Model Validation and Verification

7.1 Monitoring settlement of two test embankments in Recreio dos Bandeirantes: a case study

For the purpose of studying the effectiveness of the CPR Grouting two test embankments were built. One of them was constructed over a treated soil (Embankment A), the other one was built over an improved soil with only PVDs (Embankment B). Both were instrumented and their settlements were monitored over a period of approximately five months. Informations about the soil properties, the construction and the monitoring equipment are further discussed in details.

7.1.1 Description of the embankments

On August 14, 2014, the field works started with the area demarcation, six months later the construction of the pioneer layer.[1] On August 18, the drain system was positioned for both future embankments. An equilateral triangular pattern was adopted with spacing $S = 1.5$ m.

Embankment B The day after, in the area of embankment B the previous pioneer layer was removed (with its geotextile reinforcement), consisting in an excavation 1.30 m deep, and a new granular layer approximately 1.20 m high was placed. On August 20, there was the installation of the field instrumentation for monitoring settlement and excess pore water pressure. The embankment B construction started on September 13 and ended on September 15.

Embankment A On September 3, 2014, the CPR Grouting was applied in the area of embankment A across the whole thickness of the soft clay layer. On September

---

[1]An initial layer constructed over a weak roadbed where selected material is used to provide a stable platform for the construction of subsequent layers.
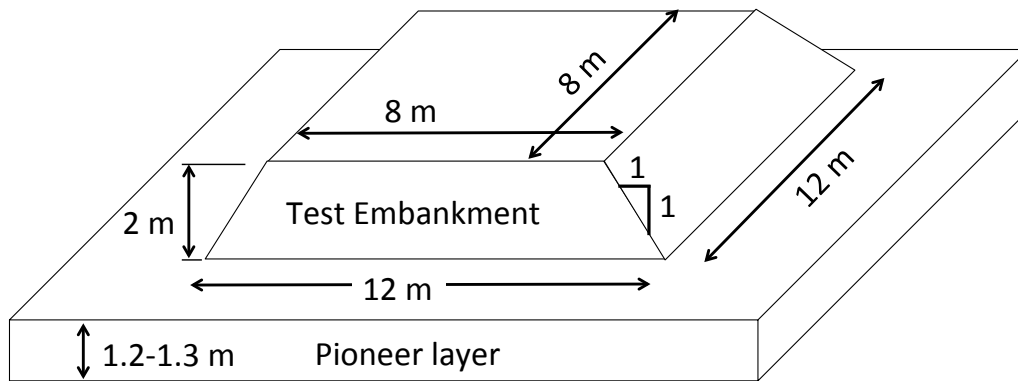
Figure 7.1: Geometry of the test embankments

9, the area was instrumented, as already done for the area of embankment B. The embankment construction started on September 16 and ended on September 19.

For both embankments the same instrumentation was adopted, namely:

- No. 3 settlement plates
- No. 2 piezometers with different deep penetration
- No. 1 inclinometer

The embankments had the same dimensions and were built using the same sandy material, to have a better experimental comparison. The embankment fill reached 2 meter high and covered and square surface of 12×12 m. The embankment side slope inclination was 1:1. For a better comprehension refer to Fig. 7.1. The unit weight of the fill used for the calculations is 17.5 kN/m^3 for both the pioneer layer and the embankments.

7.1.2 Geotechnical field characterization and modelling

7.2 Field investigations

Field investigations showed the presence of the alternation of clayey and sandy layer, a peculiarity of the whole region. For redacting of the geotechnical model, only the tests localized in the neighbourhood of the test embankment will be considered. The tests locations are shown in Figure A.1 (see Appendix), field testing included Standard

Penetration Tests (SPT), Cone Penetration Tests with pore pressure measure (CPTu), Vane Shear Test (VST) and Pressuremeter tests (PMT). Laboratory testing consisted in an oedometric test carried out on undisturbed sample.

The interpretation of the SPT logs SP3, SP9 and SP14, leads to a model divided in three layers, composed in the upper part of two clayey layers (organic brown clayey silt and grey sandy clay) above a firm and pervious sandy base. The model involves a soil volume up to a depth equal to the width of the base of the embankment. In this way, the contribution of the deeper layers are not taken into account for the calculation of the consolidation settlements. Visual inspection of the SPT logs (see Appendix) indicates that the soft soil is 8 meters deep. Its geotechnical properties have been determined during the oedometric test, that is resumed in Figure A.5 (see Appendix).

The PMT tests carried out at depths of 3.0 and 6.0 meters offered the elastic parameters to carry out the settlement analysis. The pressure-expansion curves are reported in Figure A.6 (see Appendix) and shows how "soft" the soil is. The results are summarized in Table 7.1. Specimens recovered at different depths suggested values of the unit weight around 12 kN/m^3 at the surface, with an increase to 13.5 kN/m^3 at greater depths. In the same manner, they showed that the void index decreases with depth and this feature will be enclosed in the geotechnical model, schematically represented in Fig. 7.2.

Table 7.1: Geotechnical parameters from pressuremeter tests.

Test	p_0	p_L	G	s_u
PMT 1 3m	36 kPa	50 kPa	108 kPa	3.7 kPa
PMT 1 6m	66 kPa	90 kPa	226 kPa	6.7 kPa

An important event must be added to the starting model. Actually, it is mandatory to take into consideration the previous realization of the pioneer layer, that happened approximately six month before the execution of the test. In addition, according to field measurements, it induced a consolidation settlement that was accelerated by the installation of the drain system. As a results, the stresses in the field must be corrected and this aspects must be taken into account during the settlement calculation.

The simulation of the stress history will be executed by means of a numerical
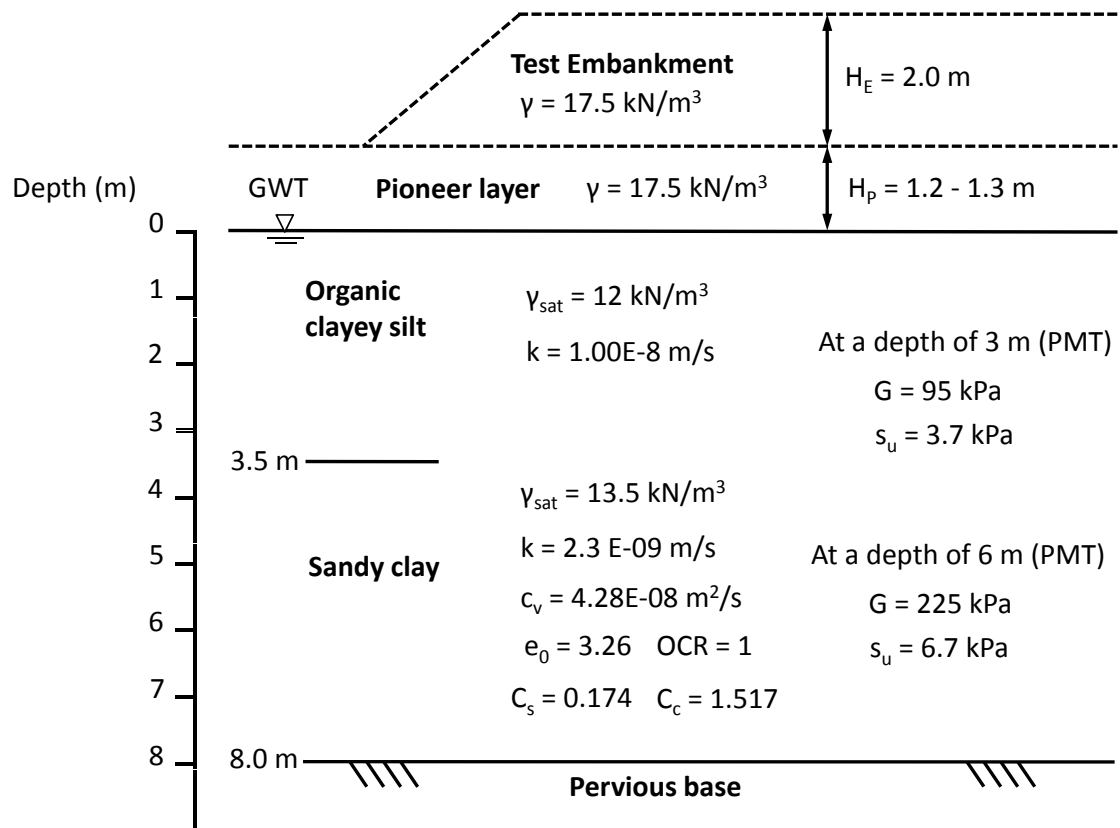
Figure 7.2: Geotechnical model

Table 7.2: Soil data sets parameters employed in the numerical analysis.

EP const. model		Sand-Embankment	Sandy Clay	Organic clayey silt
γ_{unsat}	kN/m^3	17,5	10	10
γ_{sat}	kN/m^3	20	12	13.5
k_v	m/day	1	1.987E-04	4.320E-04
k_h	m/day	1	5.962E-04	1.296E-03
E	kPa	4,000E+04	607.5	189
ν	–		0.3	0.35	0.35
G	kPa	1.538E+04	225	70
E_{oed}	kPa	5.385E+04	975	303.3
ϕ	degrees	32	26	26
c	kPa	1	1	1
ψ	degrees	2	0	0

analysis with PLAXIS, considering an equivalent circular embankment of external radius equal to $1.13 \times 6 = 6.78$ m and internal radius equal to $1.13 \times 4 = 4.52$ m. This allows an axisymmetric analysis. The PVDs installation varies the consolidation behaviour of the soil, and this will be taken into account by introducing an equivalent vertical hydraulic conductivity as illustrated by Zhang et al. (2006). In this way, the analysis will be simplified into a one-dimensional problem. For clarity, the expression that provides this transformation is here recalled:

$$k'_v = \left(1 + \frac{32}{\pi^2 F} \frac{H^2}{d_e^2} \frac{k_h}{k_v}\right) k_v \qquad (7.1)$$

where H is the height of the vertical drainage path, d_e is the equivalent diameter of the PVD unit cell, and F is the reduction factor due to spacing and smear effects. For a better comprehension of the adopted notation refer to section 6.1. The PVD parameters required to calculate the equivalent vertical permeability are given in Table 7.3. The pattern used was the equilateral triangle. With these parameters and Eq. 7.1 it is possible to establish a ratio between the real and fictitious vertical hydraulic conductivities, that is approximately equal to $k'_v = 13.86 \, k_v$. In this way, the hydraulic effect of the PVD system is treated as an equivalent vertical permeability.

In the numerical model no flow is allowed across the lateral boundaries in order to generate a vertical seepage only. The material properties are taken from the geotechnical model in Fig. 7.2. The numerical model used is shown in Figure 7.3, the element used is the 16 nodes triangle, under the axisymmetric condition. The soil behaviour is modelled using the Mohr-Coulomb soil model – which is an elasto-plastic model. The stages are those that really happened in the field, in particular they consist in:

1. the realization of the pioneer layer, with a construction time of 7 days;

2. a waiting period of 180 days;

3. the installation of the PVDs system, that is modelled modifying the vertical hydraulic conductivities;

4. a waiting period of $15 + 15 = 30$ days (the soil treatment was executed 15 days after the PVDs installation, the embankment was constructed 15 days after);

5. the application of the surface load with a ramp model of 3 days;

6. the consequent settlement observable in 150 days.

In Figure 7.4 is reported the settlement trend with time at the centreline of the embankment, at a point immediately below the pioneer layer. The profile clearly
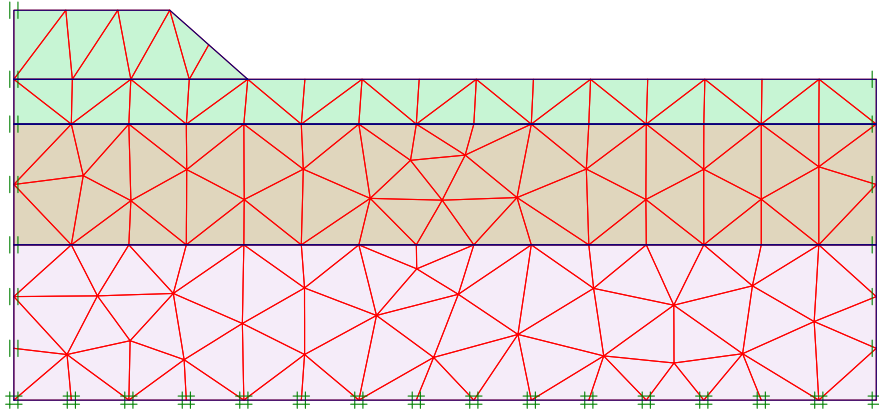
Figure 7.3: Mesh used for the numerical analysis.

identifies and acceleration after the PVD installation. The calculated settlement due to both the pioneer layer and embankment is approximately 0.80 m for the case of PVD only.

The CPR Grouting improved soil is treated as an equivalent soil model, in which the stiffness and the permeability are introduced by means of homogenization techniques. In particular, the drain system is modelled using an equivalent vertical permeability, as described in section 6.1.1. The gain in stiffness due to the treatment is calculated taken into account the increase in mean effective stress and the rigid inclusions. As a matter of fact, the elastic shear modulus of the CPR treated soil is obtained by using the following expression:

$$G' = G_0 \, \frac{p'}{p'_0} \, \frac{1}{1 - \beta^{1/3}} \tag{7.2}$$

In the above equation is stated that the stiffness is proportional to the mean effective stress, p', increased due to the grouting process. Indeed, the displacement of the ground due to the expansions leads to a radial consolidation that increases the horizontal effective stress in the ground. Furthermore, being many thousands times stiffer, the grout can the treated as a rigid inclusion within the soil mass. In this study it is seen that the Paul model is a composite model that can be employed to estimate the composite stiffness of the grouted soil. In this way a simplified analysis

Table 7.3: PVD parameters for conversion to 1D condition.

S	d_w	H	n	s	k_h/k_s	k_h/k_v
1.5 m	0.0525 m	4 m	30	3	3	3
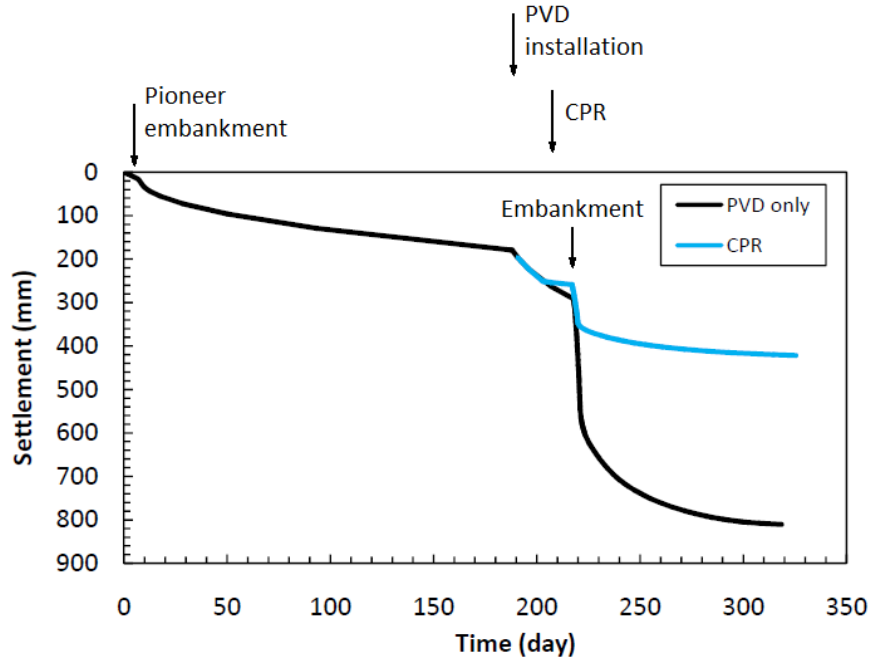
Figure 7.4: Trend of settlement with time for the whole analysis, in which the most important events are indicated.

is carried out, multiplying the original stiffness for a factor that takes into account the above mentioned aspects.

7.2.1 Homogenization of the treated soil

A detailed study of the simulated stress field has been made by means of calculations carried out using the soil parameters presented in Table 7.4 for normally consolidated soil under a overburden effective stress of $\sigma'_{v0} = 12$ kPa. A triangular pattern is chosen with a drain spacing equal to 1.5 m and a raising step of 1 m. Then, the substitution ratio is $R_S = 11.55\%$, that corresponds to a grout volume $V_g = 900$ l. The analysis showed that the best prediction was obtained considering the minimum mean effective stress, that corresponds to the maximum value of the parameter α, in its turn being upper limited by the failure condition: $\alpha < 1 - K_a$. As a consequence,

Table 7.4: Parameters of the modified Cam Clay model used for stress field calculation.

e_0	λ	κ	Λ	Γ	N	ϕ'	M	ν'
3.26	0.659	0.076	0.885	5.45	7.79	26°	1.027	0.35

the tangential earth pressure coefficient reaches its minimum, since $\alpha = 1 - K_\theta/K_r$. The best fit condition is presented in the following table:

α	K_r	K_θ	p'_0	p'
0.580	1.966	0.827	8.5 kPa	14.8 kPa

Finally, the equivalent stiffness is calculated according to Equation 7.2:

$$\frac{G'}{G_0} = \frac{p'}{p'_0} \frac{1}{1 - \beta^{1/3}} = \frac{14.8}{8.5} \times \frac{1}{1 - 0.1155^{1/3}} = 3.394$$

To calculate the equivalent vertical hydraulic conductivity the following conditions have been used:

- The treated soil is totally smeared, i.e. the diameter of the smear zone coincides to the diameter of the drain unit cell;
- The smeared soil has a conductivity equal to 1/10 that of the orginal soil;

All the calculation have been carried out according to section 6.1.1. From the calculation results that the hydraulic conductivity of the treated soil is 2.19 times that of the original one.

7.2.2 Measured settlements and prediction with new design approach

Figures 7.5 and 7.6 show the comparison between the measured and calculated settlement for both embankments. The numerical results matched well with the measured data. For the CPR embankment the measures started with the application of the 2 meters test embankment, while for the PVD only treated ground, settlements have been monitored for a weeks before the test embankment construction.
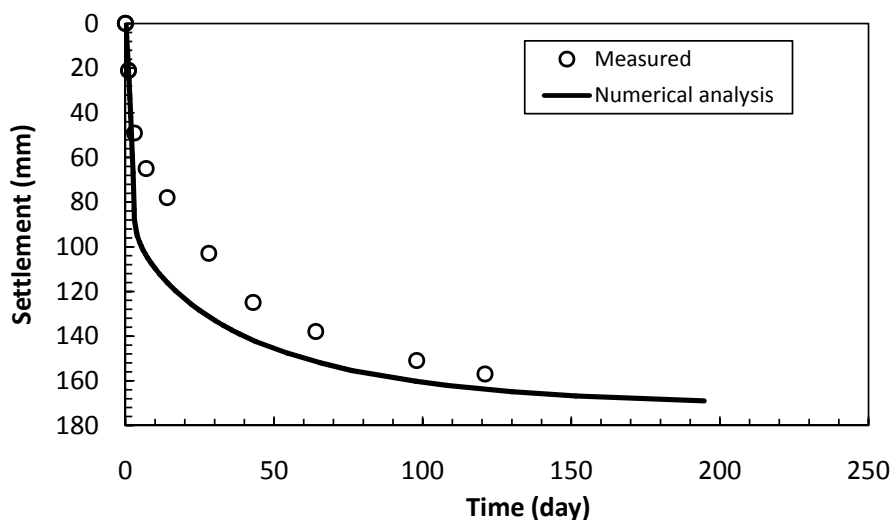
Figure 7.5: Comparison between numerical result and measured settlement for Embankment A (CPR).

7.2.3 Conclusions

The case history study shows that the homogenizationapproach reasonably simulated the field behaviour of the CPR Grouting treated soil. The numerical results demonstrated that the CPR Grouting can accelerate the consolidation of the treated ground, as well as it can minimize its settlements. However, the elasto-plastic constitutive model resulted into exaggerated immediate settlements, compared to those measured in the field for both embankments. The use of a secant stiffness caused this discrepancy.Although, for the case of CPR improved soil, the final calculated settlement was very similar to the measured one. For the embankment B (PVD only) the analysis resulted in an overestimation of the final settlement. This can be justified, if we consider that the soil surrounding the embankment was subjected to the CPR Grouting. As a consequence, the soil beneath the embankment could not displace horizontally, resulting in lesser settlement.

Equation 7.2 needs some final remarks. It should be noted that its formulation is purely arbitrary and without any experimental support. Although the stiffness increases with mean effective stress, it is not verificated that the relationship is linear. On the contrary, it seem more reasonable that the law should be nonlinear. For this
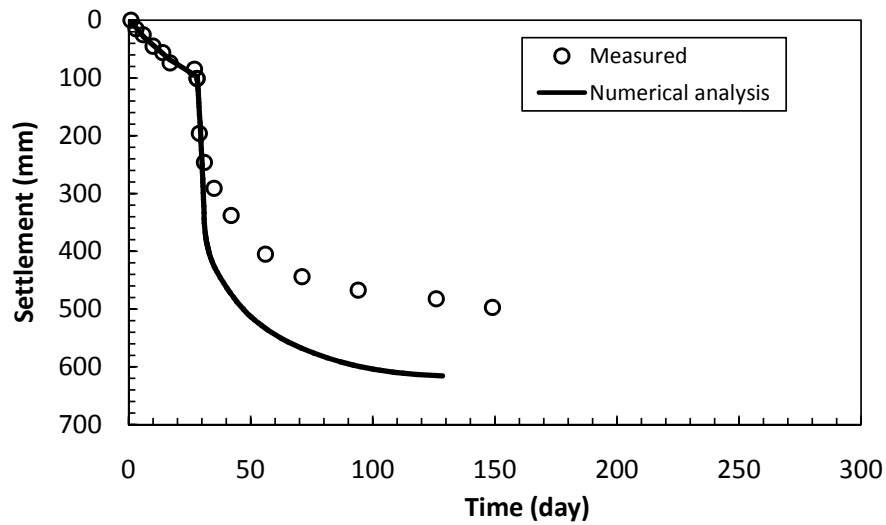
Figure 7.6: Comparison between numerical result and measured settlement for Embankment B (PVD only).

reason, Equation 7.2 shoul be rewritten in a more general form, like the following:

$$G' = G_0 \left(\frac{p'}{p'_0}\right)^m \frac{1}{1 - \chi\beta^{1/3}} \tag{7.3}$$

where m and χ are parameters that range within the interval $0.6 - 1$ and $1 - 1.24$, respectively. Further investigations are needed in order to establish a reliable value for both. Furthermore, as last remark, the use of a more complex constitutive model is highly necessar, but this goes beyond the aim of the research.

8 Comparison with DJM-PVD combined method

8.1 Dry Jet Mixing with Prefabricated Vertical Drains

Dry Jet Mixing (DJM) uses mixing blades to mix dry reagents, such as cement or lime, or other dry powders or particles with sizes less than 5 mm, with in situ soil to increase the strength and reduce the compressibility of the soft ground. DJM does not need water for slurry preparation, since DJM columns are created from the in situ saturated soil. Obviously, the reagent used depends on the soil properties and the mechanical requirements of the columns. The reagent dosage can be adjusted to different soil strata. The whole process is controlled by an advanced automatic monitoring system which continously monitorates the depth, penetration and withdrawal speeds, blade rotation speed, and reagent injection rate.

Dry Jet Mixed (DJM) and Prefabricated Vertical Drains (PVD) have been used in combination to enhance the performance of soft ground in highway construction in China. Because this tecnology can effectively reduce the settlement and increase the stability of soft ground, it rapidly sperad throughout China in 1990s. However, according to Zhang et al. (2006, 2009), the DJM installation has the following problems: (1) DJM is relatively expensive due to small column spacing (1.1 to 1.5 m); (2) the improvement depth is limited to 15 m; (3) DJM installation may reduce the strenght of the surrounding soil; (4) the DJM columns may suddenly sink into the grounf after the installation. To overcome this disadvantages, a new technique was proposed by combining the DJM method with PVDs.

Due to the similarity between the DJM-PVD and the CPR Grouting - both methods already use PVD from execution procedure to consolidate the soil - the comparison between them is considered well suitable.
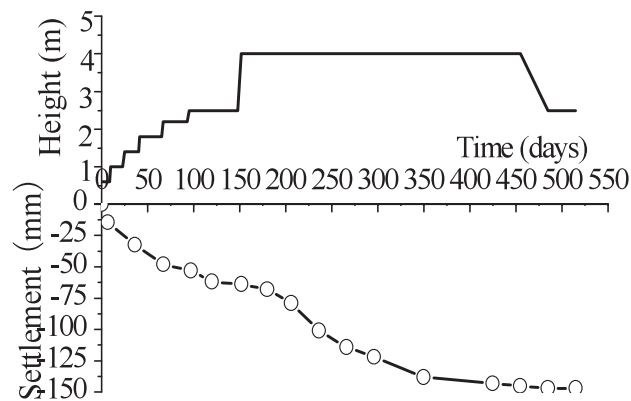
Figure 8.1: Comparison between numerical result and measured settlement for Embankment B (PVD only).

8.2 Huai-Yan highway embankment in China

Still folowing Zhang et al. (2006, 2009), to permit the construction of an highway embankment in China the DJM-PVD combined method was used. The Huai-Yan highway (a major highway in Jiangsu Province of China) has four lanes in both sides, with an embankment height of 3.7–4.3 m. The technical challenge consisted in constructing the embankment over a soft soil about 10 m thick. Indeed, the sites consist in three layers, which includes the top crust layer 1.5 to 2 m thick, the second soft clay layer with a thickness of 8.8 to 10 m, and the third hard clay base layer.

Before the installation of PVDs, a 0.3 m pioneer layer was placed. PVD was installed on a triangular pattern 2.2 m spaced, to a depth of 13 m. After that, the DJM columns were installed according to the same grid, to the same depth. The DJM column was not completely penetrated through the hard clay base layer. All colums had a diameter of 0.5 m, a common size used in China. Then, the replacement ratio used was 4,73%. The embankment construction began one month after the columns intallation. The monitored settlement at the centerline and the embankment height against time are reported in Figure 8.1. The final settlement was estimated to be 199 mm.

Table 8.1: Subsoil and embankment fill parameters adopted by Zhang et al. (2009) for FEM analysis of Huai-Yan highway embankment in China. Section K19+760

	γ (kN/m^3)	E (MPa)	ν -	c (kPa)	ϕ (°)	k_v ($\times 10^4$ m/d)
Crust	18.0	10	0.30	20	15	1
Soft clay*	16.0	2.0+0.2z	0.35	10+z	15	1.63
Hard clay	19.0	6	0.30	15	20	1.63
Embankment	20.0	30	0.30	400	35	
DJM column	**	80	0.30	400	0	

* The properties increase per linear meter depth.
** The unit weight is assumed to be the same of the surrounding soil.

Table 8.2: PVD parameters for conversion to 1D condition.

H_d	d_w	n	s	k_h/k_s	k_h/k_v	q_w	k_w/k_h
13 m	0.05 m	46.2	6	3	2	100 m^3/year	10^4

8.2.1 Numerical modelling

In an initial paper, Zhang et al. (2006) carried out a simplified consolidation analysis considering two construction stages. The first 2.0 m embankment was constructed in 50 days. After that, 75 days were left for soil consolidation, and the last 2.0 m were constructed also in 50 days. The unloading after 450 days was not considered. In a second paper, Zhang et al. (2009)) carried out a FEM analysis using PLAXIS 2D, assuming the unit cell mode in axisymmetric condition. They used the Mohr-Coulomb model (elasto-plastic constitutive model with Mohr-Coulomb failure criterion) for all layers.The parameters are provided in Table 8.1. Linear elastic model was used for the DJM columns. Further details can be obtained in their original paper. The unit cell model is reported in Figure 8.2. The PVD parameters are shown in Table 8.2.

8.3 Numerical simulation of CPR Grouting

Based on the data provided in the previous section, a numerical analysis will be carried out in order to simulate the CPR Grouting treatment. The aim of this virtual
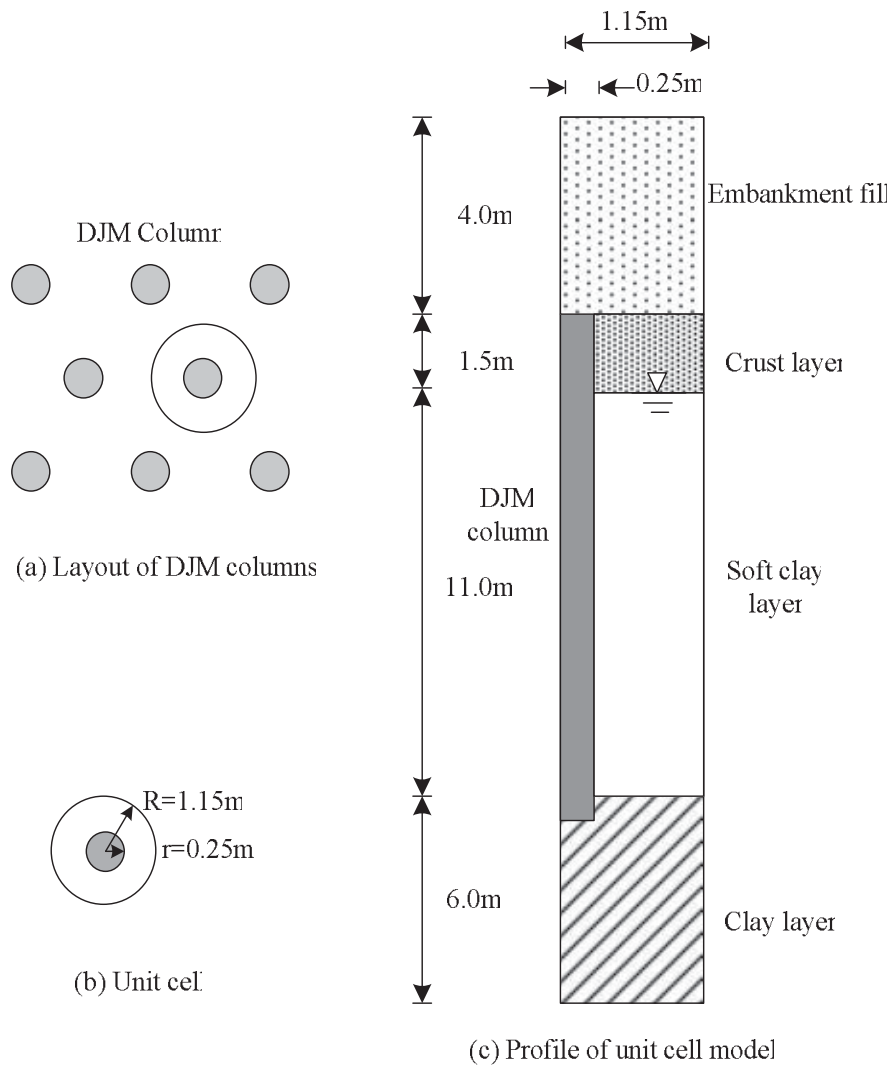
Figure 8.2: Unit cell model used by Zhang et al. (2009) for FEM analysis.

Table 8.3: Geotechnical properties of Jiangsu marine soft clay. Values from Zhang et al. (2006) and Miao and Kavazanjian Jr. (2007)[a].

w (%)	LL (%)	PI (%)	e_0 -	C_c [a]	C_s -	OCR [a]	ν -	ϕ' (°)
63.0	68.9	27.4	1.7	$-0.704 + 0.022w = 0.68$	0.1*	1	0.35	15

* Assumed value

experiment is to get a comparison between it and the DJM-PVD method. For this reason, the same replacement ratio will be used, i.e. the substitution ratio for the CPR Grouting will be very close to 4.73%. Indeed, it is choosen a drain system consisting in a triangular pattern with 2.2 m spacing, and a grout expanded volume of 800 l, so it follows that $R_S = 4.77\%$. The geotechnical parameters are those presented by Zhang et al. (2006), as average values, and the compression index is estimated according to the correlationship presented by (Miao and Kavazanjian Jr., 2007) for Jiangsu marine soft clay. The physical and mechanical indices are shown in Table 8.3.

To calculate the equivalent vertical hydraulic conductivity the conditions established in the previous chapter have been used, here recalled:

- The treated soil is totally smeared, i.e. the diameter of the smear zone coincides to the diameter of the drain unit cell;
- The smeared soil has a conductivity equal to 1/10 that of the orginal soil;

All the calculation have been carried out according to section 6.1.1. From the calculation it results that the hydraulic conductivity of the treated soil is 4.5 times the original one. The simulated stress field after the application of the CPR Grouting has been made considering a normally consolidated soil under a overburden effective stress of $\sigma'_{v0} = 57$ kPa. The minimum mean effective stress calculated is equal to 61.8 kPa, while the maximum is 74.0 kPa. An average value is considered. Then, the equivalent stiffness is calculated according to Equation 7.2:

$$\frac{E'}{E_0} = \frac{p'}{p'_0} \frac{1}{1 - \beta^{1/3}} = \frac{67.9}{47.2} \times \frac{1}{1 - 0.0477^{1/3}} = 2.26$$

The numerical model used to carry out the comparison is resumed in Figure 8.3. The construction stages are those used by Zhang et al. (2006) in their simplified analysis.

Table 8.4: Consolidation rate and dissipation of pore water pressure.

Case	u_{max} (kPa)	Consolidation degree after 455 days	Time for $U = 90\%$ (days)
Unimproved*	74.3	30.1	4620
DJM-PVD*	37.2	91.0	432
CPR	38.4	79.3	704

* Results taken from Zhang et al. (2009).

Figure 8.4 presents a comparison of the measured settlement, the numerical result obtained by Zhang et al. (2009) and the result of this study. In the present analysis, the unloading phase was not considered. It can be seen that the settlement on the top of the DJM column is not equal to that of the surrounding soil. The differential settlement is a tipical disadvantage of all ground improving methods that use columnar inclusions. The comparison verifies the competence of the numerical modelling. The simulated CPR Grouting treatment shows a better mechanical response, since its final settlement is about 150 mm, less than DJM-PVD improved ground. Hovever, the consolidation rate of CPR improved ground is lower than DJM-PVD combined improved ground. A comparison betweem excess pore pressure at the middle of soft clay layer is shown in Table 8.4.

The numerical analysis results indicate that the consolidation of the ground improved by CPR Grouting is not as fast as the DJM-PVD combined method, although the same excess pore pressure has been calculated. However, the final settlement is lower for the same substitution ratio. The better performance of the CPR Grouting is due to the consolidation process promoted during the cavity expansions. However, this process may reduce the hydraulic conductivity of the soil due to smear or it may compromit the hydraulic efficiency of the drains, leading to a longer consolidation.

ID	Name	Type	γ_{unsat} [kN/m^3]	γ_{sat} [kN/m^3]	k_x [m/day]	k_y [m/day]	ν [-]
1	Crust	Drained	18,0	18,0	1,0000E-4	4,5000E-4	0,30
2	Soft clay CPR Grouting	Undrained	16,0	16,0	3,2600E-4	7,3350E-4	0,35
3	Clay layer	Undrained	19,0	19,0	3,2600E-4	7,3350E-4	0,30
4	Embankment	Drained	20,0	20,0	0,1000	0,1000	0,30

E_{ref} [kN/m^2]	c_{ref} [kN/m^2]	φ [°]	ψ [°]	E_{incr} [kN/m^3]	c_{incr} [kN/m^3]	y_{ref} [m]	T-Strength [kN/m^2]	R_{inter} [-]
10000,0	20,0	15,0	0,0	0,0	0,0	0,0	0,0	1,00
4520,0	10,0	15,0	0,0	452,0	1,0	17,0	0,0	1,00
6000,0	15,0	20,0	0,0	0,0	0,0	0,0	0,0	1,00
30000,0	1,0	35,0	0,0	0,0	0,0	0,0	0,0	1,00

Figure 8.3: Unit cell model used in the present study for FEM analysis.
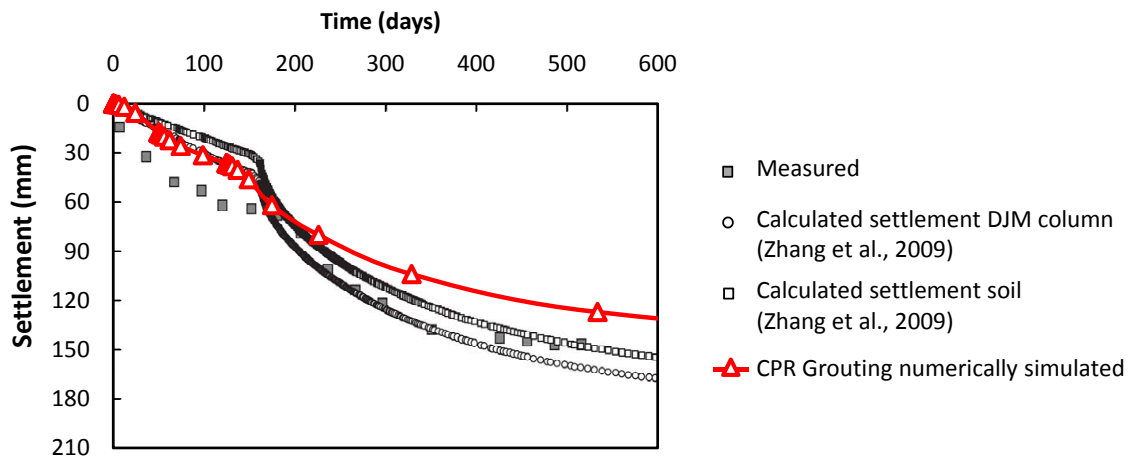
Figure 8.4: Vertical displacement at the inteface between crust and embankment.

9 Conclusions

The CPR Grouting has been investigated by means of a literature review and comparison of all similar grouting technique (especially compensation and compaction grouting) and a theoretical approach has been used in order to establish a design method for future applications. Several new concepts has been introduced in this work. First of all, the concept of unit cell has been reviewed and improved by introducing the Substitution Ratio, R_S, defined as *the volume of grout injected in an undeformed unit cell* (Eq. 4.2):

$$R_S = \frac{V_g}{Ah}$$

An expression for the prevision of the of the void ratio change due to the grouting process has been derived and it was showed that the zero grout efficiency assumption is valid in the case of normally consolidated soils and non-simultaneous injections. Neglecting the volume of the borehole, the expression becomes (Eq. 4.9):

$$e = (1 - \lambda_c R_S)(1 + e_0) - 1$$

For correct estimations, a balloon expansion test should be carried out to provide the real value of the grout efficiency or, equivalently, the volume loss ratio due to consolidation effect. Determining the coefficient λ_c by laboratory tests is crucial to predict the void ratio reduction. Note that λ_c depends mostly on OCR and R_S.

As a consequence of the void index reduction, by means of the modified Cam Clay model, the gain in undrained strength due to the grouting has been calculated knowing the compression ratio of the clay and the variation of the void ratio (Eq. 4.14):

$$\frac{s_u}{s_{u0}} = \exp\left(2.3\,\lambda_c\,R_S\,\frac{1+e_0}{C_c}\right)$$

The above expression refers only to the strength of the soil around the grout bulbs. At the present time, there is no method for estimating the bearing capacity of CPR

Grouting improved soil, that takes into account the presence of the rigid inclusion into the ground. The development of a theoretical approach for this purpose is necessary.

The cavity expansion theory outlined the stress field and excess pore pressure induced during the formation of the bulbs. The results show that generally three zones – the external elastic zone, the intermediate plastic zone, and the internal critical state failure zone – may coexist around the cavity. It is found that within the critical state region the effective stresses are practically constant and no excess pore pressure is generated in the elastic zone. The critical state model suggests to adopt a horizontal spacing between grouting points at most equal to the diameter of the critical state region around the expanding cavity. The failure mechanism nearby the surface offering the lowest limit pressure is the cylindrical one, instead the conical failure usually admitted in compaction grouting literature.

A model has been developed to provide the stress state after the dissipation of the pore pressure due to the expansions. This has been done by introducing the hypothesis that the vertical stress does not vary so much. However, the proposed method does not provide a unique result, but it allows to identify an interval of possible and admissible values of mean effective stress post CPR Grouting. Field tests are needed to validate and improve the proposed formulation.

Finally, a simplified method for predicting embankment settlement has been proposed. The simplification allows to carry out a Terzaghi's one dimensional consolidation analysis, since the equivalent parameters k_v' and m_v' are estimated correctly. In this way, a consolidation curve can be easily constructed for practically purposes by calculating an equivalent coefficient of consolidation, by its definition.

Further investigations are necessary to calibrate the model parameters for the correct modelling of the PVD drain system, indeed, although the expressions are simple (Eqs. 6.16, 6.39 and 6.40):

$$F = \ln \frac{d_e}{d_w} - 0.75 + \left[\frac{k_h}{k_s} - 1\right] \ln \frac{d_s}{d_w}$$

$$\frac{k_h'}{k_h} = \frac{c_h'}{c_h} = \frac{\mu^2}{4F}$$

$$k_v' = \left(1 + \frac{128}{\pi^2} \frac{H_d^2}{D^2} \frac{k_h'}{k_v}\right) k_v$$

they need a lot of parameters to be calibrated. The most important is the smear

zone identification, represented by the ratio d_s/d_w, that is not dependent on the PVD installation any more, but it is caused by the expansion grouting process. It must be clarified the loss of drains discharge capacity due to bending induced by the expansion of bulbs. A deeper study concernig the destructuration during cavity expansion and its effects on permeability and stiffness is strongly necessary.

The results show significant alteration of the stress state and the soil stiffness after the expansion of bulbs. As a consequence, embankment settlements are reduced due to two major effects: the ground movements and the stiffness of the composite soil. Indeed, the displacement of the ground due to the expansions leads to a radial consolidation that increases the horizontal effective stress in the ground, improving the compressibility characteristics of the soil. Furthermore, being many thousands times stiffer, the grout can the treated as a rigid inclusion within the soil mass. In this study it is seen that the Paul model is a composite model that can be employed to estimate the composite stiffness of the grouted soil (Eqs. 6.48 and 6.49):

$$m_v' = m_v(1 - \beta^{1/3}) \qquad \text{(Paul Model)}$$
$$m_v' = m_v(1 - 1.24\beta^{1/3}) \qquad \text{(Modified Paul Model)}$$

The choice of Paul model with rigid inclusions has been suggested by two aspects: (1) there are irregularities in the geometry of the bulbs - the shape is not spherical - and, in general, there is no vertical alignment and contact between them; (2) after hardened, the geogrout has strength and rigidity thousand times higher than the surrounding soil.

Many other model are available in the literature, but the Paul model is favored due to its simplicity and its approach, which considers a non-continuous dispersed reinforcement. More complex constitutive models are preferred to be used. Unfortunately, almost all of them employ a linear elastic relationship. a series of field test or a back analysis of historical field settlement curves must be carried out to give a correct expression for the estimation of the improved soil compressibility. It is necessary to point out that the conventional field tests (SPT, CPTu or Vane test) are not exhaustive to assess the mechanical properties of the treated soil, because they analyze only the soil (matrix), disconsidering the reinforcement or vice versa. Thus, not testing the whole assembly, but only one of its components, it is not correctly evaluated the gain of rigidity obtained by the ground improvement.

To validate the proposed design method two real test embankments were studied,

one constructed over a CPR Grouting improved soil, one over an PVD improved soil. The case history study shows that the homogenization approach reasonably simulated the field behaviour of the CPR Grouting treated soil. The numerical results demonstrated that the CPR Grouting can accelerate the consolidation of the treated ground, as well as it can minimize its settlements. However, the elasto-plastic constitutive model resulted into exaggerated immediate settlements, compared to those measured in the field for both embankments. The use of a secant stiffness caused this discrepancy.

It should be noted that the formulation for predicting the stiffness of the consolidated soil around the bulbs is purely arbitrary and without any experimental support. Further investigations are needed in order to establish a reliable value for the parameters m and χ in Equation 7.3, here recalled:

$$G' = G_0 \left(\frac{p'}{p'_0} \right)^m \frac{1}{1 - \chi \beta^{1/3}}$$

As last remark, the use of a more complex constitutive model (as instance, the structured critical state model) is highly necessar, but this goes beyond the aim of the research.

Bibliography

Almeida, M. S. S. and Marques, M. E. S. (2010). *Aterros sobre solos moles 2ª ed. Projeto e desempenho.* Coleção Huesker: engenharia com geossintéticos. Oficina de Textos, São Paulo.

Au, S. K. A., Soga, K., Jafari, M. R., Bolton, M. D., and K., K. (2003). Factors affecting long-term efficiency of compensation grouting in clays. *J. Geotech. Geoenviron. Eng. ASCE*, 129(3):254–362.

Au, S. K. A., Yeung, A. T., and Soga, K. (2006). Pressure-controlled cavity expansion in clay. *Can. Geotech. J.*, 43(7):714–725.

Au, S. K. A., Yeung, A. T., Soga, K., and Cheng, Y. M. (2007). Effects of subsurface cavity expansion in clays. *Géotechnique*, 57(10):821–830.

Balaam, N. and Booker, J. R. (1981). Analysis of rigid rafts supported by granular piles. *International Journal for Numerical and Analytical Methods in Geomechanics*, 5(4):379–403.

Baligh, M. (1985). Strain path method. *Journal of Geotechnical Engineering*, 111(9):1108–1136.

Barron, R. A. (1948). Consolidation of fine-grained soils by drain wells. *Transactions of the ASCE*, 113:718–742.

Bergado, D., Anderson, L. R., Miura, N., and Balasubramaniam, A. S. (1996). *Soft Ground Improvement: In Lowland and Other Environment.* Amer Society of Civil Engineers.

Botas, J. D., Velhinho, A., and Silva, R. J. C. (2008). Elastic behaviour of spherical particles reinforced metal-matrix composites. *Materials Science Forum*, pages 202–206.

Brand, E. and Brenner, R. (1981). *Soft Clay Engineering*. Developments in Geotechnical Engineering. Elsevier Science.

Campos, A. C. S. L. (2007). Características de compressibilidade de uma argila mole da zona industrial de Santa Cruz. MSc thesis, PUC Rio, Rio de Janeiro.

Cao, L. F., Teh, C. I., and Chang, M. F. (2001). Undrained cavity expansion in modified cam clay i: Theoretical analysis. *Géotechnique*, 51(4):323–334.

Carrillo, N. (1942). Simple two - and three-dimensional cases in the theory of consolidation of soils. *Journal of Mathematical Physics*, 21:11–18.

Carter, J. P., Randolph, M. F., and Wroth, C. P. (1979). Stress and pore pressure changes in clay during and after the expansion of a cylindrical cavity. *International Journal for Numerical and Analytical Methods in Geomechanics*, 3(4):305–322.

Castro, J. and Sagaseta, C. (2009). Consolidation around stone columns. influence of column deformation. *International Journal for Numerical and Analytical Methods in Geomechanics*, 33(7):851–877.

Chen, T.-l., Zhang, L.-y., and Zhang, D.-l. (2014). An fem/vof hybrid formulation for fracture grouting modelling. *Computers and Geotechnics*, 58:14–27.

Chew, S.-H. and Bharati, S. K. (2016). Arresting settlement of clay using low-pressure grouting. *Proceedings of the Institution of Civil Engineers - Ground Improvement*, 169(1):22–35.

Collins, I. F. and Yu, H. S. (1996). Undrained expansion of cavities in critical state soils. *International Journal for Numerical and Analytical Methods in Geomechanics*, 20(7):489–516.

de Mello, M. A. (2013). A consolidação profunda radial aplicada em solo compressível na Lagoa Rodrigo de Freitas/RJ. MSc thesis, Instituto Militar de Engenharia, Rio de Janeiro.

El-Kelesh, A. M., Mossaad, M. E., and Basha, I. M. (2001). Model of compaction grouting. *Journal of geotechnical and geoenvironmental engineering*, 127(11):955–964.

Fung, Y. and Tong, P. (2001). *Classical and Computational Solid Mechanics.* Advanced series in Engineering Science. World Scientific.

Gibson, R. E. and Anderson, W. F. (1961). In-situ measurement of soil properties with the pressuremeter. *Civ. Engng Public Works Rev.*, 56:615–618.

Hansbo, S. (1981). Consolidation of fine-grained soils by prefabricated drains. *Proc. 10th Int. Conf. on Soil Mech. and Found. Eng.*, 3:677–682.

Hansbo, S. (1994). *Foundation engineering*, volume 75 of Developments in Geotechnical Engineering. Newnes.

Hill, R. (1950). *The Mathematical Theory of Plasticity.* The Oxford Engineering Science Series. Oxford Press, Oxford.

Indraratna, B., Aljorany, A., and Rujikiatkamjorn, C. (2008). Analytical and numerical modeling of consolidation by vertical drain beneath a circular embankment. *Int. J. of Geomech.*, 8(3):199–206.

Indraratna, B., Rujikiatkamjorn, C., Wijeyakulasuriya, V., McIntosh, G., and Kelly, R. (2010). Soft soils improved by prefabricated vertical drains: performance and prediction.

Jones, R. (1975). *Mechanics of Composite Materials.* International student edition. Scripta Book Company.

Komiya, K., Soga, K., Agaki, H., Jafari, M. R., and Bolton, M. D. (2001). Soil consolidation associated with grouting during shield tunnelling in soft clayey ground. *Géotechnique*, 51(10):835–846.

Landau, L. and Lifshitz, E. (1970). *Theory of Elasticity.* Volume 7 of A Course of Theoretical Physics. Pergamon Press.

Lorenzo, G. A. and Bergado, D. T. (2003). New consolidation equation for soil cement pile improved ground. *Canadian Geotechnical Journal*, 40(2):265–275.

Miao, L. and Kavazanjian Jr., E. (2007). Secondary compression features of Jiangsu soft marine clay. *Marine Georesources & Geotechnology*, 25(2):129–144.

Nichols, S. and Goodings, D. (2000). Effects of grout composition, depth and injection rate on compaction grouting. *Advances in Grouting and Ground Modification*, pages 16–31.

Priebe, H. J. (1995). The design of vibro replacement. *Ground engineering*, 28(10):31.

Riccio, M., Baroni, M., and Almeida, M. (2013). Ground improvement in soft soils in rio de janeiro: the case of the athletes' park. *Proceedings of the Institution of Civil Engineers - Civil Engineering*, 166(6):36–43.

Rixner, J. J., Kraemer, S. R., and Smith, A. D. (1986). *Prefabricated Vertical Drains.* Vol. I, Engineering Guidelines. Federal Highway Administration, Washington, D.C.

Silvestri, V. and Abou-Samra, G. (2011). Application of the exact constitutive relationship of modified cam clay to the undrained expansion of a spherical cavity. *International Journal for Numerical and Analytical Methods in Geomechanics*, 35(1):53–66.

Soga, K., Au, S. K. A., Jafari, M. R., and Bolton, M. D. (2004). Laboratory investigation of multiple grout injections into clay. *Géotechnique*, 54(2):81–90.

Terzaghi, K. V. (1943). *Theoretical Soil Mechanics.* Wiley, New York.

Timoshenko, S. and Goodier, J. (1951). *Theory of Elasticity.* McGraw-Hill.

Wang, S., Chan, D., Lam, K., and Au, S. (2010). Effect of lateral earth pressure coefficient on pressure controlled compaction grouting in triaxial condition. *Soils and Foundations*, 50(3):441–445.

Weber, T. M., Plötze, M., Laue, J., Peschke, G., and Springman, S. M. (2010). Smear zone identification and soil properties around stone columns constructed in-flight in centrifuge model tests. *Géotechnique*, 60(3):197–206.

Wong, H. Y. (1974). Discussion of compaction grouting. *by Douglas R. Brown and James Warner, J. Soil Mech. and Found. Div.*, 100(5):556–559.

Wood, D. M. (1990). *Soil behaviour and critical state soil mechanics.* Cambridge University Press, Cambridge.

Ye, G., Zhang, Z., Xing, H., Huang, M., and Xu, C. (2012). Consolidation of a composite foundation with soil–cement columns and prefabricated vertical drains. *Bulletin of Engineering Geology and the Environment*, 71(1):87–98.

Yu, H.-S. (2000). *Cavity Expansion Methods in Geomechanics*. Kluwer Academic Publishers, The Netherlands.

Zhang, D., Liu, S., Du, Y. J., and Du, G. Y. (2009). Consolidation mechanism of ground improved by a combined DJM-PVD method. *Lowland Technology International IALT*, 11(2):8–13.

Zhang, D., Liu, S., and Hong, Z. (2006). Consolidation calculating method of soft ground improved by DJM-PVD combined method. *Ground Modification and Seismic Mitigation*, pages 29–36.

Zytynski, M., Randolph, M. F., Nova, R., and Wroth, C. P. (1978). On modelling the unloading-reloading behaviour of soils. *International Journal for Numerical and Analytical Methods in Geomechanics*, 2(1):87–93.
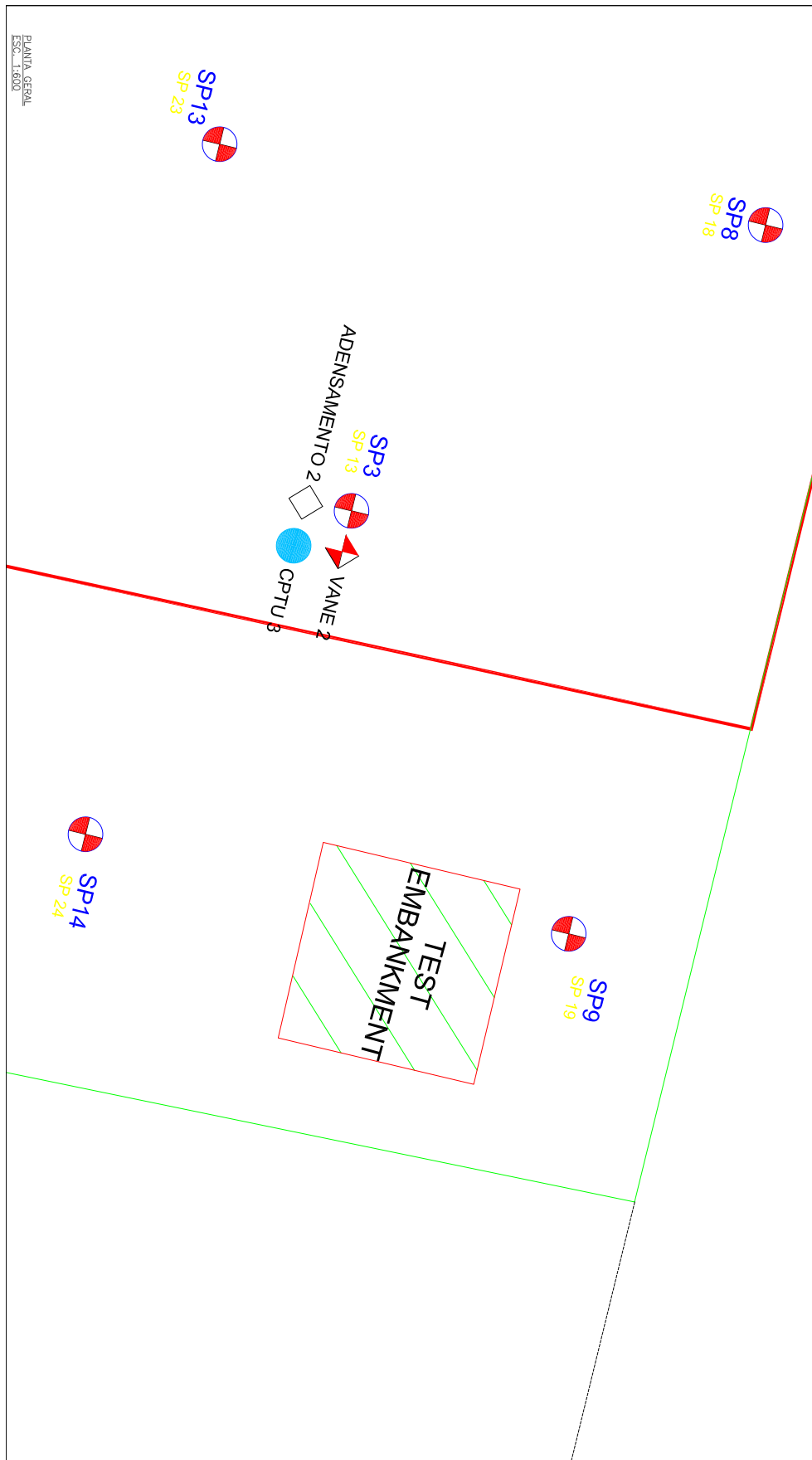
A Geotechnical field investigations

Figure A.1: Field tests locations for embankment A.

Figure A.2

Figure A.3

Curi Engenharia Ltda
Rua Dr. Borman, 06/304
Centro - Niterói - RJ.
Tel: (21) 2717-3335
curiengenhria@ig.com.br

Sondagem, Controle Tecnológico
Rebaixamento de lençol d'água

| SONDAGEM À PERCUSSÃO | INÍCIO: | 20/03/14 | COTA | ----- | **SP-24** |
| | TÉRMINO: | 20/03/14 | R.N. | ***** | |

CLIENTE: LEDUCA EMPREENDIMENTOS IMOBILIÁRIOS LTDA

LOCAL: ESTRADA DOS BANDEIRANTES COM RUA DANIEL BARRETO DOS SANTOS - RECREIO - RIO DE JANEIRO - RJ.

ESCALA DE COTAS	PERF. GEOL.	GRÁFICO DO No. DE GOLPES/30 cm — 10 20 30 40 50 60 70	GOLPES P/30 INIC.	FINAL	NÍVEL DA ÁGUA	PROF. DA CAMADA	CLASSIFICAÇÃO DO MATERIAL
			2	3	0,70		Silte argiloso, p/arenoso, c/m/materia organica, cor marrom m/escuro, consistencia mole.
			1 90	-		1.60	Areia fina e media, argilosa, c/marisco, cor cinza escuro, fofa.
			0	1		2.70	Argila siltosa, p/arenosa, c/p/marisco, cor cinza escuro, consistencia muito mole.
			0	1			
5			3	4		4.75	Areia fina, media e grossa, argilosa, cor cinza escuro, fofa a pouco compacta.
			4	5			
			6	6			
			7	10		7.55	
			9	12			
10			12	14			Areia fina e media, p/argilosa, cor cinza, medianamente compacta.
			14	18			
			11	13			
			13	16			
			12	16			
15			13	19		14.70	Continua na Próxima Página
20							

Obs.:

Amostrador - Ø E = 50.8 mm	Lavagem		R = Revestimento: 4,00 m		Sondador: SERGIO	Escala: 1/100
Ø I = 34.9 mm	Início (m):					R.J. No.
Revestimento - tubo Ø 2 1/2	Estágio 1(cm):	Leitura	N.A.(m)	Data	ROBERTO PEDREIRA FERREIRA CURI	
Martelo - 65 kg	Estágio 2(cm):	1	0,70	20/03/14	CREA-RJ 30422-D	**4277**
Altura de Queda = 75 cm.	Estágio 3(cm):	2	0,70	20/03/14		
		CURI ENGENHARIA LTDA				

Figure A.4

Date: 06/10/2013
Job: Aterro Teste
Location: Barra da Tijuca
Soil Type: Argila Mole

Borehole No.:
Sample No.: 4
Depth: 5 m

Test No.:
Operator:

MOISTURE CONTENTS

	Initial		Final	
Container:	15,12	g	14,72	g
Container + wet soil:	49,36	g	62,39	g
Wet soil:	34,24	g	47,675	g
Container + dry soil:	30,98	g	44,89	g
Dry soil:	15,86	g	30,1750	g
Water:	18,39	g	17,5	g
Moisture content:	116,0	%	58,0	%
Saturation degree:	87,57	%	100	%

Secific graviy: Gs = 2,46

SPECIMEN INFO

Height:	20	mm
Diameter:	70	mm
Area:	38,48	cm²
Volume:	76,97	cm³
Wet soil:	97,83	g
Dry soil:	45,30	g
Ring:	14,92	g
Bulk density:	1,271	g/cm³
Dry density:	0,589	g/cm³

Initial void ratio e_0 = 3,257

Pacheco Silva's method (1970)
C_c = 1,517 C_s = 0,174
σ'_m = 13,2 kPa
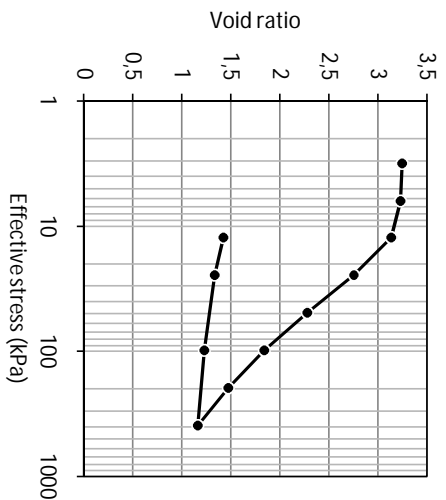
RESULTS

	Loading								Unloading		
Masses (kg)	1,23	2,461	4,808	9,616	19,232	38,465	76,93	153,86	38,465	9,616	4,808
Stresses (kPa)	3,14	6,27	12,26	24,51	49,02	98,05	196,10	392,20	98,05	24,51	12,26
H (mm)	19,95	19,86	19,42	17,64	15,41	13,35	11,63	10,17	10,48	10,98	11,40
ΔH (mm)	0,05	0,14	0,58	2,36	4,59	6,65	8,37	9,83	9,52	9,02	8,60
Δe	0,011	0,030	0,123	0,502	0,977	1,416	1,782	2,092	2,026	1,920	1,831
$e = e_0-\Delta e$	3,247	3,228	3,134	2,755	2,280	1,842	1,476	1,165	1,231	1,337	1,427
δp' (kPa)	3,14	3,14	5,98	12,26	24,51	49,03	98,05	196,10	-294,2	-73,54	-12,26
δe	0,011	0,019	0,094	0,379	0,475	0,439	0,366	0,311	-0,066	-0,106	-0,089
$(1+e_1)$	4,257	4,247	4,228	4,134	3,755	3,280	2,842	2,476	2,165	2,231	2,337
m'_v (kPa⁻¹)	7,974E-04	1,438E-03	3,703E-03	7,479E-03	5,157E-03	2,727E-03	1,314E-03	6,402E-04	1,036E-04	6,488E-04	3,121E-03
c_v (m²/s)	8,340E-07	1,400E-06	3,410E-07	5,730E-08	2,970E-08	4,140E-08	3,820E-08	4,660E-08			
k (m²/s)	6,650E-09	2,013E-08	1,263E-08	4,285E-09	1,532E-09	1,129E-09	5,020E-10	2,983E-10			

Average value within the field loading path

m'_v	5,121E-03
c_v	4,280E-08
k	2,315E-09

1 kgf = 9,81 N

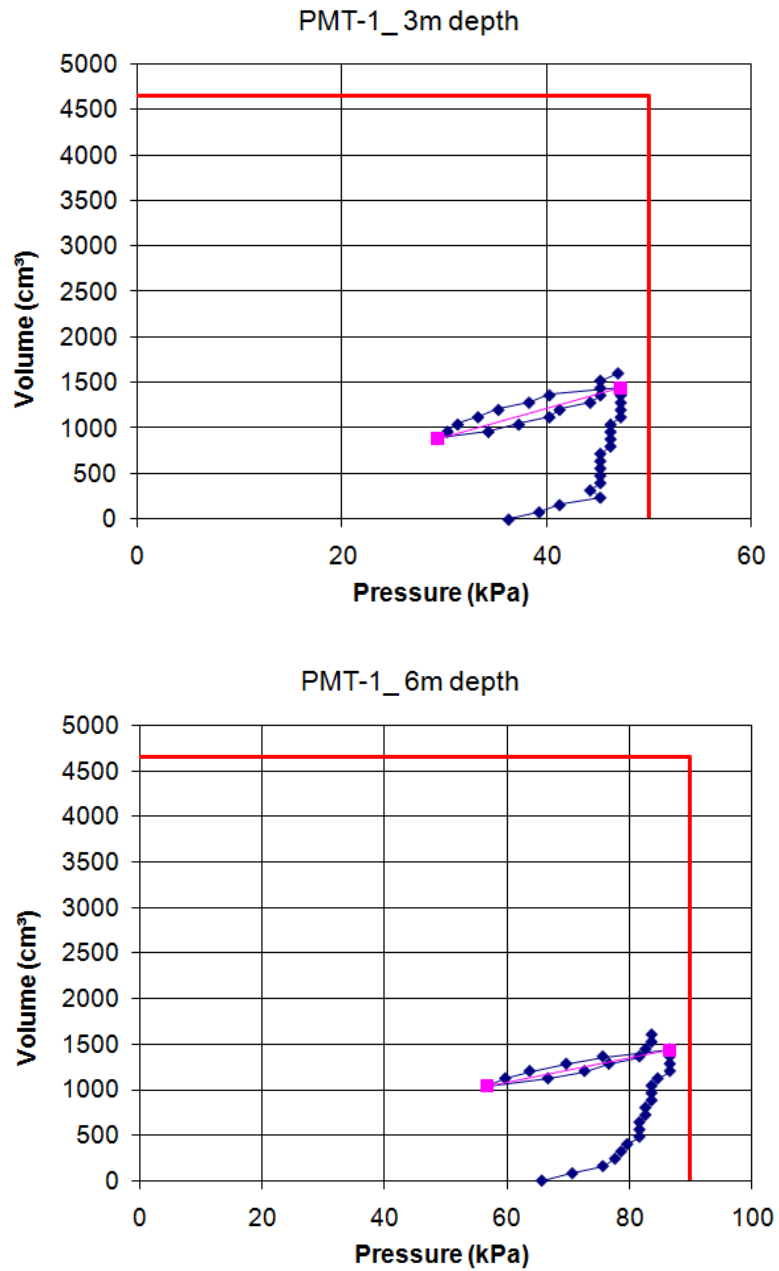Void ratio vs Effective stress (kPa)

Figure A.5: Oedometer test results.

Figure A.6: Pressure-expansion curves from pressuremeter tests.